1975

Moessbauer Studies Of Tin (iv) And Iron (iii) Acetylacetonates

Tsun Kong Sham

MOSSBAUER STUDIES OF
TIN (IV) AND IRON (III) ACETYLACETONATES

by

Tsun Kong Sham

Department of Chemistry

Submitted in partial fulfillment
of the requirements for the degree of
Doctor of Philosophy

Faculty of Graduate Studies
The University of Western Ontario
London, Ontario

June, 1975

To My Parents

ABSTRACT

^{119}Sn Mössbauer spectra of six coordinate Organotin(IV) acetylacetonates, $R_2Sn(L_2)_2$, or $RSnCl(L_2)_2$, (R = Me, Ph, L_2 = β -diketonate, or substituted β -diketonates) have been measured. The quadrupole splittings (QS) are used to assign structures of these compounds. For dimethyl compounds, Mössbauer and nmr evidence indicates that there is appreciable Sn 5S character along the Sn-C bond.

The compounds, $MSnCl(L_2)_2$, or $MSnCl_3\ L'_2$ (M = $Mn(CO)_5$, $Mn(CO)_4Ph_3P$, $Fe(CO)_2$ cp, $Mo(CO)_3$ cp; L_2 = acetylacetonate, 8-hydroxyquinolinate; L'_2 = 2,2' bipyridine, 1,10-phenanthroline) have been prepared. Mössbauer and Infrared studies indicate that the tin atom is six coordinate. Octahedral partial quadrupole splittings (pqs) are calculated for the metal groups. Correlation of octahedral pqs with tetrahedral pqs reveals that the ratio for $\{pqs\}^{oct}/\{pqs\}^{tet}$ is 0.75 ± 0.05, slightly greater than the theoretically expected 0.67.

Five coordinate organotin-acetylacetonates, R_3SnL_2, R_2SnClL_2 (R = Me, Ph, L_2 = anions of acetylacetone, benzoylacetone, and dibenzolmethane) have been prepared for the first time. Quadrupole Splittings are used to distinguish possible isomers. An X-ray single crystal determination of $Ph_3SnBzBz$ confirms the cis-R_3SnL_2 structure while quadrupole splittings indicate that the Me_3SnL_2 compounds have the mer structure.

A regression method is used to distinguish structural isomers of

five coordinate organotin (IV) compounds by their quadrupole splittings. By use of the new and literature data, partial quadrupole splittings are calculated for many ligands in trigonal-bipyramidal structures. Comparison of theory with experiment indicates that the additive model gives a consistent account of the relationship between quadrupole splittings and stereochemistry in trigonal-bipyrimidal organotin (IV) compounds. The ^{119}Sn partial quadrupole splitting parameters are used to derive partial quadrupole splitting parameters for ^{121}Sb (V) compounds.

Line broadening effects in Mössbauer spectra of ferric acetylacetonates ($Fe(AcAc)_3$) diluted in aluminum, or gallium acetylacetonates ($Al(AcAc)_3$, $Ga(AcAc)_3$) are studied. The broadenings observed are temperature and concentration dependent. The line broadening is therefore attributed to electron spin relaxation. At low temperature (4.2^0 K) and low concentration (1%), the resolved paramagnetic hyperfine structure is observed.

^{60}Co γ radiation has been used for the irradiation of the diluted ferric acetylacetonate systems. Mössbauer linewidth narrowing is observed for most of the samples after irradiation. At low $FeAcAc_3$ concentrations, Fe (II) high spin species is detected. The presence of Fe (II) high spin species indicates an effective radiolytic mechanism.

Room temperature spectra have been observed for bis (1-3-propanedionato) dimethyltin (IV). From the Goldanskii - Karyagin asymmetry in the room temperature spectrum of <u>trans</u> $Me_2Sn(AcAc)_2$, the calculated difference in mean square amplitudes parallel and perpendicular to

Me-Sn-Me axis is in good agreement with the crystallographic value.

Finally, the ^{119}Sn Mössbauer quadrupole splittings of distorted $Me_2Sn(IV)$ structures are also discussed.

ACKNOWLEDGEMENTS

I would like to thank those numerous people who have shown interest and offered suggestions during this work. I am especially grateful to my Supervisor, Dr. G. M. Bancroft, for his invaluable advice and constant encouragement. Special thanks are also due to Dr. M. G. Clark of the University of Cambridge for his great help in the theory of the additive model; and to Drs. N. C. Payne and B. W. Davies of this department for their great interest and instruction in the structural determination of organotin compounds.

I also owe Drs. H. C. Clark, V. G. Kumar Das for informative suggestions, and Dr. J. R. Bolton for the esr facilities.

Also, I am indebted to the Cancer Research Centre, U.W.O., for the ^{60}Co radiation facilities and the Chemistry Department, the University of Western Ontario, for its financial support.

Finally, I would like to thank my friends and colleagues for their assistance and in particular, reference is made to Dr. Alex Chen D.D.S. and Miss Y. M. Yiu for their encouragement during this work.

TABLE OF CONTENTS

LIST OF TABLES

LIST OF FIGURES

ABBREVIATIONS

Me - methyl

Ph - phenyl

AcAc - anion of acetylacetone

BzAc - anion of benzoylacetone

BzBz - anion of dibenzoylmethane

TfAc - anion of trifluoroacetylacetone

HfAc - anion of hexafluoroacetylacetone

oxin - anion of 8 - hydroxyquinoline

Py - pyridine

bipy - bipyridine

phen - phenanthroline

DMSo - dimethyl sulphoxide

HMPA - hexamethyl phosphoramide

OPO - methylene bis(diphenylphosphine oxide)

diphoso - ethyelenebis(diphenylphosphine oxide)

OAsO - methylene bis(diphenylarsine oxide)

bipyo - 2,2'-bipyridine N N'-dioxide

DMF - dimethyl formamide

DMA - dimethyl acetamide

pyo - pyridine oxide

pip - piperidine

Salen H_2 - bis(salicylaldehyde)ethylenediimine

terpy - 2,2',2" terpyridyl

dtc - N, N' dimethylthiocarbamate

esr - electron spin resonance

nmr - nuclear magnetic resonance

U.V. - ultra violet spectroscopy

Et - ethyl

Pr - propyl

Cp - cyclopentadienyl

efg, EFG - electric field gradient

CS - centre shift

QS - quadrupole splitting

pfg - partial field gradient

pqs - partial quadrupole splitting

eV - electron volt

Γ - Mössbauer half width

tet - tetrahedral

oct - octahedral

tbe - trigonal bipyrimidal equatorial

tba - trigonal bipyrimidal axial (apical).

CHAPTER 1

Introduction to Chemical Application of Mössbauer Spectroscopy

A. The Mössbauer Effect

The recoilfree nuclear gamma resonance (Mössbauer effect) was discovered by R. L. Mössbauer in 1957[1], and received extensive attention after it was shown[2,3] in 1959-1960 that ^{57}Fe exhibited this effect, and that hyperfine interaction in compounds can be detected. The Mössbauer effect has now become an established technique, Mössbauer spectroscopy[4,5]. Although over 40 nuclei exhibit this effect[5], only two isotopes, ^{119}Sn, and ^{57}Fe, are widely studied; since spectra are most easily obtained for these isotopes[4,6,7].

The characteristics[4,6,7] of Mössbauer spectroscopy are

1. that transitions are between nuclear levels with high energy separation (10^4 ~ 10^5 ev).
2. that the γ radiation is produced by a radioactive source, and the energy of the γ rays are modulated by the Döppler effect.
3. that the γ radiation is highly monochromatic (10^{-10}- 10^{-6} ev in width).
4. that it is a solid state phenomenon. In general both the source and the absorber must be in either a solid or frozen solution.
5. that the quality of the spectrum is greatly improved by cooling the source and the absorber to a low temperature and

6. that the Mössbauer absorption can be dominent even when the resonant nucleus is a minor constituent of the absorber.

B. Parameters

The Hamiltonian of interaction between the nucleus and the surrounding electrons in diamagnetic systems (^{119}Sn (IV), ^{57}Fe (II) low-spin etc.) gives rise to the two normally observed parameters of a Mössbauer spectrum - the Centre Shift (CS) and the Quadrupole Splitting (QS). The Centre Shift measures the variations in the coulombic interaction between the nucleus and the electronic environment in different compounds of the same element relative to a standard source. The dominant term in the centre shift is given by

$$cs = \frac{4\pi}{5} Ze^2R^2 \left(\frac{\delta R}{R}\right) \{|\psi(0)_s|^2 - |\psi(0)_s|^2\} \qquad (1.1)$$

absorber source

where Z = nuclear charge

e = protonic charge

$R = \frac{1}{2}$ (Rex + Rgr); average radius of the excited and the ground state

δR = Rex - Rgr

$|\psi(0)_s|^2$ = s electron density at the nucleus

For ^{119}Sn, since $\delta R/R$ is positive, the cs increases as $|\psi(0)_s|^2$ increases. The cs is also sensitive to p and d electrons which can have a shielding effect on the s electrons and therefore effect $|\psi(0)_s|^2$. A minor term,

usually referred to as a second order Döppler shift due to thermal motion of the nucleus, sometimes accounts for a small contribution to centre shift. However, this term is usually very small and can be neglected in the interpretation of spectra run at low temperature.

The second term in the nuclear Hamiltonian is the result of the interaction of the nuclear quadrupole moment, Q, with the electric field gradient due to other charges in the crystal. The deviation of the nucleus from spherical symmetry gives rise to the nuclear quadrupole moment. Nuclei whose spin is 0 or $\frac{1}{2}$ have a zero quadrupole moment; thus the ground state of ^{119}Sn and ^{57}Fe, with $I = \frac{1}{2}$, cannot exhibit quadrupole splitting. In ^{119}Sn and ^{57}Fe spectra, the observed quadrupole splitting is therefore due to the interaction of the first excited state (I = 3/2) nuclear quadrupole moment Q_{ex}, with the electric field gradient defined by a 3 x 3 tensor,

$$EFG = \begin{bmatrix} V_{xx} & V_{xy} & V_{xz} \\ V_{yx} & V_{yy} & V_{yz} \\ V_{zx} & V_{zy} & V_{zz} \end{bmatrix} \qquad (1.2)$$

where $V_{ij} = \frac{\partial^2 V}{\partial i \partial j}$, V = electrostatic potential, i,j = x,y,z

The components of the electric field gradient, Vij for point charges e, a distance r_i from the Mössbauer atom in polar coordinates are shown in Table 1.1.

It is apparent that Vij is a sum of independent contributions from Zi. This additivity is in fact the basis of the additive model for Mössbauer quadrupole splittings. It is usually possible to choose an appropriate axes system (denoted X, Y, Z; often the molecular axes) in which the EFG

Figure 1.1

(a). Nuclear energy levels, the isomer shift, and quadrupole splitting for $I_{gr} = 1/2$, $I_{ex} = 3/2$.

(b). Resultant Mössbauer spectrum.

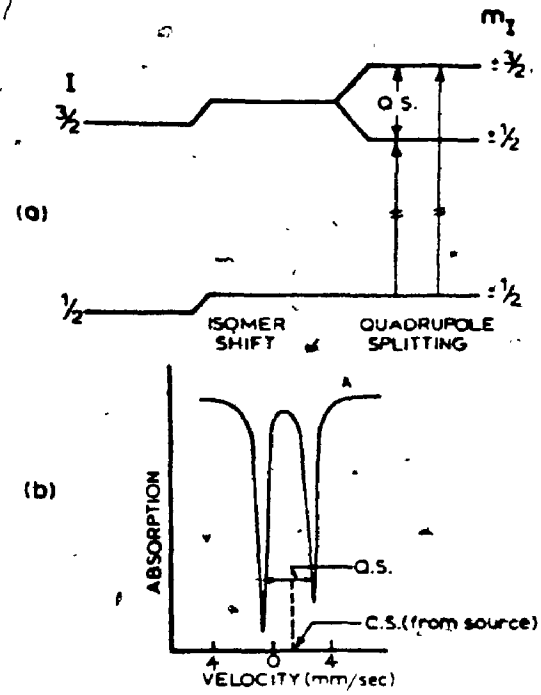

Table 1.1

Components of Electric Field Gradient Tensor for a point charge of 1 protonic charge e

Components	Coordinates
$V_{xx} = er^{-3}(3\sin^2\theta\cos^2\phi - 1)$ $V_{yy} = er^{-3}(3\sin^2\theta\sin^2\phi - 1)$ $V_{zz} = er^{-3}(3\cos^2\theta - 1)$ $V_{xy} = V_{yx} = er^{-3}(3\sin^2\theta\sin\phi\cos\phi)$ $V_{xz} = V_{zx} = er^{-3}(3\sin\theta\cos\theta\cos\phi)$ $V_{yz} = V_{zy} = er^{-3}(3\sin\theta\cos\theta\sin\phi)$	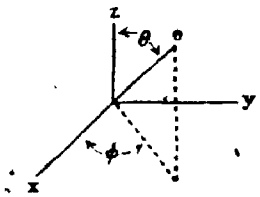

tensor is diagonalised. The Laplace equation requires that the sum of the second derivatives of the electrostatic potential vanishes:

$$V_{zz} + V_{yy} + V_{xx} = 0 \qquad (1.3)$$

Thus, there are two independent components. These are usually chosen as V_{zz}, often denoted eq, and η, the asymmetry parameter defined as

$$\eta = \frac{(V_{xx} - V_{yy})}{V_{zz}} \qquad (1.4)$$

where the components follow the convention that

$|V_{zz}| \geq |V_{yy}| \geq |V_{xx}|$, making $0 \leq \eta \leq 1$

The energy levels arising from the interaction of nuclear electric quadrupole moment with electric field gradient for $I_{ex} = 3/2$, $I_{gr} = 1/2$ is expressed as:

$$E_Q = \frac{e^2qQ}{4I(2I - 1)} [3M_I^2 - I(I + 1)] (1 + \eta^2/3)^{1/2} \qquad (1.5)$$

where $eq = V_{zz}$

I = nuclear spin

$M_I = I, I-1, \ldots -I$

For ^{119}Sn, transitions occur between $I = 3/2$ and $I = 1/2$ nuclear levels. Since the selection rule requires $\Delta M_I = 0, \pm 1$, the Mössbaur spectrum will consist of 2 lines, arising from the following transitions:

$I = 1/2$, $M_I = \pm 1/2 \rightarrow I = 3/2$, $M_I = \pm 3/2$

$I = 1/2$, $M_I = \pm 1/2 \rightarrow I = 3/2$, $M_I = \pm 1/2$

The transition probabilities for these transitions are the same for powder samples. The quadrupole splitting can be expressed as:

$$QS = \frac{1}{2}e^2qQ\ (1 + \eta^2/3)^{1/2} \qquad (1.6)$$

A typical Mössbauer spectrum is shown in Figure 1.1, along with corresponding transitions. The sign of the quadrupole splitting in this case is positive. However, it is usually impossible to extract the sign of the quadrupole splitting from a two line spectrum. For ^{119}Sn, and ^{57}Fe (II), (low spin) compounds, the sign is usually obtained in the presence of a strong magnetic field[17,18]. However, the magnetic perturbation method involves considerable experimental difficulties[17], and has not been routinely used. It is important to realize that valuable chemical information can be obtained if the sign of q is known. Thus, if $Q > 0$ as in ^{57}Fe case, $QS > 0$ implies $q \gtrsim 0$. For ^{119}Sn case, $Q < 0$ and hence $QS > 0$ implies $q < 0$ in tin compounds. In a <u>trans</u> MA_2B_4 compound, a negative q implies that electron density is concentrated along the A-M-A axis and a positive sign implies the opposite.

Magnetic hyperfine interactions arise in the presence of a magnetic field (external or internal). In diamagnetic systems, magnetic hyperfine interaction can only occur in the presence of an external magnetic field. However, in paramagnetic or ferromagnetic systems this is not necessarily the case (the latter is not important in this study and will not be discussed further). Paramagnetic hyperfine structures[19] can be obtained when electronic fluctuations are slow relative to Mössbauer transitions time scale. The spin relaxation can be seen readily if the effective field approximation is assumed valid. A change in electron spin orientation, for example, from + 5/2 to - 5/2 in the Fe^{3+} case, generates an inversion of the effective magnetic field. If this process takes place at a time interval short

compared with the lifetime of the nuclear excited state, the net magnetic field felt at the nucleus will average to zero. In this case, no magnetic spectrum will result. If the magnetic field fluctuates at a very slow rate, the effective magnetic field seen by the nucleus is no longer zero, and the magnetic spectrum will appear as a six line pattern. Spectra for intermediate relaxation times, however, are more difficult to predict. Theoretical treatment can be found in a paper[8] by Blume and Tjon. Qualitatively, the relaxation rate may be reflected by the line width: as the relaxation rate is gradually decreased, the original single line (or doublet) begins to broaden and splits into small broad peaks at the wings. These eventually sharpen into a well resolved magnetic spectrum. The energy levels can be expressed as:

$$E_{M_I} = (\mu M_I/I)\, H_{hmf}(t) \qquad (1.7)$$

where μ = nuclear magnetic moment

I = nuclear spin

$M_I = I, I-1, \ldots -I$

$H_{hmf}(t)$ = time dependent effective magnetic field felt by the nucleus; vanishes when the relaxation rate is fast compared to the Mössbauer transitions.

Two mechanisms are responsible for the rate of relaxation of the paramagnetic systems (e.g. Fe^{3+}). The spin-spin interaction with neighbouring ions, always leads to a short relaxation time. In general, magnetic structures are not obtained unless the paramagnetic species is diluted in a diamagnetic matrix[9]. Thus spin-spin relaxation does not depend on temperature; but depends on iron-iron distances. Another process is the

spin-lattice interaction where energy is transferred from the spin system to phonon mode of the lattice through spin orbit coupling. This is a temperature dependent process since it involves lattice vibration. In high spin Fe(III) ion , which has zero orbital angular momentum, spin-lattice relaxation is slow, and the relaxation rate is usually determined by the spin-spin relaxation. Spectra of ferric acetylacetonates due to spin relaxation will be discussed in Chapter 6.

C. The Additive Model for ^{119}Sn Quadrupole Splittings

The interpretation of Mössbauer quadrupole splittings in organotin (IV) compounds has been greatly facilitated by the application of additive treatment[10,11] in which the Q S of a compound is expressed as a sum of independent contributions from each ligand about the nucleus. For the calculation of ^{119}Sn quadrupole splittings, two formulations, the point charge model[11], and the molecular orbital model[12] have been used. These models rest on the assumption that the electric field gradient V at the nucleus must be additive. Thus for a compound MABC . . .

$$V = V(A) + V(B) + V(C) + \ldots \qquad (1.8)$$

Although these models can be equally used in practice, the more sophisticated molecular orbital approach which will be discussed in most part of this thesis is herein summarized.

In the simplified picture of this model[12], one considers a close-shell molecule in which the central atom M forms n σ bonds with n ligands (A, B, C, . . . N). The n valence molecular orbitals ψ_i (i = 1,2, . . . n) may be transformed into a set of ortho normal localized orbitals ϕ_L (L = A, B, C, . . . N), localized in the region of a particular metal-

ligand bond. This transformation should not change the matrix elements, V_{ij}, of the electric field gradient tensor V at the nucleus. Further, V_{ij} may be written as a sum of one electron matrix element:

$$V_{ij} = \sum_{L=A}^{N} (1 - R_L)(\phi_L|v_{ij}|\phi_L) = \sum_{L=A}^{N} v_{ij}(L) \qquad (1.9)$$

where $v_{ij} = -er^{-5}(3x_i x_j - r^2\delta ij)$. EFG operator

R_L = Sternheimer factor for distorted inner orbital shell corrections.

$vij^{(L)}$ = contribution of ligand L to V_{ij}

It becomes obvious that ϕ_L, and hence $v_{ij}(L)$, depends mainly on the properties of that particular M-L bond, provided that ϕ_L is well-localized into the region close to the M-L bond axis. Thus, those localized orbitals provide the natural framework for discussion of additivity. Clark et al[12] formulated the tensor $v_{ij}(L)$ in terms of the local axes with z directed along the M-L bond; in this form the tensor is defined as 'partial field gradient' (pfg) due to L.

The above model can be further simplified by assuming that the localized orbital can be written as a linear combination of a metal hybrid orbital h_L (formed from atomic orbitals), and a ligand orbital χ_L.

$$\phi_L = C_1 h_L + C_2 \chi_L \qquad (1.10)$$

The orbitals ϕ_L, h_L, and χ_L may all be taken as real, so that C_1 and C_2 are also real. The matrix element in Eq. (1.9) may be written

$$(\phi_L|V_{ij}|\phi_L) = C_1^2(h_L|V_{ij}|h_L) + 2C_1C_2(h_L|V_{ij}|\chi_L) + C_2^2(\chi_L|V_{ij}|\chi_L) \qquad (1.11)$$

As V_{ij} depends on $\langle r^{-3}\rangle$, the three terms on the right will fall off roughly as $1 : 10^{-1} : 10^{-2}$. Although, Sternheimer effects may increase

the third term (lattice contribution) by one order of magnitude, the contribution of the last two terms are considered negligible relative to the first term (valence contribution). In this case, using local axes system, Eq. (1. 9) becomes

$$V_{zz}(L) = 2(1 - R_L)(h_L|V_{zz}|h_L)C_1^2 = 2[L]e \qquad (1.12)$$

where [L] (analogous to $\frac{Z_i}{r_i^3}$ of Table 1.1) is the partial field gradient due to a cylindrical M-L bond. For practical reasons, another parameter, {L}, the partial quadrupole splitting is defined as

$$\{L\} = \frac{1}{2} e^2|Q|\{[L] - b[X]\} \qquad (1.13)$$

Where $b = 1$ for $\{L\}^{tet}$, $\{L\}^{oct}$ and $\{L\}^{tba}$;

$b = \frac{4}{3}$ for $\{L\}^{tbe}$;

X is a reference ligand (eg. Cl, Br) whose pfg is always chosen as zero relative to that of other ligands[12], since absolute pqs cannot be obtained.

Eq. (1.11), and (1.12) imply that different hybrids are used for different structures: tetrahedral, octahedral, and trigonal-bipyramidal. Table (1.2) shows the appropriate hybrids, and the corresponding [L] expressions derived by use of eq. (1.12).

Assuming that Sternheimer effects are constant, theoretical calculations[12] for valence orbitals of tin indicate that the ratio $\langle r^{-3}\rangle_d : \langle r^{-3}\rangle_p$ and $\langle r^{-3}\rangle_{sd} : \langle r^{-3}\rangle_p$ are of order of magnitude 10^{-2} and 10^{-3} respectively. Thus, the [L] values in Table (1.2) can be considered as arising from p orbital imbalance and approximate to

Table 1.2

Calculation of Partial Field Gradients in Important Structural Types[a,b]

Tetrahedral

$$h_z^{\text{tet}} = \tfrac{1}{2}s + \frac{\sqrt{3}}{2}p_z$$

$$[\mathrm{L}]^{\text{tet}} = -\tfrac{2}{15}\langle r^{-3}\rangle_p\,\sigma_{\mathrm{L}}^{\text{tet}}$$

Octahedral

$$h_z^{\text{oct}} = \frac{1}{\sqrt{6}}s + \frac{1}{\sqrt{2}}p_z + \frac{1}{\sqrt{3}}d_{z^2}$$

$$[\mathrm{L}]^{\text{oct}} = \left(-\tfrac{1}{5}\langle r^{-3}\rangle_p - \tfrac{2}{21}\langle r^{-3}\rangle_d - \frac{\sqrt{2}}{3\sqrt{5}}\langle r^{-3}\rangle_{sd}\right)\sigma_{\mathrm{L}}^{\text{oct}}$$

Trigonal-bipyramidal

Apical

$$h_z^{\text{tba}} = \frac{1}{\sqrt{2}}\cos\theta\, s + \frac{1}{\sqrt{2}}p_z + \frac{1}{\sqrt{2}}\sin\theta\, d_{z^2}$$

$$[\mathrm{L}]^{\text{tba}} = \left(-\tfrac{1}{5}\langle r^{-3}\rangle_p - \tfrac{1}{7}\sin^2\theta\langle r^{-3}\rangle_d - \frac{1}{\sqrt{5}}\sin\theta\cos\theta\langle r^{-3}\rangle_{sd}\right)\sigma_{\mathrm{L}}^{\text{tba}}$$

Equatorial

$$h_z^{\text{tbe}} = \frac{1}{\sqrt{3}}\sin\theta\, s + \frac{\sqrt{2}}{\sqrt{3}}p_z + \frac{1}{2\sqrt{3}}\cos\theta\, d_{z^2} - \tfrac{1}{2}\cos\theta\, d_{x^2-y^2}$$

$$[\mathrm{L}]^{\text{tbe}} = \left(-\tfrac{4}{15}\langle r^{-3}\rangle_p + \tfrac{1}{21}\cos^2\theta\langle r^{-3}\rangle_d - \frac{1}{3\sqrt{5}}\cos\theta\sin\theta\langle r^{-3}\rangle_{sd}\right)\sigma_{\mathrm{L}}^{\text{tbe}}$$

$$\eta_{\mathrm{L}}^{\text{tbe}} = \left|\frac{15\cos^2\theta\langle r^{-3}\rangle_d - 21\sqrt{5}\cos\theta\sin\theta\langle r^{-3}\rangle_{sd}}{28\langle r^{-3}\rangle_p - 5\cos^2\theta\langle r^{-3}\rangle_d - 7\sqrt{5}\cos\theta\sin\theta\langle r^{-3}\rangle_{sd}}\right|$$

[a] tet = tetrahedral, oct = octahedral, tba = trigonal-bipyramidal-apical, tbe = trigonal-bipyramidal-equatorial.

[b] From Ref. *12*

$$[L]^{tet} = -\frac{3}{10}\langle r^{-3}\rangle_p \, \sigma_L^{tet} \qquad (1.14)$$

$$[L]^{oct} = -\frac{1}{5}\langle r^{-3}\rangle_p \, \sigma_L^{oct} \qquad (1.15)$$

$$[L]^{tba} = -\frac{1}{5}\langle r^{-3}\rangle_p \, \sigma_L^{tba} \qquad (1.16)$$

$$[L]^{tbe} = -\frac{4}{15}\langle r^{-3}\rangle_p \, \sigma_L^{tbe} \qquad (1.17)$$

The empirical parameter $\sigma_L^{superscript}$ is proportional to $2C_1^2$, and should be very similar for all the structures. Thus the above equations (1.14 - 1.17) lead to the following important consequences.

1. The quadrupole splittings found for compounds restricted to the same coordination number can be compared using Table (1.1) (replacing $\frac{Zi}{r_i^3}$ by [L], appropriate molecular coordinates, and eq. (1.6).

2. Different pqs values should be assigned to coordination numbers.

3. Provided that $\sigma_L^{tet} \sim \sigma_L^{oct} \sim \sigma_L^{tba} \sim \sigma_L^{tbe}$ is valid, as might be expected; the ratio, $[L]^{tet}$: $[L]^{oct}$: $[L]^{tba}$: $[L]^{tbe}$, should be 1:0.67: 0.67: 0.89. Most of the work described in this thesis strongly supports the above consequences and hence substantiates the applicability of additive model in terms of Molecular orbital treatment. Details will be discussed in Chapter 3 and Chapter 5.

For the molecular structures of low symmetry, it is very convenient to express QS in terms of symmetrized parameters[13], S_{02}, S_{03} instead of q, and η.

The characteristics of the EFG gives

$$\text{determinant } |V_{ij} - \lambda\delta_{ij}| = 0 \qquad (1.18)$$

which can be written as:

$$\lambda^3 + S_{02}\lambda - S_{03} = 0 \qquad (1.19)$$

where the coefficient of the λ^2 vanishes is a direct consequence of the Laplace equation. In an arbitrary cartesian coordinate, the values of S_{02}, S_{03}, are[14]:

$$S_{02} = \begin{vmatrix} V_{11} & V_{12} \\ V_{21} & V_{22} \end{vmatrix} + \begin{vmatrix} V_{22} & V_{23} \\ V_{32} & V_{33} \end{vmatrix} + \begin{vmatrix} V_{33} & V_{31} \\ V_{13} & V_{11} \end{vmatrix} \qquad (1.20)$$

$$= -\frac{3}{4} e^2 q^2 (1 + \frac{1}{3}\eta^2)$$

$$S_{03} = \begin{vmatrix} V_{11} & V_{12} & V_{13} \\ V_{21} & V_{22} & V_{23} \\ V_{31} & V_{32} & V_{33} \end{vmatrix} = \frac{1}{4} e^3 q^3 (1 - \eta^2) \qquad (1.21)$$

Thus the quadrupole splitting for $^{119}Sn(IV)$ or $^{57}Fe(II)$ low spin compounds is

$$QS = \frac{1}{2} e^2 qQ (1 + \frac{1}{3}\eta^2)^{1/2}$$

$$= \text{sign}\,\{S_{03}\} eQ\,(-\frac{1}{3} S_{02})^{1/2} \qquad (1.22)$$

where sign $\{S_{03}\}$ denotes the sign of S_{03} and Q is the scalar quadrupole moment of the nucleus. Both (q, η), and (S_{02}, S_{03}) are used for calculation of quadrupole splittings in this study whenever appropriate.

Distortions from ideal geometry are usually ignored when the additive model is applied to a real chemical system[12]. The present uncertainty on the effect of distortion is also discussed in this context.

D. Mössbauer Resonance Techniques

In this thesis, all the spectra of ^{119}Sn and ^{57}Fe resonance except three were run by routine methods[4,7,15] most often used in Mossbauer laboratories. Two ^{119}Sn magnetic spectra and one ^{57}Fe liquid helium temperature spectrum were run at PCUM, Harwell, England, and are described in Chapter 5 and Chapter 6 respectively. A 10 mci radioactive source of $Ba^{119m}SnO_3$ and a 50 mci radioactive source of ^{57}Co doped in Copper matrix were used for ^{119}Sn and ^{57}Fe spectra respectively. The source was driven by a electromechanical vibrator (Austin Science Associates, U.S.A.), which provided the linear velocity range of interest: $\pm$ 5mms^{-1} for the ^{119}Sn; $\pm$ 4mms^{-1} for diamagnetic ^{57}Fe; and $\pm$ 12 mms^{-1} for the paramagnetic ^{57}Fe spectra. Mirror image spectra were produced since the vibrator was driven by a sawtooth wave form.

A Perspex or Perspex-aluminum holder containing 70 to 100 mg solid sample (normally powder) was sealed and cooled to liquid nitrogen temperature with the holder in a Copper block covered by a thin styrofoam lid. With the Cu block immersed into a liquid N_2 dewar, the temperature at the sample was 110 $\pm$ 5K. Room temperature spectra were obtained by similar set up except that an empty dewar was used or by taping the sample holder in front of the counter. γ-rays were selected using a single channel analyzer, and detected by a proportional counter. Counts from the detector were stored in a 512 channel analyzer whose channels were synchronized with the velocity scan so that the same velocity increment was associated with each channel. Calibration of the linearity of the instrument was performed using accurate positions of the four lines of a ^{57}Fe spectrum obtained from a 99.99% natural iron foil absorber at room temperature.

An updated version of a FORTRAN IV program written by Dr. A. J. Stone[16], was used to compute all the spectra using digital outputs obtained from the spectrometers. Lorentzian line shapes were fitted to all the peaks encountered in the spectra since Mössbauer absorption peaks are Lorentzian. The deconvolution of small but visibly unresolved splittings was achieved by the constraint functions in this program.

The quality of the spectra was judged by the statistical χ^2. χ^2 values between 450-500 for ~500 degrees of freedom were obtained for most spectra. With the exception of some room temperature spectra, the counts per channel were in a range of 400,000 - 1,000,000. Higher counts/channel were always required for room temperature or low ^{57}Fe concentration spectra. In some cases, ^{57}Fe enriched samples were used to improve the quality of the spectra.

E. References

1. R. L. Mössbauer, Z. Physik. 151, 124 (1958); Naturwissenschaflen 45, 538, (1958).

2. O. C. Kistnerand, A. W. Sunyar, Phys. Rev. Lett. 4, 412, (1960).

3. J. P. Schiffer, and W. Marshall, Phys, Rev. Lett. 3, 556 (1959).

4. N. N. Greenwood and T. C. Gibb, "Mössbauer Spectroscopy", Chapman and Hall, London (1971).

5. J. G. Stevens, and L. H. Bowen, Analyt. Chem. 46, 287 (1974).

6. G. K. Wertheim, "Mössbauer Effect: Principles and Applications", Academic Press, N. Y. (1964).

7. G. M. Bancroft, "Mössbauer Spectroscopy. An Introduction for Inorganic Chemists and Geochemists", McGraw-Hill, U. K. (1973).

8. M. Blume, and J. A. Tjon, Phys. Rev. 165, 446 (1968).

9. H. H. Wickman, M. P. Klein and D. A. Shirley, Phys. Rev. 152, 345 (1966).

10. G. M. Bancroft, and R. H. Platt, Adv. Inorg. Chem. Radiochem. 15 59 (1972) and references therein.

11. R. V. Parish, and R. H. Platt, Inorg. Chim. Acta 4, 65 (1970).

12. M. G. Clark, A. G. Maddock, and R. H. Platt, J. Chem. Soc. Dalton, 281 (1972).

13. M. G. Clark, J. Chem. Phys. 54, 697 (1971).

14. M. G. Clark, Molec. Phys. 20, 257 (1971).

15. V. I. Goldanskii, and R. H. Herber, eds., "Chemical Application of Mössbauer Spectroscopy". Academic Press, N. Y. (1968).

16. A. J. Stone, appendix to G. M. Bancroft, W. K. Ong, A. G. Maddock, R. H. Prince and A. J. Stone, J. Chem. Soc. (A), 1966, (1967).

17. W. M. Reiff. Coord. Chem. Rev. 10, 37, (1973).

18. T. C. Gibb, J. Chem. Soc. (A), 2503 (1970).

19. H. H. Wickman "Mössbauer Effect Methodology" 2, 39, 1966. ed. K. J. Gruverman, Plenum Press, N. Y.

CHAPTER 2

Mössbauer Studies of Six Coordinate Organotin(IV) Acetylacetonates

A. Introduction

Before the work described in this chapter was started, considerable effort[1,2,3,4] had been expended in the study of the stereochemistry of organotin acetylacetonates, both in solution and in the solid state. However, there is still controversy over the structures of these compounds; even though the X-ray study of $Me_2Sn(AcAc)_2$[5] confirms the trans-structure proposed from Mössbauer quadrupole splittings. For example, McGrady and Tobias[2] assigned the trans structure to $Ph_2Sn(AcAc)_2$ from nmr data, whereas Mössbauer quadrupole splitting strongly suggests the cis-configuration. Also, dipole moment measurements[4] in solution indicated that all the diorganotin(IV) acetylacetonates have the distorted cis structure. Moreover, $RSnCl(AcAc)_2$ (R = Me,Ph) compounds have been assigned the cis and trans configurations by different research groups from nmr[6] and infrared[3] evidence respectively. However, recent structural determinations[7,8] show that $Cl_2Sn(AcAc)_2$ has the cis- configuration in the solid state as well as in solution.

It is commonly recognized that in the trans-R_2Sn compounds

whose stereochemistry follows Bent's rule as described[2] previously, most of the Sn_{5s} character is concentrated in the Sn-C bonds, and the Sn-L bonds involve only 5p characters. However, Parish and Platt[9] have pointed out that in cis-R_2Sn structures, the Sn5S character in the Sn-C bond should be considerably less than in the trans-R_2Sn cases, and Mössbauer centre shifts values supported this interpretation.

In this work, the compounds, $R_{2-x}Cl_xSnL_2$ (x = 0, 1, 2, R = Me, Ph, L = anion of acetylacetone(AcAc), benzoylacetone(BzAc), dibenzoylmethane(BzBz), trifluoroacetylacetone(TfAc), and hexafluoroacetylacetone(HfAc)) and Cl_4SnHL have been prepared and studied by use of Mössbauer spectroscopy with three objectives in mind; first, to use Mössbauer quadrupole splittings to assign structures of these compounds; second, to use the variation in centre shifts (C S), quadrupole splittings (Q S), and nmr coupling constants ($^2J_{^{119}Sn-CH_3}$) to examine the Sn-L and Sn-C bond characteristics; and finally, to study the variation of s character in Sn-C bonds and of the corresponding quadrupole splittings in cis-Ph_2SnL_2 structures in terms of the degree of distortion. In addition, the sign of the quadrupole splittings for the dimethyl compounds have been determined by use of the observed Goldanskii - Karyagin asymmetry in the spectra and the recent X-ray data.

B. Results and Discussion

The ^{119}Sn Mössbauer parameters for seventeen tin(IV) β-diketonates are listed in Table 2.1, along with previously reported values (in brackets), and related phenyl tin oxinates (oxinate = anion of

Table 2.1

Mössbauer Parameters for Sn(IV)acetylacetones*

	Compound	C S	Q S
1.	$Me_2Sn(AcAc)_2$	1.16 (1.18)[a]	+ 4.02 (3.93)[a]
2.	$Me_2Sn(BzAc)_2$	1.06	3.87
3.	$Me_2Sn(BzBz)_2$	1.18	+ 4.08
4.	$Me_2Sn(TfAc)_2$	1.32	+ 4.36
5.	$Me_2Sn(HfAc)_2$	1.43	+ 4.47
6.	$Ph_2Sn(AcAc)_2$	0.71 (0.74)[a]	2.07 (2.14)[a]
7.	$Ph_2Sn(BzAc)_2$	0.73	2.23
8.	$Ph_2Sn(BzBz)_2$	0.73	2.15
9.	$Ph_2Sn(TfAc)_2$	0.89	2.53
10.	$Ph_2Sn(HfAc)_2$	1.18	2.71
11.	$Cl_2Sn(AcAc)_2$	0.15 (0.25)[b]	0.54
12.	$Cl_2Sn(BzAc)_2$	0.08	0.54
13.	$Cl_4Sn(HAcAc)$	0.41	0.70
14.	$Cl_4Sn(HBzAc)$	(0.47)[c]	0.65
15.	$[Cl_4SnAcAc][PyH]$	(0.47)[c]	~ 0
16.	$[Cl_4SnAcAc][Et_3NH]$	0.45	~ 0
17.	$ClSnMe(AcAc)_2$	0.61	1.78
18.	$ClSnPh(AcAc)_2$	0.61	1.77
19.	$ClSnPh(BzBz)_2$	0.63	1.64
20.	$Ph_2Sn\ oxin_2$	(0.73)[b]	(1.65)[b]
21.	$ClSnPh\ oxin_2$	(0.67)[b]	(1.48)[b]

* In mms^{-1} at 110°K. Errors are $\pm$ 0.02 mms^{-1} except where specified. Line widths are 1.10 $\pm$ 0.10 mms^{-1}.

a. Reference 1 b. Reference 10 c. Reference 30

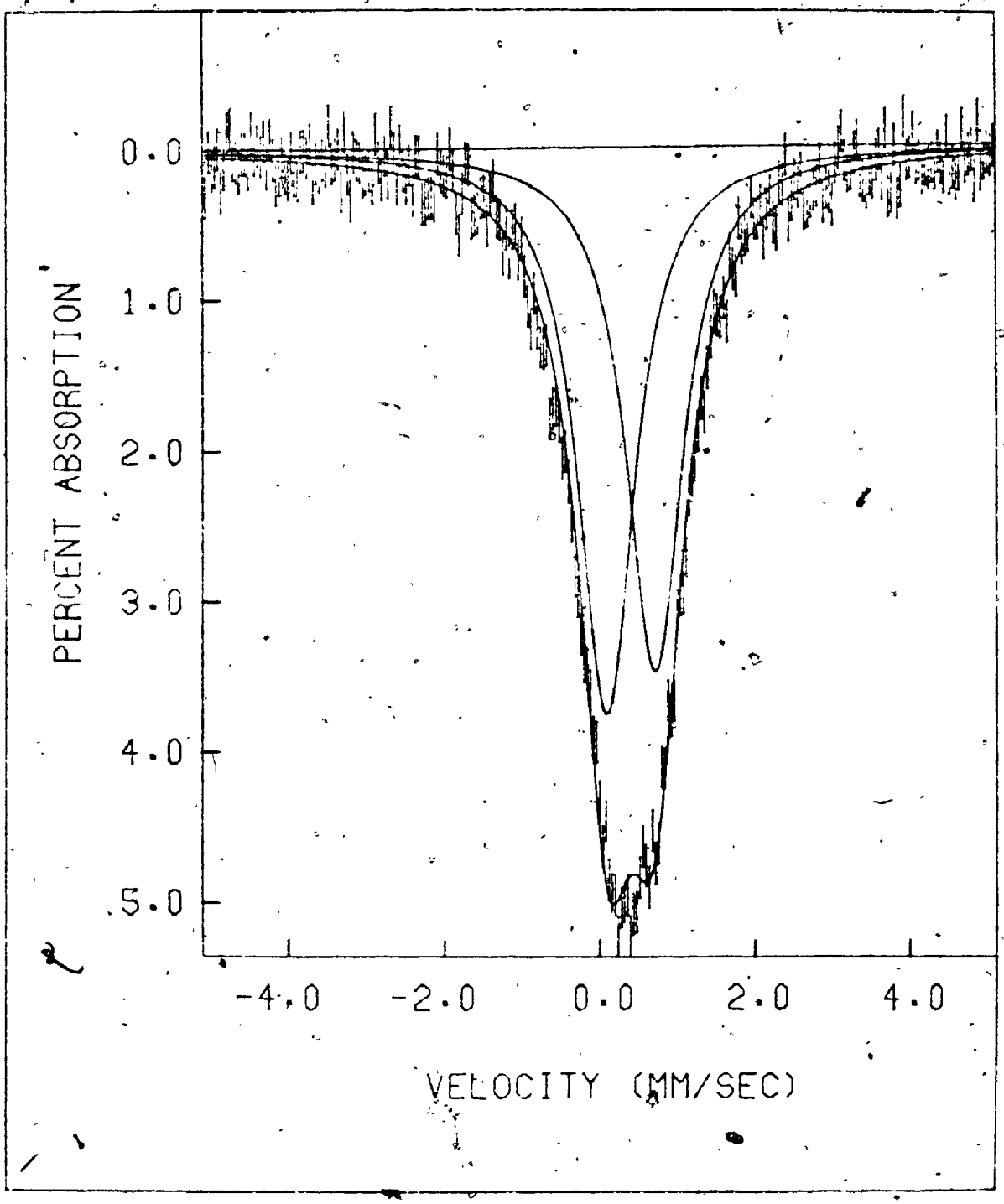

Figure 2.1 Mössbauer Spectrum of $Cl_4Sn(HBzAc)$ at 110°K

quadrupole splittings are likely to be positive since other cis-Ph_2Sn compounds have positive signs[12]. The discrepancy, both in the magnitude and in the signs, however, can be readily rationalized by use of a recently proposed model[12,13] in which distortion is included. In cis-Ph_2SnL_2 compounds, as the electroegativity of L increases, the s character tends to maximize in the Sn-C bond[14], hence the C-Sn-C angle tends to open towards a trans structure where maximum character in the C-Sn bond can be achieved. Assuming that {Ph} is essentially a constant in an octahedral coordination sphere, and {Ph} >> {L/2} (this is in fact the case), the quadrupole splitting will increase as L becomes more electronegative. ~~This is~~ consistent with X-ray data where no cis-R_2SnL_4 structure with a C-Sn-C angle less than 100° has ever been discovered. It is very likely that the ∠C-Sn-C angle in Ph_2SnL_2 is in the order: BzAc ~ AcAc ~ BzBz < TfAc < HfAc.

The structures of $ClSnMe(AcAc)_2$, $ClSnPh(AcAc)_2$, and $ClSnPh(BzBz)_2$ cannot be obtained from quadrupole splittings. The predicted quadrupole splittings for trans-Me and Ph isomers are + 1.94, + 1.78, + 1.86 mms^{-1} respectively, while the predicted splittings for cis-isomers are + 2.03, + 1.87, + 1.89 mms^{-1} respectively, compared to the observed values of 1.78, 1.77, and 1.64 mms^{-1}. Although the observed values are closer to those predicted for the trans-isomers, the predicted quadrupole splittings for cis and trans isomers are too similar to assign these structures[14]. However, recent nmr studies[6] suggest that $ClSnMe(AcAc)_2$ and $ClSnPh(AcAc)_2$ are the cis-isomer in solution, and dipole moment data[17]

8-hydroxylquinoline). The values obtained in this study are in good agreement with those found in the literature[1, 10, 11]. The nmr coupling constants and the intensity ratios of the Mössbauer doublets for dimethyl compounds are given in Table 2.2. A typical spectrum with a small quadrupole splitting in shown in Figure 2.1. The large decrease in χ^2 on going from a one peak to a two peak fit for $Cl_2Sn(AcAc)_2$, $Cl_2Sn(BzAc)_2$, $Cl_4Sn(HAcAc)$, and $Cl_4Sn(HBzAc)$ strongly supports the presence of a small quadrupole splitting for these compounds. For example, χ^2 decreased from 655 to 547 for a one and two peak fit respectively with ~500 degrees of freedom to $Cl_2Sn(AcAc)_2$. The error in these small quadrupole splittings is, of course, much larger than that for the resolved splittings.

1. Structure and Quadrupole Splittings

From Table 2.1, it is immediately apparent that the dimethyl compounds can be assigned the trans-structure, whereas the diphenyl compounds can be assigned the cis-structure; since they have quadrupole splittings[1, 10] in the range of 4 mm s^{-1} and 2mm s^{-1} respectively. The similarity of quadrupole splittings for $Cl_2Sn(AcAc)_2$ and $Cl_4Sn(HAcAc)$ which must be cis is entirely consistent with the cis structure assigned to $Cl_2Sn(AcAc)_2$[7].

However, it is apparent that the quadrupole splittings for the cis-Ph_2SnL_2 isomers are substantially larger than that expected on the basis of the additive model[10] where regular geometry is assumed. Thus, if we use the previously derived partial quadrupole splittings[11],

(pqs), - 1.03 mms^{-1} and - 0.95 mms^{-1}, for Me and Ph respectively, we can derive pqs values for AcAc/2, BzBz/2, and HfAc/2 of - 0.03, - 0.01 and + 0.09 mms^{-1}, respectively, from the trans-Me_2Sn compounds. The EFG, and QS expressions[10] used for these calculations are given by:

$$V_{zz} = \{4[R] - 4[L/2]\}e \quad (2.1)$$

$$V_{yy} = \{2[L/2] - 2[R]\}e \quad (2.2)$$

$$V_{xx} = \{2[L/2] - 2[R]\}e \quad (2.3)$$

$$\eta = 0 \quad (2.4)$$

$$QS = \frac{1}{2} e^2qQ = \frac{1}{2} e^2Q\{4[R] - 4[L/2]\} \quad (2.5)$$

where $\frac{1}{2} e^2|Q|[R] = \{R\} = - 1.03\ mms^{-1}$ is the previously derived pqs value for Me. Thus, taking into account that Q for ^{119}Sn is negative, eq. (2.5) can be expressed in terms of pqs parameters

$$- QS = 4\{R\} - 4\{L/2\} \quad (2.6)$$

For $Me_2Sn(AcAc)_2$, QS = + 4.02 mms^{-1}, eq. (2.6) becomes

$$- 4.02 = - 4.12 - 4\{AcAc/2\} \text{ and } \{AcAc/2\} = - 0.03\ (mms^{-1})$$

Using these values, we can predict the quadrupole splittings for cis-$Ph_2Sn(AcAc)_2$, cis-$Ph_2Sn(BzBz)_2$, and cis-$Ph_2Sn(HfAc)_2$ of - 1.84, - 1.88, and - 2.08 mms^{-1}, compared to the observed quadrupole splittings of 2.07, 2.15 and 2.71 mms^{-1}, respectively. It is obvious that the deviation between observed and predicted quadrupole splittings increases with the increase in the electronegativity of L. The signs of these

quadrupole splittings are likely to be positive since other cis-Ph_2Sn compounds have positive signs[12]. The discrepancy, both in the magnitude and in the signs, however, can be readily rationalized by use of a recently proposed model[12,13] in which distortion is included. In cis-Ph_2SnL_2 compounds, as the electroegativity of L increases, the s character tends to maximize in the Sn-C bond[14], hence the C-Sn-C angle tends to open towards a trans structure where maximum character in the C-Sn bond can be achieved. Assuming that {Ph} is essentially a constant in an octahedral coordination sphere, and {Ph} >> {L/2} (this is in fact the case), the quadrupole splitting will increase as L becomes more electronegative. ~~This is~~ consistent with X-ray data where no cis-R_2SnL_4 structure with a C-Sn-C angle less than 100° has ever been discovered. It is very likely that the ∠C-Sn-C angle in Ph_2SnL_2 is in the order: BzAc ~ AcAc ~ BzBz < TfAc < HfAc.

The structures of $ClSnMe(AcAc)_2$, $ClSnPh(AcAc)_2$, and $ClSnPh(BzBz)_2$ cannot be obtained from quadrupole splittings. The predicted quadrupole splittings for trans-Me and Ph isomers are + 1.94, + 1.78, + 1.86 mms^{-1} respectively, while the predicted splittings for cis-isomers are + 2.03, + 1.87, + 1.89 mms^{-1} respectively, compared to the observed values of 1.78, 1.77, and 1.64 mms^{-1}. Although the observed values are closer to those predicted for the trans-isomers, the predicted quadrupole splittings for cis and trans isomers are too similar to assign these structures[14]. However, recent nmr studies[6] suggest that $ClSnMe(AcAc)_2$ and $ClSnPh(AcAc)_2$ are the cis-isomer in solution, and dipole moment data[17]

indicates that the related compound $ClSnPh(oxin)_2$ has the cis-configuration. The Mössbauer spectrum of the frozen solution of $Me_2Sn(AcAc)_2$ in benzene was also recorded. The computed CS and QS are 1.08 and 3.85 mms^{-1}, respectively. These values along with those obtained by Herber et al[16] in butylbenzene, 0.97, and 2.76 mms^{-1} for CS and QS, respectively, are small compared with those for the neat solid (CS = 1.16 mms^{-1} QS = 4.02 mms^{-1}). These results clearly indicate that a structural change, as recently studied by Serpone, et al[17], occurs in solution. A larger QS observed in benzene than in butylbenzene is probably due to some degree of crystallization when the benzene solution is frozen. Another possibility in the solvent dependence of the acetylacetonate exchange[17].

2. Correlations of Centre Shifts with Quadrupole Splittings and with nmr $^2J_{119Sn-CH_3}$

It is now generally recognized that in trans-$Me_2Sn(AcAc)_2$, the Sn-C bonds involve most of the Sn 5S character, while the bonds to the acetylacetonates involve mainly Sn 5p character. The centre shift-quadrupole splitting correlation for dimethyl compounds (Fig. 2.2) strongly supports the above argument and moreover suggests that this argument can be applied to all these compounds. Thus the Sn-L bonds in these compounds contain little Sn 5S character. As the electronegativity of the equatorial ligands increases, the p orbital imbalance $[-N_{pz} + \frac{1}{2}(N_{p_x} + N_{p_y})]$ becomes more negative, the field gradient becomes more negative, and the quadrupole splitting becomes more positive[12]. If the chelates are only involved in bonding with Sn5p orbitals, a withdrawal of p electrons increases $[\psi(0)_{5s}]^2$ by deshielding and the centre shift will increase with

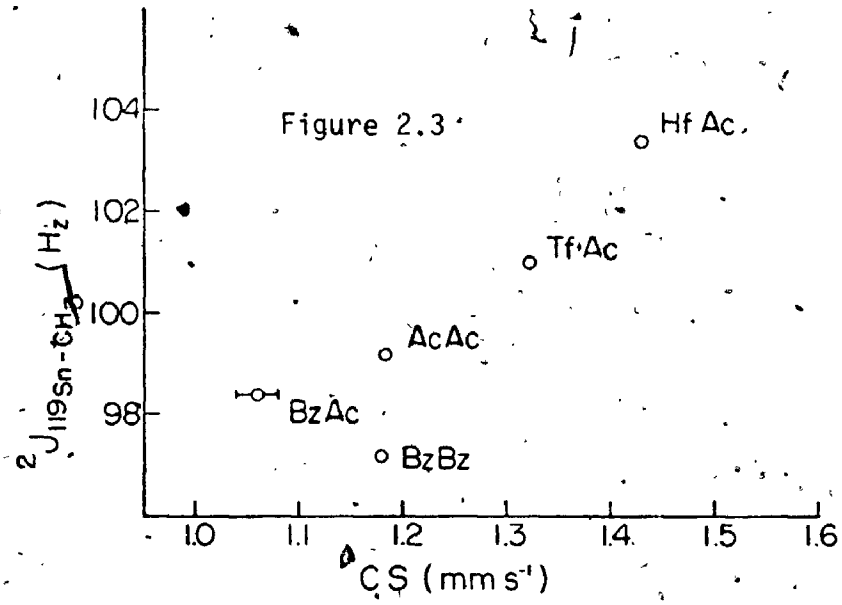

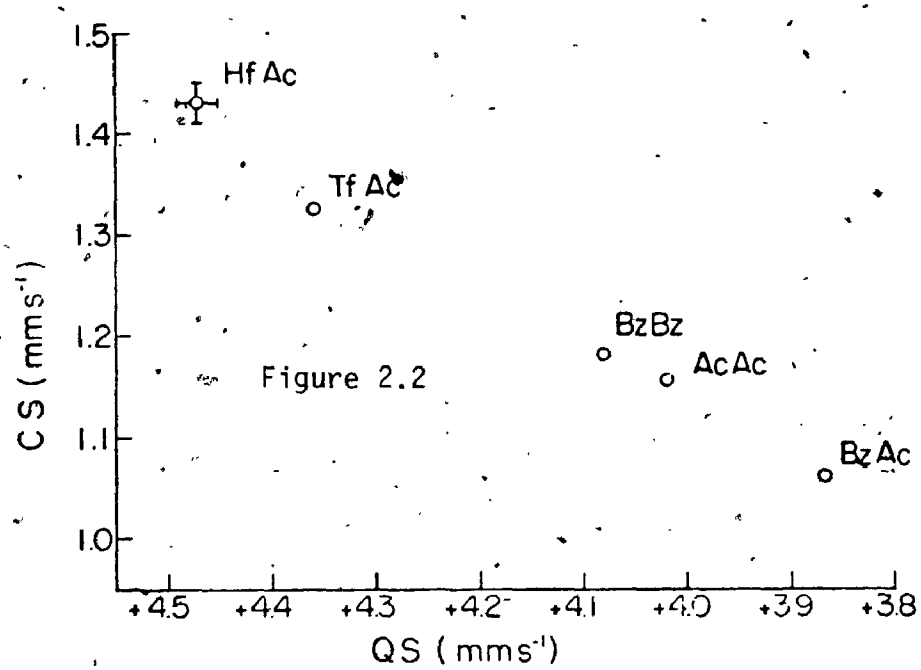

Figure 2.2 Plot of CS vs. QS for <u>trans</u> Me_2SnL_2 Compounds

Figure 2.3 Plot of $^2J(^{119}Sn\text{-}CH_3)$ vs. CS for <u>trans</u> Me_2SnL_2 Compounds

an increase of quadrupole splittings. This correlation is very similar to that for IX compounds (X = Na, K, Br, Cl, I)[18] where the IX bond is thought to involve only I 5p orbitals. If the Sn-L bonds contain considerable s character, an opposite trend would be expected[19].

The diphenyl compounds all have a substantially lower cs than the dimethyl compounds and this smaller cs is consistent with a smaller 5s character in the Sn-Ph bond than in the Sn-Me bond, and also with a cis-configuration[9]. On this argument, there will be an appreciable s character in the Sn-L bonds in the cis diphenyl compounds, and as the eletronegativity of L increases one would expect a small cs increase (or perhaps a decrease) than in the dimethyl compounds, and a poor or negative correlation between CS and QS; provided that the s character in the Sn-L bonds does not change at all. However, according to Bent's rule[16] and the recent proposed model[13], one would expect an increase in CS as well as QS as the electronegativity of L increases, since Sn tends to maximize the 5s character in Sn-C bonds and opens the C-Sn-C angle. The CS-QS correlation is not good for the diphenyl compounds, but a substantial increase in CS and in QS is observed as the electronegativity of L increases. This trend is consistent with the argument in terms of distortion[13]. It would appear that any change in Mössbauer parameters of the cis compounds is accompanied by the change of the s character in the Sn-C bond.

The correlation between $^2J_{^{119}Sn-CH_3}$ and the centre shift (Fig. 2.3) is consistent with little Sn 5s character in the Sn-L bonds in dimethyl compounds. Pidcock et al[20] has assumed that the Fermi contact term is the dominant term determining ^2J and that in a series of compounds such as the dimethyl compounds, the factors affecting $^2J_{^{119}Sn-CH_3}$ are just $[\psi(0)_{5s}]^2_{Sn}$,

α^2 (the s character in the Sn-C bond), and the degree of covalency in the Sn-C bond. According to Pidcock[20], the nmr $[\psi(0)5s]^2_{Sn}$ refers to the square of the amplitude of the atomic wave function at the nucleus; and the α^2 and covalency represent how much this orbital is involved in bonding. In contrast, the Mössbauer centre shift ($[\overline{\psi}(0)5s]^2$) has included these three terms; but when comparing with ^2J, it is convenient to separate the ^{119}Sn centre shift into similar terms.

$$CS \propto [\psi(0)5s]^2_{Sn} \sum_{bonds} \alpha^2 \times \text{Covalency}$$

Since Fig. 2.2. indicates that virtually all the Sn 5s character is in the Sn-C bonds, α^2 and the covalency are constant. Variation in $[\psi(0)5s]^2$ thus changes the CS, and $[\psi(0)5s]^2$ can only be changed by shielding effects of p electrons which are concentrated in the plane. As the electronegativity of the equatorial ligands increases, there will be more p electron density delocalized on to the ligands, hence both the CS and ^2J values will increase. This interpretation is consistent with the observed positive correlation (Fig. 2.3). It is interesting to compare $^2J_{^{119}Sn-CH_3}$ values due to p dehsielding with those due to change of s character in the Sn-C bond. In contrast to 2.3, a recently observed correlation[21] between $^2J_{^{119}Sn-CH_3}$ and CS of $Me_{4-x}SnM_x$ compounds (X = 1-3, M = $Co(CO)_4$, $Mn(CO)_5$, $Fe(CO)_2Cp$,) in which the s character of the bonds and Bent's rule determines ^2J, gives a negative slope. The observed variation in $^2J_{^{119}Sn-CH_3}$ of the $Me_{4-X}SnM_X$ system is ~20 Hz which is large compared with a range of only ~5 Hz observed in Me_2SnL_2 systems.

3. Goldanskii and Karyagin Asymmetry

All dimethyl compounds show pronounced asymmetric doublets in their spectra obtained from powder samples. The area ratios $I_+/I_- = R$ (I_+, and I_- are the areas for the positive and negative velocity lines, respectively) for these compounds are given in Table 2.2. For $Me_2Sn(AcAc)_2$, I_+/I_- (0.91 $\pm$ 0.05) is in good agreement with that reported by Herber et al[16]. Similar asymmetric doublets have been observed in tin[22-25] and iron[26,27] compounds; and have been attributed to Goldanskii-Karyagin effect[23,24] (due to anisotropic vibration of the Mössbauer nucleus). Flin et al[27] showed that the area ratio $(I_{3/2}/I_{1/2})$ of the two lines depends on $\langle Z^2\rangle - \langle X^2\rangle$, where $\langle Z^2\rangle$ and $\langle X^2\rangle$ are the mean square vibrational amplitudes parallel and perpendicular, respectively to the electric field gradient axis Z. In trans Me_2SnL_2 compounds, $\langle Z^2\rangle$ corresponds to the mean square vibrational amplitude of the tin atom along the Me-Sn-Me bond axis (the Z EFG axis), while $\langle X^2\rangle$ corresponds to the mean square vibrational amplitude in the plane of the acetylacetonates. If $\langle Z^2\rangle < \langle X^2\rangle$, then $R > 1$; if $\langle Z^2\rangle > \langle X^2\rangle$, then $R < 1$. This result can be important, if $\langle Z^2\rangle - \langle X^2\rangle$ is known from X-ray studies. First, if Mössbauer Spectra can be obtained at room temperature, then, the observed $(I_{3/2}/I_{1/2})$ can be compared with that calculated from X-ray data. Room temperature spectra of $Me_2Sn(AcAc)_2$ have been obtained; and the measured R value is in good agreement with that derived from X-ray data (details will be given in the Appendix). Moreover, if the sign of $\langle Z^2\rangle - \langle X^2\rangle$ is known, R can be used to determine the sign of the quadrupole splitting. In the trans-Me_2SnL_2 compounds, the X-ray study of $Me_2Sn(AcAc)_2$ shows that $\langle Z^2\rangle > \langle X^2\rangle$, and $(I_{3/2}/I_{1/2})$ must be less than 1. This immediately identifies the positive velocity line as the $\pm$ 3/2 line, and indicates that all dimethyl compounds have positive quadrupole splitting (from Table 2.2).

The positive QS of $Me_2Sn(AcAc)_2$ agrees with the sign previously determined using the magnetic pertubation method[12].

C. Experimental

With the exception of the new compounds, all the organotin (IV) β-diketonates were prepared using methods available in the literature[2-4, 28-31]. Some synthetic routes which leads to the formation of these compounds are summarized in the following reactions:

$$R_2SnO + HL \xrightarrow{H_2O} R_2SnL_2 + H_2O \qquad (2.7)$$

$$R_2SnCl_2 + 2\,NaL \xrightarrow{C_6H_6} R_2SnL_2 + 2NaCl \qquad (2.8)$$

or or

$$2\,TlL \qquad 2\,TlCl \qquad (2.9)$$

$$RSnCl_3 + 2HL \xrightarrow{H_2O} RSnClL_2 + 2HCl \qquad (2.10)$$

$$RSnCl_3 + 2TlL \xrightarrow{C_6H_6} RSnClL_2 + 2TlCl \qquad (2.11)$$

where R = Me, Ph; L = β-diketonates. Compounds 1,3 (Table 2.1) were prepared using eq. (2.7)[2]. Compounds 2-4 were prepared via eq. (2.8)[2], while compounds 5-10 were prepared by eq. (2.9)[4]. Compounds 17, and 18 were formed following eq. (2.10)[3]. However, Compound 19 can only be prepared using eq. (2.11) reported here. The purity of compounds was checked by m.p., infrared, n.m.r., chemical analyses (chemalytic, inc., Arizona, U.S.A.) and Mössbauer spectra. The synthesis of $PhSnClBzBz_2$ is reported as follows.

Bis (1,3-diphenyl-1,3-propanedionato)phenylchlorotin(IV), $PhSnCl(BzBz)_2$ - Phenyltintrichloride (0.46 gm) was added rapidly to a benzene solution of $TlBzBz$[4] (1.37 gm). The reaction mixture was stirred for 1 hour under a

nitrogen atmosphere. The white precipitate (TlCl) was discarded and the solution was evaporated to dryness under vacuum. The yellow residue was recrystallized in benzene. The yield was ~0.83 gm.

The melting points and analyses (observed values in parentheses) for the new compounds are: $Me_2Sn(TfAc)_2$, m.p. 105-106, C 32.3(32.0), H3.14 (2.86); $Ph_2Sn(TfAc)_2$, m.p. 66-68, C 45.6(45.8), H 3.11(2.95); and $PhSnCl(BzBz)_2$ m.p. 227-228 C 61.0(60.92); H 3.98(4.03).

The nmr spectra for dimethyl compounds were obtained in deuterochloroform solution. The $^2J_{^{119}Sn-CH_3}$ values are in good agreement with those previously reported. Mössbauer spectra were obtained as described in Chapter 1. All centre shifts are reported with respect to the centre of a room temperature $BaSnO_3$ - $BaSnO_3$ spectrum.

D. References

1. B. W. Fitzsimmons, N. T. Seeley and A. W. J. Smith, Chem. Comm. 390, (1970); ibid, J. Chem. Soc. (A), 143, (1969).

2. M. M. McGrady and R. S. Tobias, J. Am. Chem. Soc., 87, 1909 (1965).

3. Y. Kawasaki, T. Tanaka, J. Chem. Phys. 43, 3396 (1965); R. Ueeda, Y. Kawasaki, T. Tanaka, R. Okawara, J. Organomet. Chem. 5, 194, (1966).

4. C. Z. Moore and W. H. Nelson, Inorg. Chem. 8, 138 (1969).

5. G. A. Miller and E. O. Schlemper, Inorg. Chem. 12, 677 (1973).

6. N. Serpone and K. A. Hersh, Inorg. Chem. 13, 2901, (1974).

7. G. A. Miller and E. O. Schlemper, unpublished (ref. 13 in ref. 5 above).

8. R. Jones, Jr. and R. C. Fay, Inorg. Chem. 12, 2599 (1973).

9. R. V. Parish and R. H. Platt, Inorg. Chimica, Acta. 4, 589 (1970).

10. G. M. Bancroft and R. H. Platt, Adv. Inorg. Radiochem. 15, 59 (1972).

11. M. G. Clark, A. G. Maddock and R. H. Platt, J. Chem. Soc. (Dalton), 281 (1972).

12. R. V. Parish and C. E. Johnson, J. Chem. Soc. (A), 1906 (1971).

13. G. M. Bancroft and T. K. Sham, Inorg. Chem., submitted.

14. H. A. Bent, J. Inorg. Nucl. Chem., 19, 43 (1961).

15. F. P. Mullens, Can. J. Chem. 48, 1677 (1970).

16. R. H. Herber, M. F. Leary and Y. Hazony, J. Chem. Phys. 60, 5070, (1974).

17. N. Serpone and R. Ishayek, Inorg. Chem. 13, 52 (1974).

18. G. M. Bancroft, "Mössbauer Spectroscopy" An Introduction for Inorganic Chemists and Geochemists", McGraw-Hill, England (1973).

19. J. K. Lees and P. A. Flinn, J. Chem. Phys. 48, 882 (1968).

20. A. Pidcock, R. E. Richards and L. M. Venanzi, J. Chem. Soc. (A), 1707 (1966); and A. Pidcock, private communication.

21. G. M. Bancroft and K. D. Butler, J. Chem. Soc. (Dalton), 1694 (1973).

22. S. V. Karyagin, Doklady, Akad. Nauk, S.S.S.R. 140, 1102 (1963).

23. V. I. Goldanskii, E. F. Makarov and V. V. Kharpoo, Phys. Lett. 3, 344 (1963).

24. R. H. Herber and S. Chandra, J. Chem. Phys. 52, 6045 (1970).

25. R. H. Herber, S. Chandra and Y. Hazony, J. Chem. Phys. 53, 3330 (1970).

26. G. M. Bancroft, M. J. Mays and B. E. Prater, J. Chem. Soc. (A) 956 (1970).

27. P. Flinn, S. L. Ruby and W. L. Kehl, Science 143, 1434 (1964).

28. W. H. Nelson and D. F. Martin, J. Inorg. Nucl. Chem. 27, 89 (1965).

29. A. L. Allred and D. W. Thompson, Inorg. Chem. 7, 1196 (1968).

30. D. W. Thompson, J. F. Lefelhocz and K. S. Wong, Inorg. Chem. 11, 1139 (1972).

CHAPTER 3

Preparation and Mössbauer Spectra of Six Coordinate Sn-Mn Compounds: The Ratio of Six Coordinate to Four Coordinate Partial Quadrupole Splittings

A. Introduction

Although extensive studies on four coordinate tin-metal bond compounds have been documented, relatively little chemistry of six coordinate tin compounds containing such a tin-metal bond is known[2,3]. Thus, only seven compounds have been prepared - often in low yield. Patmore and Graham first reported three cobalt carbonyl derivatives of six coordinate tin acetylacetonates. Bonatti and Minghetti[3] reported another four six coordinate compounds containing a Sn-Fe, Sn-Co, or Sn-Mo bond.

No example of six coordinate Sn-Mn compounds has been reported. However, Mössbauer pqs parameters[4,5,6] as well as the extensive organotin chemistry[7], strongly suggest that $Mn(CO)_5^-$, along with other metal groups should show chemical characteristics comparable to that of the organogroups; and, therefore, six coordinate tin-manganese compounds should be readily prepared. In this Chapter, a series of novel six coordinate tin compounds (mainly containing Sn-Mn bonds) is reported. These compounds are prepared by use of reactions analogous to those encountered in organotin chemistry. The infrared and Mössbauer spectra of these compounds and some related compounds are discussed in some detail.

The EFG expressions for structures I, III and IV are given in Table 3.3. Using previously derived $\{L\}^{oct}$ values (mm s^{-1}) for AcAc/2 (-0.03[20]), bipy/2(-0.08[8]), phen/2 (-0.04[8]), oxin/2(-0.05[27]), ph(-0.95[8]) and Cl(0.00[8]), we can now derive $\{M\}^{oct}$ values (Table 3.4) from the quadrupole splittings in Table 3.2. To provide the overall best $\{M\}^{oct}$ values, averaged $\{M\}^{oct}$ values are calculated except for those determined from oxin compounds (except for compound 12 of course). The Q S values for $R_2Sn(oxin)_2$ compounds[21] vary over a wide range, and the {oxin} value seems less well defined than the other values. For $Mn(CO)_5$, the $\{Mn(CO)_5\}^{oct}$ values (mm s^{-1}) derived from compounds 1,2,3,4,7 and 8 (assuming the <u>fac</u> structure for compounds 3 and 4) are -0.76, -0.69, -0.70, -0.64, -0.73 and -0.71 respectively giving an average value of -0.71 $\pm$ 0.03 mm s^{-1}. Considering the wide variation in structure and bonding about the Sn in these six compounds, the consistency of these values is satisfactory. For example, the $\{Mn(CO)_5\}^{oct}$ values derived from compounds 7 and 8 with electropositive Ph groups are very similar to those derived from the halide compounds.

If structure IV is taken for the phen and bipy $MSnCl_3$ adducts, the $\{Mn(CO)_5\}^{oct}$ value derived from the Q.S. for compounds 3 and 4 are both -0.58 mm s^{-1}, very much smaller than the -0.71 average given above. The additivity treatment strongly suggests that these adducts all have the <u>fac</u> structure.

In Table 3.4, it is apparent that the $\{L\}^{oct}$ value are all substantially smaller than the $\{L\}^{tet}$ values. The four coordinate {M} values in Table 3.4 were derived from the nearly tetrahedral R_3SnM compounds[4] wherever possible. Since a Q.S has not been resolved for $Ph_3SnMn(CO)_4$-PPh_3, a $\{Mn(CO)_4PPh_3\}^{tet}$ value has been derived by plotting the (Q S) of

$RSnCl_3 \cdot$(bipy) and $RSnCl_3 \cdot$(phen) compounds in a simple addition reaction:[11, 12]

$$RSnCl_3 + L \xrightarrow{C_6H_6} RSnCl_3L \qquad (3.3)$$

Our preparations of $MSnXL_2$ and $MSnCl_3L$ compounds were carried out by analogous reactions to those given above. Reaction (3.2) rather than (3.1) was used because the $MSnCl_3$ compounds tend to decompose in aqueous solution.

The analogous reactions for R_2SnCl_2 compounds readily yield the expected six coordinate compounds, $R_2Sn(AcAc)_2$, $R_2Sn(oxin)_2$, R_2SnCl_2 phen and R_2SnCl_2 bipy. However, the reactions of M_2SnCl_2 compounds, and the above ligands are not clearly understood at the present time. For example, the reaction of $[Fe(CO)_2cp]_2$ $SnCl_2$ and oxin[3] gives $[Fe(CO)_2cp]$ $SnCl(oxin)_2$ instead of $[Fe(CO)_2cp]_2$ Sn $oxin_2$ as an isolated product. Reactions of $[Fe(CO)_2cp]_2$ $SnCl_2$ and $[Mo(CO)_3cp]_2$ $SnCl_2$ with Tl AcAc and Tl oxin gave products which were very light and air sensitive. The Mössbauer and infrared evidence suggested that the six coordinate M_2SnL_2 (L = AcAc or oxin) may well be present. Because of the previous preparation of trans-$[Co(CO)_4]_2$[2] and the preparation of trans-$Mn(CO)_5$-$SnPhCl_2$phen reported here, it seems likely that the dimetal compounds could be prepared under the proper conditions.

2. Infrared Spectra and Structures

The use of CO stretching frequencies in the 1900-2200 cm^{-1} region of IR spectra has greatly facilitated the structure elucidation of metal carbonyl complexes[13, 14, 15]. $Mn(CO)_5L$ (L = Cl, Br) compounds with a C_{4v} symmetry have a three band (2a + e) pattern in the carbonyl

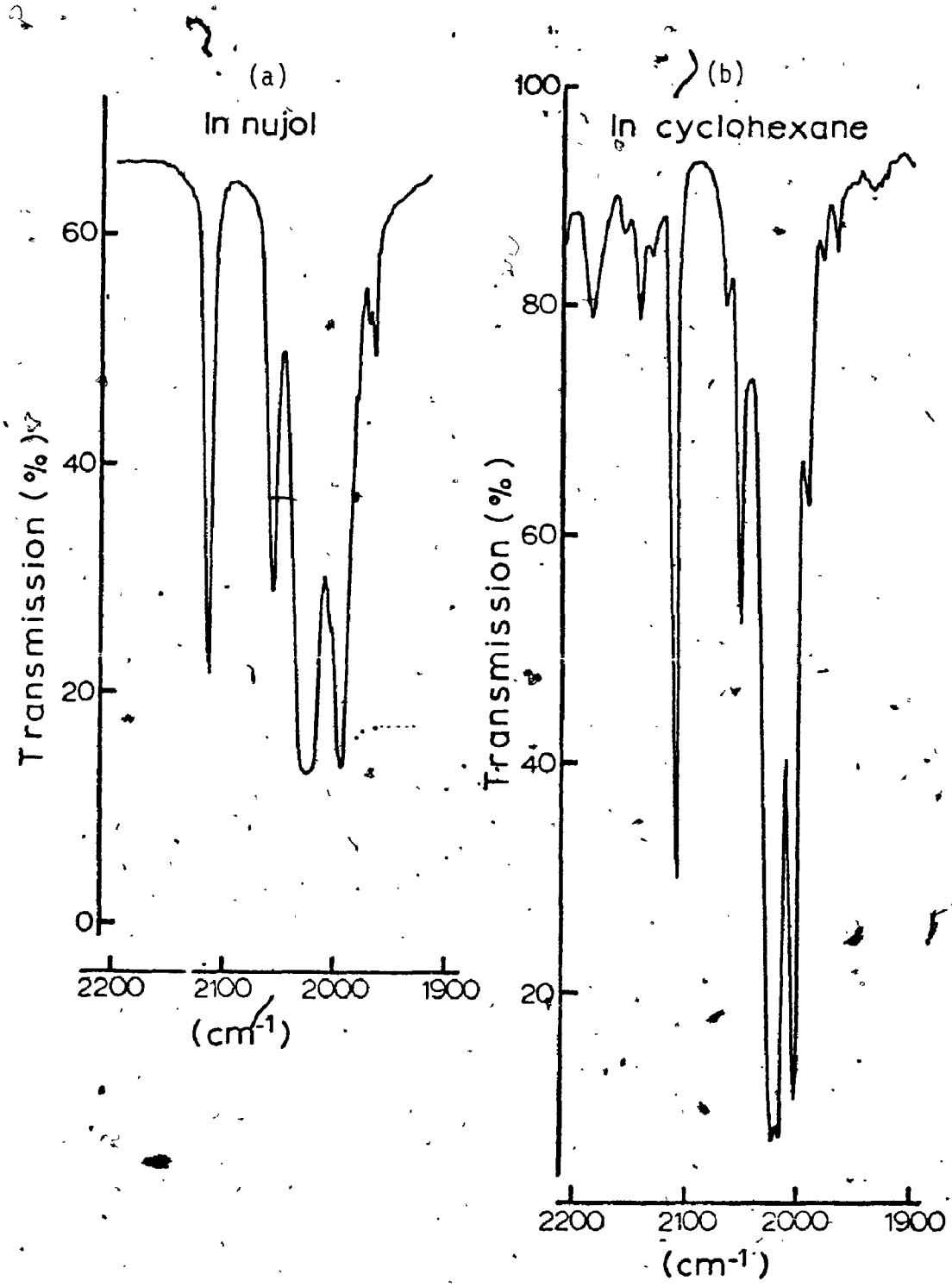

Figure 3.1 Infrared Spectra of $Mn(CO)_5SnCl(AcAc)_2$ in the CO Stretching Frequency Region

(a) in nujol (b) in cyclohexane

region. As the symmetry of the L group decreases (i.e. when L = $SnCl_3$, SnR_3) the normally IR inactive band (b_1) begins to appear and at the same time the e band begins to broaden and eventually splits into a doublet as L becomes less symmetric.

The above variation in infrared spectra with symmetry is very useful in assigning the structure of many of the $Mn(CO)_5$ compounds. All compounds show at least four bands including a b_1 band of appreciable intensity (Table 3.1 and Figure 3.1). In $Mn(CO)_5SnCl(AcAc)_2$, the broad e band in nujol (Figure 3.1a) splits in cyclohexane solution (Figure 3.1b) These similar spectra strongly suggest that the symmetry of the molecule is the same in both solid and solution, and that the local symmetry of all our $Mn(CO)_5$ compounds is lower than C_{4v}.

For the AcAc and oxin compounds (1,2 and 6, Table 3.1), the C_{4v} trans structure can be ruled out, leaving us with the cis structure for all three compounds, (I, Figure 3.2). It seems likely that the previously prepared analogues, $MSnCl(oxin)_2$(M = $Fe(CO)_2cp$, $Mo(CO)_3cp$)[3] and $Co(CO)_4SnCl(AcAc)_2$ also have the cis configuration. These structures are consistent with the Mössbauer quadrupole splittings (vide infra) and the cis structure for the $RSnCl(AcAc)_2$[16] compound.

The CO stretching bands observed for $Mn(CO)_5SnPhCl_2$(phen) alone cannot be used to assign structures with confidence. However, the Mössbauer quadrupole splitting (vide infra) shows that this compound has the trans structure (II, Figure 3.2). The infrared data is consistent with this structure. Also, the analogous Ph compound has the same structure confirmed by X-ray study[17].

The other phen and bipy adducts (compounds 3 and 4) can have either the fac (III) or mer (IV) structures (Figure 3.2). Because both

Table 3.1

CO Infrared Stretching Bands of Tin-Metal Bond Compounds

	Compound	CO IR bands (± 2cm^{-1})						
		a_1	b_1	e	a_1'	k_1	k_2	k_1
1.	cis-$Mn(CO)_5SnCl(AcAc)_2$[a]	2112 (2110)	2055 (2051)	2025 (2022)[b]	1995 (2006)	16.20	17.05	0.25
2.	cis-$Mn(CO)_5SnCl(oxin)_2$	2110	2031	2016	2010	16.39	16.66	0.12
3.	fac-$Mn(CO)_5SnCl_2bipy$	2016	2073	2021[b]	2010	16.58	17.35	0.43
4.	fac-$Mn(CO)_5SnCl_3phen$	2114	2070	2035[b]	2010	16.47	17.30	0.29
5.	trans-$Mn(CO)_5SnPhCl_2phen$	2109	2063	2012[b]	2000	16.41	17.19	0.42
6.	cis-$Mn(CO)_5SnPh(AcAc)_2$	2118	2068	2021[c]	2001[c]	16.75	17.27	0.39
7.	$Mn(CO)_5SnCl_3$[d]	2122	2070	2043	2037	16.91	17.31	0.20
8.	$Mn(CO)_5SnPh_3$[d]	2093	2027	2002	2002	16.34	16.64	0.23
9.	$Mn(CO)_5SnMe_3$[d]	2089	2021	1998	1991	16.29	16.49	0.24
10.	$Mn(CO)_4Ph_3PSnCl_3$	2090	2042	1993	--	--	16.81	0.38
11.	$Mn(CO)_4Ph_3PSnPh_3$	2049	1989	1947	--	--	15.98	0.31
12.	fac-$Mn(CO)_4Ph_3PSnCl_3bipy$	2072	2026	1974	--	--	16.58	0.41
13.	fac-$Mn(CO)_4Ph_3PSnCl_3phen$	2071	2027	1972	--	--	16.59	0.44

a. Values in parentheses are obtained from cyclohexane solution spectrum.

b. Doublets

c. Broad.

structures have symmetries lower than C_{4v}, it is not possible to distinguish these structures from the infrared data. However, the Mössbauer quadrupole splittings (vide infra) suggest that these compounds, the other analogous $Fe(CO)_2cp$ complexes, and the Ph and Me analogues[17] all have the fac structure.

The force constants k_1, k_2 and k_i have been calculated using the Cotton-Kraihanzel[13] method. They are compared with those calculated previously for the four coordinate compounds $Mn(CO)_5SnCl_3$ and $Mn(CO)_5SnR_3$ (R = Me, Ph)[18]. There are no discernable trends in the infrared stretching frequencies or the k's in the six coordinate compounds. The k's and stretching frequencies for the six coordinate compounds nearly all lie between those for the four coordinate $Mn(CO)_5SnCl_3$ and $Mn(CO)_5SnMe_3$. Considering the axial CO a_1' band, it is apparent that this band in the six coordinate compounds lies close to that for $Mn(CO)_5SnPh_3$ rather than $Mn(CO)_5SnCl_3$ ~~which has~~ more s character in the Mn-Sn bond. This result is perhaps surprising because for the halide complexes at least, the Cl and O bonding atoms are all electronegative compared to the three Ph in $Mn(CO)_5SnPh_3$; and one expects that the increase in electronegativity of L in $Mn(CO)_5SnL_3$ (e.g. from L = Ph to L = Cl) increases the σ withdrawal effect in the Sn-Mn bond and hence increases the positive charge in the Mn, decreases the electron density in the trans CO antibonding orbital and increases the a_1' frequency. There appears then to be more electron density in the CO antibonding orbitals in the six coordinate complexes than might have been expected.

The CO stretching pattern of $Mn(CO)_4PPh_3SnCl_3L$ compared with $Mn(CO)_4PPh_3SnCl_3$ and $Mn(CO)_4PPh_3SnPh_3$ is similar to that of $Mn(CO)_5SnCl_3L$

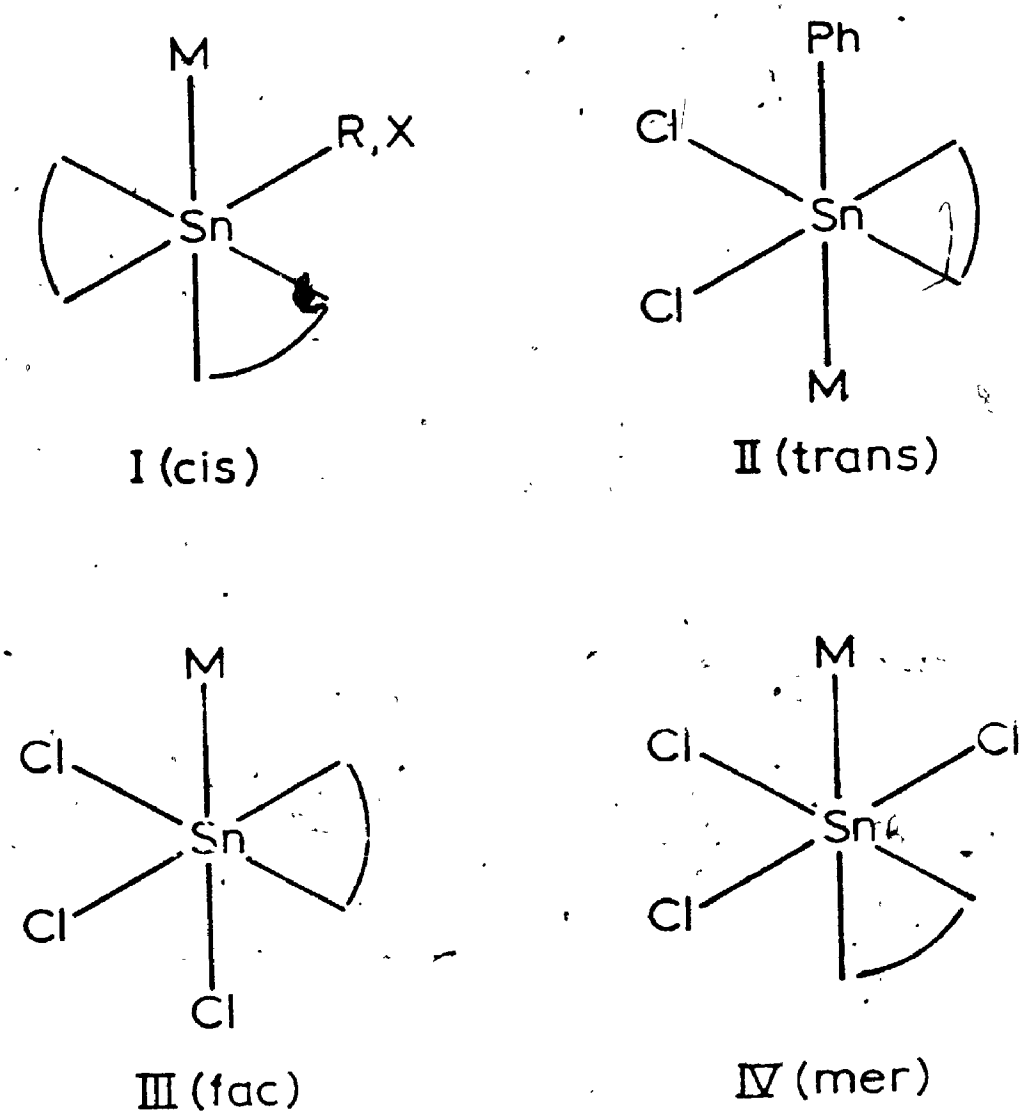

Figure 3.2 Structures of Six Coordinate Sn(IV)-Metal Compounds

compared with $Mn(CO)_5SnCl_3$ and $Mn(CO)_5SnPh_3$. The CO frequencies for $Fe(CO)_2cpSnCl_3$·phen are 2029, 2023, (doublet), 1974, similar to that of $Fe(CO)_2cpSnCl_3$·bipy, but lower than that of $Fe(CO)_2cpSnCl_3$.

C. Mössbauer Quadrupole Splittings and Ratio of Partial Quadrupole Splittings.

The ^{119}Sn Mössbauer parameters along with the ^{57}Fe Mössbauer parameters for the $Fe(CO)_2cp$ compounds are given in Table 3.2, while typical ^{119}Sn and ^{57}Fe spectra are shown in Figure 3.3. The ^{57}Fe centre shifts (C S) are very similar to those for four coordinate $SnFe(CO)_2cp$ compounds[19], while the quadrupole splittings (Q S.) are about 0.1 mm s^{-1} smaller than for the four coordinate compounds.

Qualitatively, the ^{119}Sn quadrupole splittings and centre shifts for the six coordinate compounds are smaller than those for the corresponding four coordinate $MSnCl_3$ species (compounds 13-15, Table 3.2). Compared to the six coordinate Ph analogues (17-20, Table 2), the M-Sn compounds have larger centre shifts and lower quadrupole splittings. The above quadrupole splitting trends are due to the fact that $|\{L\}^{oct}| < |\{L\}^{tet}|$[8], and that $|\{M\}| < |\{Ph\}|$ in both coordinations. The quantitative interpretation of these results is given below, while the centre shift trends are discussed in the next section.

The infrared evidence presented earlier strongly suggests that all the AcAc and oxin derivatives (1,2,7,9,12, Table 3.2) have the cis structure (I, Figure 3.2). The large Q S for compound 8 is only consistent with the trans structure II, since the cis structure would give a Q S of less than 2 mm s^{-1}. The phen and bipy $MSnCl_3$ adducts could have either structure III or IV, but the additivity treatment discussed below indicates that these compounds have the fac structure (III).

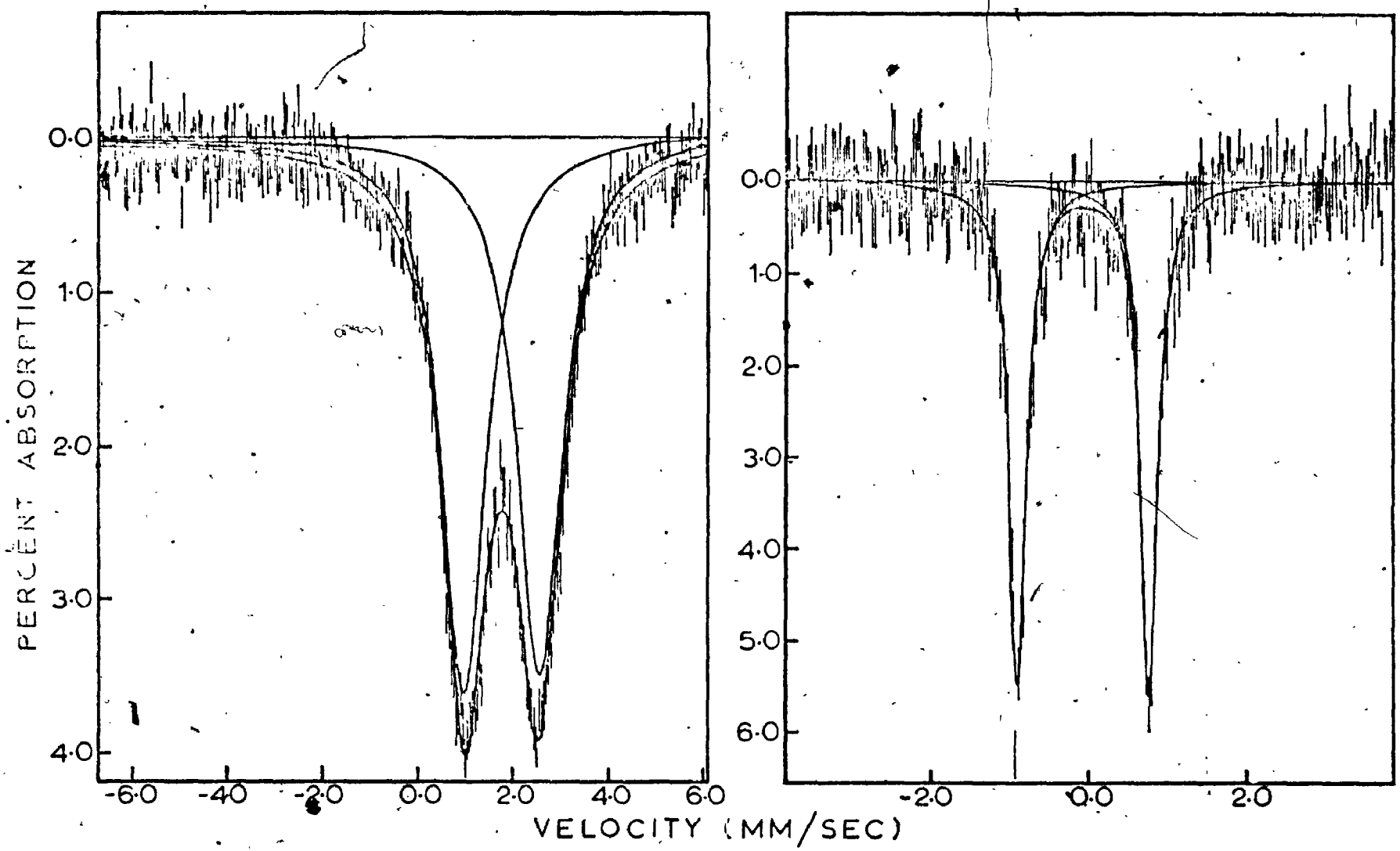

Figure 3.3 Typical Mossbauer Spectra: (a) ^{119}Sn spectrum of $Fe(CO)_2CpSnCl_3bipy$

(b) ^{57}Fe spectrum of $Fe(CO)_2CpSnCl_3bipy$

Table 3.2

^{119}Sn Mossbauer Parameters for Six Coordinate Sn-Metal Compounds and Related Compounds*

	Compound	C.S.	Q.S.	Γave	Ref.
1.	cis-$Mn(CO)_5SnCl(AcAc)_2$	1.11	1.49	1.06	a.
2.	cis-$Mn(CO)_5SnCl(oxin)_2$	1.05	1.33	1.04	a.
3.	fac-$Mn(CO)_5SnCl_3bipy$	1.40	1.24	0.94	a.
4.	fac-$Mn(CO)_5SnCl_3phen$	1.35	1.20	0.99	a.
5.	fac-$Mn(CO)_4Ph_3PSnCl_3bipy$	1.51	1.33	1.01	a.
6.	fac-$Mn(CO)_4Ph_3PSnCl_3phen \cdot C_6H_6$	1.52	1.33	1.01	a.
7.	cis-$Mn(CO)_5SnPh(AcAc)_2$	0.95	1.72	1.07	a.
8.	trans-$Mn(CO)_5SnPhCl_2phen$	1.70	3.25	1.28	a.
9.	fac-$Fe(CO)_2cpSnCl_3phen \cdot C_6H_6$	1.47(0.35)	1.29(1.71)	1.05(0.31)	a.
10.	fac-$Fe(CO)_2cpSnCl_3bipy$	1.53(0.35)	1.43(1.70)	1.01(0.27)	a.
11.	cis-$Fe(CO)_2cpSnCl(oxin)_2$	1.14(0.34)	1.31(1.65)	1.00(0.30)	a.
12.	cis-$Mo(CO)_3cpSnCl(oxin)_2$	1.10	1.27	1.01	a.
13.	$Mn(CO)_5SnCl_3$	1.65	1.60		b.
14.	$Mn(CO)_4Ph_3PSnCl_3$	1.70	1.69		a.
15.	$Fe(CO)_2cpSnCl_3$	1.75(0.32)	1.83(1.80)		b.
16.	$Mo(CO)_3cpSnCl_3$	1.69	1.71		c.
17.	$PhSnCl_3bipy$	0.87	1.50		d.
18.	$PhSnCl(AcAc)_2$	0.61	1.78		e.
19.	$Ph_2Sn(AcAc)_2$	0.71	2.07		e.
20.	$PhSnCl(oxin)_2$	0.67	1.48		f.

* At 110°. Units are mm s^{-1}. Values in bracket are for ^{57}Fe. Errors are ± 0.02 mm s^{-1}

a) This work b) ref. 4 c) ref. 6 d) F.P. Mullins, Can.J.Chem. 48,1677(1970).

e) ref. 20 f) ref. 21.

The EFG expressions for structures I, III and IV are given in Table 3.3. Using previously derived $\{L\}^{oct}$ values (mm s^{-1}) for AcAc/2 (-0.03[20]), bipy/2(-0.08[8]), phen/2 (-0.04[8]), oxin/2(-0.05[27]), ph(-0.95[8]) and Cl(0.00[8]), we can now derive $\{M\}^{oct}$ values (Table 3.4) from the quadrupole splittings in Table 3.2. To provide the overall best $\{M\}^{oct}$ values, averaged $\{M\}^{oct}$ values are calculated except for those determined from oxin compounds (except for compound 12 of course). The Q S values for $R_2Sn(oxin)_2$ compounds[21] vary over a wide range, and the {oxin} value seems less well defined than the other values. For $Mn(CO)_5$, the $\{Mn(CO)_5\}^{oct}$ values (mm s^{-1}) derived from compounds 1,2,3,4,7 and 8 (assuming the fac structure for compounds 3 and 4) are -0.76, -0.69, -0.70, -0.64, -0.73 and -0.71 respectively giving an average value of -0.71 ± 0.03 mm s^{-1}. Considering the wide variation in structure and bonding about the Sn in these six compounds, the consistency of these values is satisfactory. For example, the $\{Mn(CO)_5\}^{oct}$ values derived from compounds 7 and 8 with electropositive Ph groups are very similar to those derived from the halide compounds.

If structure IV is taken for the phen and bipy $MSnCl_3$ adducts, the $\{Mn(CO)_5\}^{oct}$ value derived from the Q.S. for compounds 3 and 4 are both -0.58 mm s^{-1}, very much smaller than the -0.71 average given above. The additivity treatment strongly suggests that these adducts all have the fac structure.

In Table 3.4, it is apparent that the $\{L\}^{oct}$ value are all substantially smaller than the $\{L\}^{tet}$ values. The four coordinate {M} values in Table 3.4 were derived from the nearly tetrahedral R_3SnM compounds[4] wherever possible. Since a Q.S has not been resolved for $Ph_3SnMn(CO)_4$-PPh_3, a $\{Mn(CO)_4PPh_3\}^{tet}$ value has been derived by plotting the (Q S) of

Table 3.3

EFG Expressions for Structures I, III, and IV

Isomer	EFG Expression
I	$V_{zz}/e = 2[M] - [L] - [R]$
	$V_{yy}/e = 2[R] - [M] - [L]$
	$V_{xx}/e = 2[L] - [R] - [M]$
III ([Cl] = 0)	$V_{zz}/e = 2[M] - 2[L]$
	$V_{yy}/e = [L] - [M]$
	$V_{xx}/e = [L] - [M]$
IV ([Cl] = 0)	$V_{zz}/e = 2[M] + [L]$
	$V_{yy}/e = -[M] - 2[L]$
	$V_{xx}/e = [L] - [M]$

Table 3.4

Derived Octahedral pqs Values along with

Previously Derived Tetrahedral pqs Values

L	$\{L\}^{oct}$	estimator*	$\{L\}^{tet}$	ref.
Cl,Br	0.0	--	0.0	8
I	-0.14	--	-0.17	8
$Mo(CO)_3cp$	-0.66	12	-0.75	a
$Mn(CO)_5$	-0.71	1,3,4,7,8	-0.97	4
$Mn(CO)_4PPh_3$	-0.73	5,6	-1.01	b
$Fe(CO)_2cp$	-0.74	9,11	-1.08	4
Ph	-0.95	ref. 8	-1.26	8
Me	-1.03	ref. 8	-1.37	8

* refer to compounds in Table 3.3

a K.D. Butler, Ph.D. Thesis, University of Western Ontario, 1974.

b By interpolation, see text.

the $MSnCl_3$ compounds (M = $Fe(CO)_2$ cp, $Mn(CO)_5$, $Co(CO)_4$, $Mo(CO)_3$ cp and $Mn(CO)_4PPh_3$) versus the known $\{M\}^{tet}$ values. The interpolated $\{Mn(CO)_4PPh_3\}^{tet}$ values ~~is -1.01~~ mm s^{-1}. The smaller $\{M\}^{oct}$ values are entirely consistent with previous predictions based on a molecular orbital treatment[8] in which the pqs values can be approximated by:

$$\{L\}^{tet} = -|\tfrac{1}{2} e^2Q| \tfrac{3}{10} < r^{-3} >_p \sigma^{tet} \qquad (3.4)$$

$$\{L\}^{oct} = -|\tfrac{1}{2} e^2Q| \tfrac{1}{5} < r^{-3} >_p \sigma^{oct} \qquad (3.5)$$

for sp^3 hybridized Sn^{IV}, and d^2sp^3 (or sp) hybridized Sn respectively. In these expressions, the σ parameters describe the involvement of the tin hybrid in the M-Sn bond. As the donor properties of M increase, σ increases. Taking the ratio of the two expressions above, $\{L\}^{oct}/\{L\}^{tet} = 0.67(\sigma^{oct}/\sigma^{tet})$. Provided that $\sigma^{oct} \sim \sigma^{tet}$, the ratio of $\{L\}$ values should be close to 0.67, assuming that the $<r^{-3}>_p$ are the same.

The ratio of the $\{L\}$ values in Table 3.4 is always close to 0.75, and a regression of $\{L\}^{oct}$ versus $\{L\}^{tet}$ (Figure 3.4) gives a good linear plot with the equation:

$$\{L\}^{oct} = 0.75\ \{L\}^{tet} + 0.01(\text{mm s}^{-1}) \qquad (3.6)$$

The intercept is very close to 0.00 mm s^{-1} as it should be, and the r value (0.991) shows that this is a very good correlation. The slope of 0.75 is slightly larger than the value of 0.67 for equal σ values. The value of 0.75 could be due to σ^{oct} being larger than σ^{tet}. Another possible reason for the larger ratio is that the $\{L\}^{tet}$ values were derived from R_3SnX(Ph, alkyl) and R_3SnM (M = $Mn(CO)_5$, cp, $Mo(CO)_3$ cp)

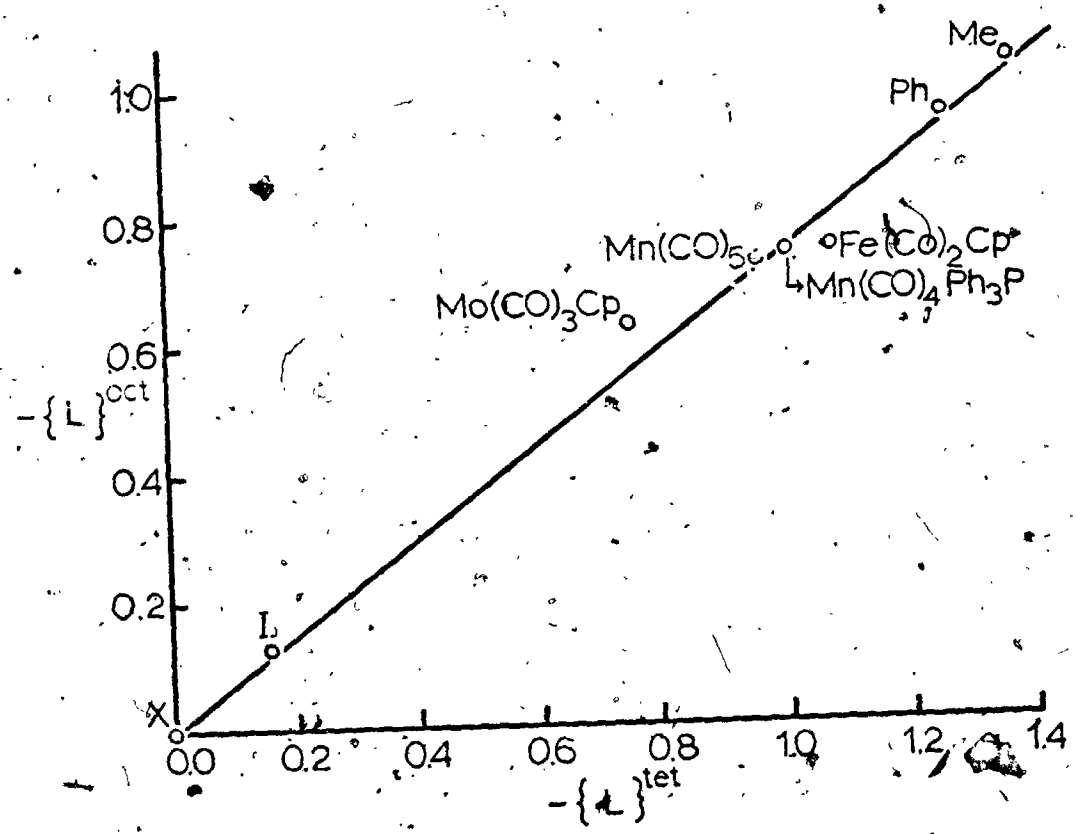

Figure 3.4

Plot of $\{L\}^{oct}$ vs. $\{L\}^{tet}$ for Seven Ligands

compounds in which the S character in the SnR or SnM bond respectively is slightly greater than that expected on the basis of sp^3 hybridization. This greater S character makes the $\{L\}^{tet}$ values less negative than expected, resulting in an increase in $\{L\}^{oct}/\{L\}^{tet}$. A similar effect could take place to decrease $|\{L\}^{oct}|$, but this effect should be smaller. The very large structural distortions possible in tetrahedral compounds compared to octahedral compounds is consistent with this argument.

It is interesting to note that the order of $\{M\}^{oct}$ values is identical to the order of $\{M\}^{tet}$ values. The relative bonding properties of the metal moieties are the same in six and four coordination, and the bonding properties of two metal moieties are consistently different. Thus, as in four coordination, the p donor ability increases in the order:

$$I < X < < Mo(CO)_3\ cp < Mn(CO)_5 < Mn(CO)_4PPh_3 < Fe(CO)_2\ cp < Ph < Me$$

Parish et al[6] have recently reported $|\{L\}^{tet}|$ values for metal moieties which are significantly smaller than the values in Table 3:4. For example, the metal {M} values derived from the nearly tetrahedral $Bu_3SnFe(CO)_2$ cp and $Me_3SnMn(CO)_5$[4] are -1.08 mm s^{-1} and -0.97 mm s^{-1} respectively, while those derived[6] from $Fe(CO)_2$ $cpSnCl_3$ and $Mn(CO)_5SnCl_3$ are -0.95 mm s^{-1} and -0.83 mm s^{-1} respectively[6]. As has been pointed out[19], this variation is largely due to the increase in S character in the Sn-M bond from the $MSnR_3$ compounds to the $MSnCl_3$ compounds. Since the derivation of $\{L\}^{tet}$ (eq. 3.4) refers to sp^3 hybridization, for the purpose of comparing pqs for different coordinations, it seems more reasonable to determine the $\{L\}^{tet}$ values from structures closest to

tetrahedral whenever possible. Variations in $\{L\}^{tet}$ values can often then be discussed[19] on the basis of varying S character in the Sn-M bond. If Parish's $\{L\}^{tet}$ values are used for a similar regression analysis, then the slope of the line becomes 0.77. This larger value is consistent with the argument that there is more S character in the Sn-M bond in $MSnCl_3$ than in $MSnR_3$.

Besides the apparent interpretive advantages, $\{L\}^{tet}$ values (Table 3.4) usually give significantly better agreement between the predicted and observed Q S[22] than those derived from $MSnCl_3$. Thus for 32 dihalide compounds M_2SnX_2, $RMSnX_2$ and $MM'SnX_2$ (R = Me, Ph, M,M' = $Cr(CO)_3$ cp, $Mo(CO)_3$ cp, $W(CO)_3$ cp, $Mn(CO)_5$, $Co(CO)_4$, $Fe(CO)_2$ cp; X = Cl, Br, I), a plot of predicted versus observed QS gives a slope of 0.83 and r = 0.92, using $\{L\}^{tet}$ values derived from R_3SnM compounds. Parish's values, however, give the slope and r value of 0.72 and 0.78 respectively. For 67 organometallic Sn compounds, the correlation coefficient is 0.98 in both cases, but the slope of 1.01 obtained from values in Table 3.4 is significantly lower than 1.07, using Parish's values. For overall additive treatment of Q S, $\{L\}^{tet}$ values derived from less distorted structures seem to be better working values than those derived from $MSnCl_3$[6].

D. Centre Shifts and Bonding

The centre shifts of all the compounds given in Table 3.4 are smaller than those of the corresponding four coordinate structures. Several other features arise from these CS values. First, in contrast to Q S, and in agreement with the four coordinate results, the CS of metal-tin compounds are larger than those of the corresponding organotin compounds. For example, the CS and QS for $PhSnCl(AcAc)_2$ are 0.61 and

1.78 mm s^{-1} respectively; whereas those for $Mn(CO)_5SnCl(AcAc)_2$ are 1.11 and 1.49 mm s^{-1} respectively. This indicates that the Sn-M bond contains more S character than the Sn-R bond. Second, the CS always increases in the order, $MSnClL_4 < MSnCl_3L'_2 < MSnCl_3$ (L = O donors L' = N donors). A similar trend has been observed for organotin analogues. This would suggest that nitrogen containing ligands are always better donors than oxygen and chloride ligands. This is in general consistent with the pqs assigned to these ligands[8]. Finally the smaller CS in <u>cis</u> $Mn(CO)_5SnPh(AcAc)_2$ than that in <u>trans</u> $Mn(CO)_5SnPhCl_2$phen is consistent with previous observations[20].

It is now possible to compare the S character in the Sn-L bond in the following order,

$$Cl, Br << Ph \leq Me < Mn(CO)_5 \leq Mo(CO)_3\ cp$$

$$< Mn(CO)_4\ PPh_3 \leq Fe(CO)_2\ cp$$

This order is established by directly comparing CS of the compounds (Table 3.4). It is obvious that this order is identical to that derived for four coordinate compounds. Thus, the arguments used to establish the S character series for four coordinate compounds are entirely satisfactory for the six coordinate analogues[4]. The difference in P donor strength and CS character between a R-Sn and a M-Sn bond is now clear, since results from two different structural types come to the same conclusion.

E. Experimental

The compounds in Table 3.5 were prepared for the first time.

Table 3.5

Analytical Data for New Sn-Metal Bond Compounds

	Compound	m.p.	Obs. C	Obs. H	Cal. C	Cal. H
1.	cis-$Mn(CO)_5SnCl(AcAc)_2$	128-130	32.90	2.58	32.99	2.50
2.	cis-$Mn(CO)_5SnCl(oxin)_2$	122(d)	45.18	2.31	43.34	1.90
3.	fac-$Mn(CO)_5SnCl_3bipy$	134-135(d)	31.27	1.40	31.29	1.35
4.	fac-$Mn(CO)_5SnCl_3phen$	152-154(d)	34.40	1.24	33.19	1.31
5.	fac-$Mn(CO)_4PPh_3SnCl_3bipy$	120-122(d)	48.56	3.13	47.40	2.86
6.	fac-$Mn(CO)_4PPh_3SnCl_3phen \cdot C_6H_6$	126-128(d)	52.37	3.14	52.64	3.20
7.	cis-$Mn(CO)_5SnPh(AcAc)_2$	141(d)	42.82	3.25	45.31	2.38
8.	trans-$Mn(CO)_5SnPhCl_2phen$	139-140(d)	42.90	1.88	43.04	2.04
9.	fac-$Fe(CO)_2^{cp}SnCl_3 \cdot phen \cdot C_6H_6$	141-142	45.72	2.95	45.47	2.90

TlL (L = acetylacetonate (AcAc) or 8-hydroxyquinolinate (oxin)) and the four coordinate M-Sn precursors were prepared by previously published methods[23, 24, 25]. Compounds 1, 2 and 7 were prepared by reacting $Mn(CO)_5$-$SnCl_3$ or $PhCl_2SnMn(CO)_5$ with the appropriate TlL. The white precipitates of TlCl were discarded and the filtrates were evaporated to dryness. The crude products were recrystallized in n-hexane. The yields were about 40%. The products are slightly light sensitive and decompose in air. The bipyridyl (bipy) and phenanthroline (phen) adducts were obtained by pipetting benzene solutions of the ligand into the benzene solution of the corresponding $MSnCl_3$ or $PhCl_2SnM$[M = $Mn(CO)_5$, $Mn(CO)_4PPh_3$, $Fe(CO)_2$ cp]. Precipitates formed immediately. The solids were washed with benzene and then centrifuged. The yield was not less than 90%. These adducts are slightly soluble in nonpolar solvents, but moderately soluble in acetone.

The melting points and chemical analyses of the new compounds are listed in Table 3.5. Satisfactory purity was not obtained for two compounds (2 and 7) which decompose readily on standing at room temperature. However, Mössbauer spectra gave narrow lines for these compounds. In some cases, chathrated benzene molecules were present (compounds 6 and 9), as has been found previously for six coordinate Sn-Co derivatives. Representative preparations are described below.

<u>$Mn(CO_5)SnCl(C_5H_7O_2)_2$</u> - A benzene suspension of Tl $C_5H_7O_2$ was prepared from 0.617 gm of Tl $C_3H_7O_2$ and 20 ml freshly distilled benzene. To the above solution, a benzene solution of 0.465 gm $Mn(CO)_5SnCl_3$ in 10 ml benzene was added. The reaction mixture was stirred at room temperature for an hour. The white precipitate (TlCl) were discarded. The filtrate was evaporated to dryness under vacuum, then

extracted with refluxing n-hexane. The n-hexane solution was concentrated and left in the refrigerator overnight. White crystals were collected and the yield was about 0.22 g.

<u>$Mn(CO)_5SnCl_3.C_{12}H_8N_2$</u> - A benzene solution (10 ml) containing 0.1068 gm of 1, 10-phenanthroline was added dropwise to a stirring benzene solution of 0.249 g $Mn(CO)_5SnCl_3$ in a centrifugal tube. The shining yellow solid formed immediately was washed with dried benzene and centrifuged 0.29 gm of the pure product was obtained.

Other previously prepared six coordinate compounds were characterized by their melting points and infrared CO stretching frequencies.

Mössbauer spectra were recorded at 110K° as described in Chapter 1.

Infrared spectra of nujol mulls were taken using a Perkin-Elmer 621 spectrometer.

F. References

1. E. H. Brook and R. J. Cross, Organomet. Chem. Rev. (A), 227, 6, (1970).

2. D. J. Patmore and W. A. G. Graham, Inorg. Chem. 1879, 6, (1967).

3. F. Bonati and G. Minghetti, J. Organomet. Chem. 332, 16, (1969).

4. G. M. Bancroft, K. D. Butler, A. T. Rake and B. Dale, J.C.S. (Dalton), 2025, (1972), and references.

5. G. M. Bancroft and K. D. Butler, J.C.S. (Dalton), 1694, (1973).

6. R. J. Dickinson, R. V. Parish, P. J. Rowbotham, A. R. Manning and P. Hackett J.C.S. (Dalton), 425, (1975).

7. R. C. Poller, Chemistry of Organotin Compounds, Academic Press, N.Y. (1970).

8. M. G. Clark, A. G. Maddock, and R. H. Platt, J.C.S. (Dalton) 281, (1972).

9. K. Kawasaki, R. Veeda, T. Tanaka, and R. Okwara, J. Oraanomet. Chem. 5, 194, (1966).

10. G. M. Bancroft and T. K. Sham, unpublished results.

11. D. Blake, G. E. Coates and J. M. Tate, J. Chem. Soc., 756, (1961).

12. J. E. Ferguson, W. R. Roper and C. J. Wilkins, J. Chem. Soc., 3716, (1965).

13. F. A. Cotton andC. S. Kraihanzel, J. Am. Chem. Soc., 4432, 84, (1962).

14. W. A. G. Graham, Inorg. Chem., 7, 315 (1968).

15. L. M. Haines and M. H. B. Stiddard, Adv. Inorg. Chem. Radiochem., 12, 53, (1969).

16. N. Serpone and K. A. Hersh, Inorg. Chem. 2901, 13, (1974).

17. P. G. Harrison, T. J. King and J. A. Richards, J. Chem. Soc. (Dalton) 1723, (1974).

18. W. Jetz, P. B. Simons, J. A. J. Thompson and W. A. G. Graham, Inorg. Chem., 5, 2271, (1966).

19. G. M. Bancroft and A. T. Rake, Inorganica Chimica Acta, 13, 175 (1975).

20. G. M. Bancroft and T. K. Sham, Can. J. Chem., 52, 1361 (1974).

21. G. M. Bancroft and R. H. Platt, Adv. Inorg. Chem. Radiochem., 15, 59, (1972).

22. G. M. Bancroft and K. D. Butler, Inorganica Chimica Acta, in press.

23. W. H. Nelson and D. F. Martin, J. Inorg. Nucl. Chem., 27, 87, (1965).

24. R. D. Gorsich, J. Am. Chem. Soc., 84, 2456 (1962).

25. F. Bonati and G. Wilkinson, J. Chem. Soc., 179, (1964).

Chapter 4

Preparation and Mössbauer Studies of Five Coordinate Organotin (IV) Acetylacetonates: X-Ray Structure of (1,3-Diphenyl-1,3-Propanedionato) Triphenyl Tin (IV)

A. Introduction

It is shown in Chapter 3 that Mössbauer quadrupole splittings for four, and six coordinate tin compounds are best described in terms of partial quadrupole splittings (pqs) derived on the basis of the molecular orbital additive model[1]. It would appear that the same treatment should be applicable to the five coordinate tin structures. The ρ value[2], (QS/CS), and the additive treatment[1] have been used to distinguish between five coordinate isomers[3,4]. However, as Clark et al[5] have pointed out, the five coordinate quadrupole splitting treatment has been hindered by the paucity of structural data as well as the necessity of assigning partial quadrupole splittings to both axial and equatorial groups.

Relatively little structural information has been available[6] for five coordination organotin (IV) compounds in spite of the fact that a large number of these compounds[7] have been synthesized. Thus, X-ray structures are known for just seven monomeric five coordinate compounds: $Me_3SnCl(C_6H_5N)$[8], $[Me_2SnCl_3]^-$[9], $[Me_2SnCl_2]^-$[10],

$Me_3SnNO_3.H_2O$[11], $Me_3SnCH_3COCH_2PPh_3$[12], $Me_2SnCl(S_2CN(Me)_2)$[13] and $Ph_3SnONPhCOPh$[14], where Me = CH_3 and Ph = C_6H_5. In the above structures, all the methyl compounds have the equatorial configuration, whereas $Ph_3SnONPhCoPh$, which has two equatorial C-Sn bonds and an apical C-Sn bond, has the less common all -cis structure. Correspondingly, the methyl compounds have quadrupole splittings[2] in a region of ~3.3 mm s^{-1} ($\pm$ 0.04), where as $Ph_3SnONPhCoPh$ has a quadrupole splitting of -1.94 mm s^{-1}[14].

With two objectives in mind; first, to prepare new five coordinate isomers with β-diketonates; and second, to assign structures from their quadrupole splittings, a series of five coordinate compounds of triorgano β-diketonates of the type Me_3SnL_2 and Ph_3SnL_2 [L_2 = anions of acetylacetone (AcAc), benzoylacetone (BzAc) and dibenzoylmethane (BzBz)] has been prepared and characterized. A related compound, $Ph_2SnClBzBz$ has also been studied. The X-ray crystal study confirms that $Ph_3SnBzBz$ has the all -cis configuration. The Mössbauer quadrupole splittings for the triphenyl compounds are consistent with this structure and strongly suggest that $Ph_2SnClBzBz$ has the equatorial structure and that trimethyl compounds have the unknown mer structure.

B. Preparation and Spectroscopic Studies

All the five coordinate compounds discussed in this Chapter were prepared by use of the thallium salt method[15,16,17], which has been described in the previous two chapters. The products were formed very smoothly via the following reaction.

Table 4.1 Melting points, analyses, proton nmr and infrared data for five coordinate acetylacetonates.

Compound	M.P., °C	Analyses, % calc (found) C	H	τ	$^2J_{^{119}Sn-CH_3}$ (Hz)	ν_{Sn-C} (cm^{-1})
$Me_3SnAcAc$	176-177	36.03 (36.50)	4.99 (5.08)	9.6[illegible]	60.8	574m, 556s
$Me_3SnBzAc$	126-128	(48.05) 56.70	(5.58) 5.22	9.62	60.5	589m, 550s
$Me_3SnBzBz$	164d	56.66 (55.86)	4.69 (4.94)	9.62	59.2	585w, 548w
$Ph_3SnAcAc$	98-100d	58.95 (61.4)	4.42 (4.45)			
$Ph_3SnBzAc$	63-65	65.52 (65.79)	4.67 (4.73)			
$Ph_3SnBzBz$	135-136	68.38 (69.12)	4.47 (4.57)			
$Ph_2SnClBzBz$	147-149	61.00 (60.92)	3.9 (4.03)			

$$R_3SnCl + TlL_2 \xrightarrow[\text{atm.}]{N_2} R_3SnL_2 + TlCl\downarrow \qquad (4.1)$$

where R = CH_3, C_6H_5; L_2 = β-diketonates.

The white thallium chloride precipitated immediately and the desired product was subsequently obtained from the solution.

The analyses, colour, melting points; along with nmr parameters and infrared ν_{Sn-C} bands for methyl compounds are given in Table 4.1. All trimethyl compounds tended to disproportionate both in solution and in the solid state. While $Me_3SnAcAc$ and $Me_3SnBzBz$ were stable for several weeks, $Me_3SnBzAc$ tended to disproportionate rapidly, i.e.

$$2Me_3SnBzAc \rightarrow Me_2Sn(BzAc)_2 + Me_4Sn$$

This was proved in solution by the presence of Me_4Sn (τ = 9.9, $^2J_{^{119}Sn-CH_3}$ = 54 Hz) in a benzene solution shortly after preparation. Thus, a good elemental analysis could not be obtained for $Me_3SnBzAc$ due to its instability. Similar disproportionation reactions have been found for Me_3Sn oxin[18] and $Cl_3SnAcAc$[19]. No Me_4Sn signal was detected in the nmr spectra of $Me_3SnAcAc$ and $Me_3SnBzBz$ shortly after preparation; but their nmr spectra taken three months after preparation were very similar to the corresponding diorgaontin analogues[20]. The triphenyl compounds are more stable than the trimethyl compounds, although a really satisfactory analysis could not be obtained for $Ph_3SnAcAc$.

The infrared spectra of these compounds are very similar to those of their corresponding six coordinate diorgano analogues[21]. For the trimethyl compounds, however, the multiple infrared Sn-C frequencies show that the three Me groups are not in equivalent positions in the solid state and that the two oxygens are not in axial positions. In contrast, trimethyl tin compounds with C_{3v} symmetry have only one Sn-C frequency characteristic of the three Me groups.

The n.m.r. chemical shifts and the coupling constants $^{2}J_{^{119}Sn-CH_3}$ for the trimethyl compounds (Table 4.1) are characteristic of five coordinate trimethyl species such as $Me_3SnBr(Ph_3PO)$ ($^{2}J_{^{119}Sn-CH_3}$ = 66 Hz)[22]. The fact that the three non equivalent methyls in trimethyl tin compounds (presumably, two axial, and one equatorial; or two equatorial and one axial) have only one resonance signal is not surprising; since similar one peak resonance has been observed for $Me_3Sn(oxin)$[18] and other trimethyl Sn cations[22]. This is probably due to rapid intramolecular interconversion or intermolecular interconversion processes similar to those described by Serpone et al[23]. The three possible configurations for R_3SnL_2 compounds are:

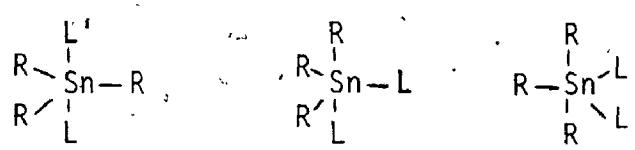

I II III

where structures I, II, and III are denoted equatorial, all-cis, and mer structures respectively. When L_2 acts as a chelating ligand,

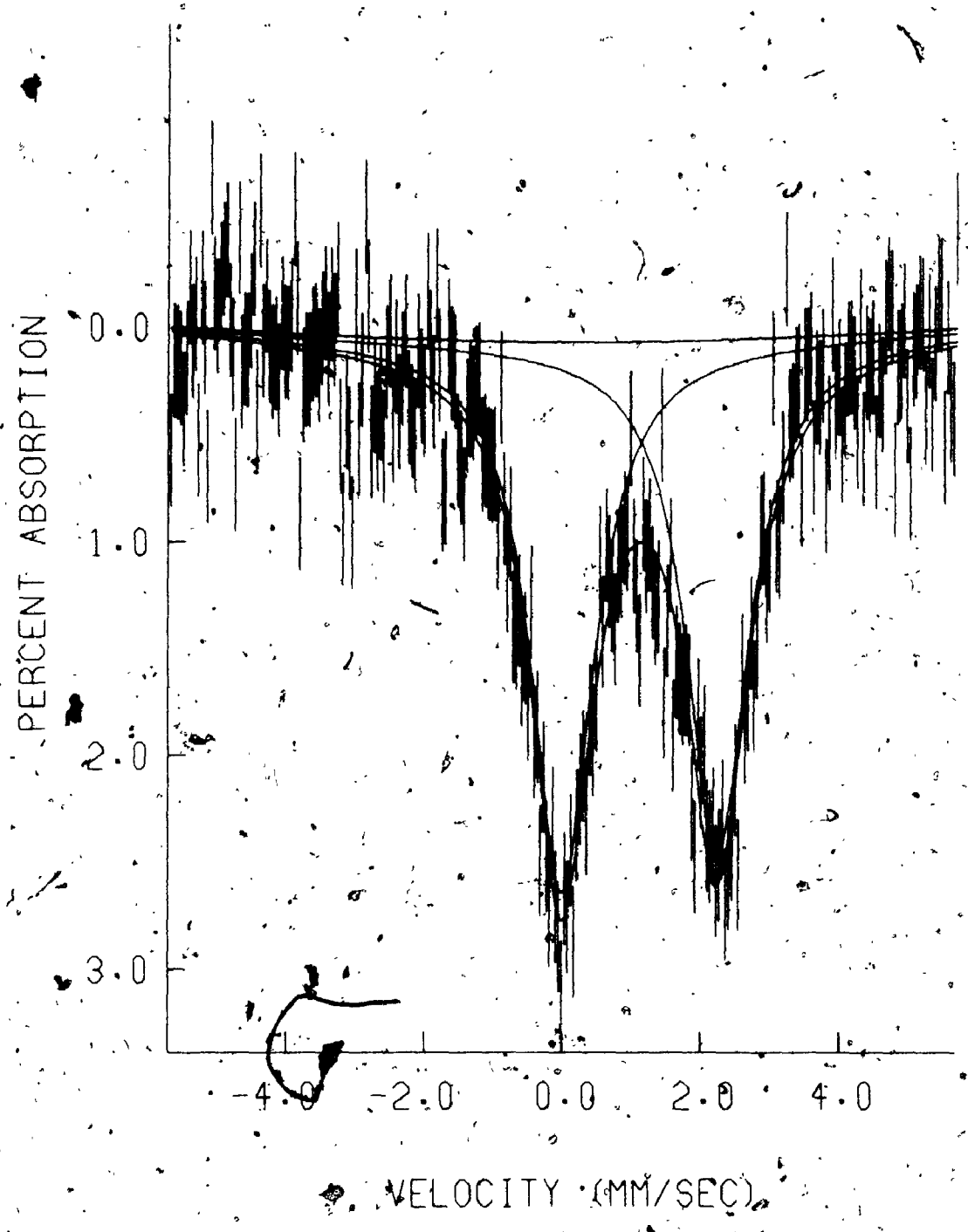

Figure 4.1 Mössbauer Spectrum of Ph_3SnO_2Bz

Table 4.2

Mössbauer Parameters (mm s^{-1} at 110K)[†]

Compound	CS	QS	Ref.
$Me_3SnAcAc$	1.21	3.81	a
$Me_3SnBzAc$	1.13	3.69	a
$Me_3SnBzBz$	1.15	3.86	a
$Me_2Sn(AcAc)_2$	1.16	4.02	a
$Me_2Sn(BzAc)_2$	1.06	3.87	a
$Me_2Sn(BzBz)_2$	1.18	4.08	a
Me_4Sn	1.31	0	b
$Ph_3SnAcAc$	1.09	1.38	a
$Ph_3SnBzAc$	1.08	2.25	a
$Ph_3SnBzBz$	1.13	2.25	a
$Ph_2Sn(AcAc)_2$	0.71	2.07	a
$Ph_2Sn(BzAc)_2$	0.73	2.23	a
$Ph_2Sn(BzBz)_2$	0.73	2.15	a
Ph_4Sn	1.22	0	b
$Ph_2SnClBzBz$	1.11	2.61	a

[†]Errors are ± 0.02 mm s^{-1}. Line widths are 1.10 ± 0.10 mm s^{-1}.

χ^2 values for all spectra are 005 ± 40 for ~500 degrees of freedom.

a. This work. b. References 1, Table 4.2

the mer structure can be achieved by either a monomer as III or a dimer in which L_2 bridges two R_3Sn moieties. It is reasonable to rule out the dimer; since the structural data for $Me_2Sn(AcAc)_2$, $Cl_2Sn(AcAc)_2$[24], and $Ph_3SnBzBz$ reported in this study indicate that the diketonates do not act as a bridging ligand. Also the steric requirement of the chelating ligand along with the infrared evidence indicates that structure I is very unlikely. Hence structures II and III are possible isomers of these compounds.

Mössbauer parameters for the triorganotin β diketonates along with their related species are given in Table 4.2. A spectrum of $Ph_3SnBzBz$ is shown in Fig. 4.1. It is immediately apparent that the trimethyl compounds have much larger quadrupole splittings than those of the triphenyl cpmpounds. Also, the trimethyl compounds have similar quadrupole splittings to their trans dimethyl analogues[20] while the triphenyl compounds have similar quadrupole splittings to the cis diphenyl analogues[20]. These results are readily rationalized if the trimethyl compounds have the mer structure and triphenyl compounds have the all -cis structure. To illustrate this, a rough calculation of quadrupole splittings for these species has been performed. In Table 4.3, assuming[25] that the axial and equatorial ligands have the same partial field gradients (or partial quadrupole splittings) and that the five coordinate partial quadrupole splittings are given by the octahedral values ({Me} = - 1.03 mm s^{-1}, {Ph} = -0.95 mm s^{-1}) and {L} = 0, we calculate quadrupole splittings for structures of interest (Table 4.3, structures I to V). The results in Table 4.3 show that these calculations are entirely consistent with the splittings observed if the trimethyl and the triphenyl compounds are assigned

Table 4.3

EFG Components and Predicted Quadrupole Splittings

for Five and Six Coordinate Isomers

	Species	EFG Components	Me compound*	Ph compound*
I	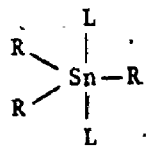	$V_{zz}/e = 4[L] - 3[R]$ $\eta = 0$	-3.09	-2.85
II	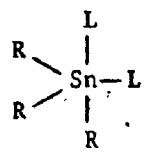	$V_{11}/e = -\frac{3}{2}[R] + [L]$ $V_{22}/e = +\frac{3}{2}[R] - 2[L]$ $V_{33}/e = +[L]$	1.78 (η=1)	1.65 (η=1)
III	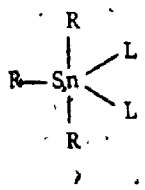	$V_{11}/e = -\frac{1}{2}[L]$ $V_{22}/e = -3[R] + \frac{5}{2}[L]$ $V_{33}/e = 3[R] - 2[L]$	3.55 (η=1)	3.28 (η=1)
IV	trans-R_2SnL_4	$V_{zz}/e = 4[R] - 4[L]$	+4.12	+3.80
V	cis-R_2SnL_4	$V_{zz}/e = -2[R] + 2[L]$	-2.06	-1.90

*Predicted Quadrupole Splittings for Structures (in mm s^{-1})

the mer and the all -cis configurations respectively. The quadrupole splitting for $Ph_3SnAcAc$ is surprisingly small relative to its analogous compounds, and cannot be rationalized readily. The quadrupole splitting of $Ph_2SnClBzBz$ is consistent with an equatorial structure, since the related species, $Ph_2SnCl_3^-$ has a similar Q S (2.60 $mm\ s^{-1}$). It is interesting to compare a series of phenyltin compounds containing BzBz (Table 4.2). The centre shifts increases as the number of phenyl groups increases. This is, of course, expected since the phenyl group is a good σ donor. The substantial increase in CS and QS from $Ph_2Sn(BzBz)_2$ to $Ph_2SnClBzBz$ can be attributed to the increase in 5S character in the Sn-C bond as well as the increase of C-Sn-C angle as described in Chapter 2. Also, the CS for trimethyl compounds are large compared with the triphenyl series. This result is in good agreement with the S character series[26] derived for four coordinate and six coordinate compounds.

C. The Crystal Structure of (1,3-diphenyl-1,3-propanedionato)-Triphenyl Tin (IV), $Ph_3SnBzBz$.

1. Experimental

Yellow crystals of $Ph_3SnBzBz$ were recrystallized from dry benzene. A crystal was sealed in a capillary tube. A preliminary photographic examination of the zones h(0-2)ℓ, (0-1)kℓ, and hk(0-1) showed the crystals to be monoclinic. Systematic absences of h0ℓ, ℓ = 2n + 1 and 0k0, k = 2n + 1 uniquely identify the space group as $P2_1/c$ (C_{2h}^5, No. 14)[27]. The density was measured by flotation in a mixture of n-pentane and carbon tetrachloride. The observed density

1.46(1) g cm^{-3}, agrees well with the calculated value of 1.440 g cm^{-3} assuming four molecular units in the cell. There are no crystallographic symmetry constraints imposed on the molecule. The unit cell dimensions, a = 13.216(5), b = 9.443(4), c = 22.344(9)A, and β = 109.42(2)^{o}, were determined by a least-squares refinement of the angular settings of 23 reflections with $15<2\theta<31^{o}$, centered on a four circle diffractometer with MoKα_1 radiation (λ = 0.70926A) at a temperature of 21°.

For data collection a crystal of approximate dimensions 0.15 x 0.20 x 0.30 mm was mounted in a Lindemann capillary such that the long dimension, [010], was offset from colinearity with the diffractometer spindle axis. ω-scans of a number of low-angle axial reflections showed an average width of 0.08^{o}, which was considered acceptable[28]. Intensities were recorded on a Picker FACS-1 automatic four-circle diffractometer, using prefiltered (Nb foil, 0.07 mm) MoKα radiation. The take-off angle of 1.6^{o} gave 90% of the maximum Bragg intensity available for a given reflection. The crystal to counter distance was 32.0 cm and the aperture was 4 mm square. All reflections in the range $1.5<2\theta<45^{o}$ in the octants $hk\ell$ and $\bar{h}k\ell$ were collected in 3 shells.

The Miller index range was $-14<h<13$, $0<k<10$, and $0<\ell<24$. The θ-2θ scan technique was used at a scan rate of 1.0^{o} per min, with a scan range of 0.8^{o}, corrected for dispersion. Background counts were made for 10 sec with a stationary crystal and counter at the ends of each scan. Coincidence losses were minimized for strong reflections by employing Cu foil attenuators. Five standard reflections,

(004), (00$\bar{4}$), (200), (43$\bar{1}$), and (020) were recorded at periodic intervals throughout the data collection process, as a check of machine and crystal stability. Only random fluctuations ($\pm$ 2%) in the intensities of all five standards were observed.

A total of 3833 reflections were measured and the recorded intensities were corrected for background, Lorentz and polarization effects. A standard deviation, σ, was assigned to each reflection such that $\sigma(I) = [\text{count} + 1/4(t_c/t_b)^2(b_1 + b_2) + (pI)^2]^{1/2}$ where $I = \text{count} - 1/2(b_1 + b_2)(t_c/t_b)$, count = total count measured in time t_c, and b_1 and b_2 are the background counts each measured in time t_b. The 'ignorance factor', p, was initially chosen as 0.02[29]. A statistical examination of the standard reflection suggested a value of 0.013 was more appropriate. In the final cycle of least-squares refinement p was chosen as 0.014 to give a value close to 1.0 for the error on an observation of unit weight.

Absorption correction trials[30] using $\mu = 9.1\ cm^{-1}$ showed transmission factors ranging from 0.888 to 0.906, a variation of 2%. No absorption correction was made to the data. Of the 3833 observations, 2104 had $I>3\sigma(I)$ and were used in the solution and early refinement of the structure.

2. Structure solution and refinement

The position of the Sn atom was located from a three dimensional Patterson synthesis. Two cycles of least-squares refinement on F, minimizing the function $\Sigma w(|F_o|-|F_c|)/\Sigma|F_o| = 0.259$ and $R_2 = (\Sigma w(|F_o|-|F_o|)^2/\Sigma wF_o^2) = 0.296$. The weight, w, is defined as $w = 4F_o^2/\sigma^2(F_o)^2$.

The atomic scattering factors for neutral Sn, O, and C atoms were taken from Cromer and Waber[31], whilst that for H was taken from Stewart et al[32]. Anomalous dispersion contributions to the real and imaginary parts of the structure factor were included for Sn, the values used being those of Cromer and Liberman[33]. The other 25 non hydrogen atoms were located from a difference fourier synthesis at this stage. Two cycles of refinement with the Sn, the backbone atoms of the propanedionato ligand allowed to vibrate isotropically, and the five phenyl rings defined as rigid groups with D_{6h} symmetry, C-C' = 1.392A [34], led to agreement factors R_1 = 0.063 and R_2 = 0.083. At this stage the non group atoms were assigned anisotropic thermal parameters and the phenyl group C atoms given individual temperature factors. Five more cycles led to agreement factors R_1 = 0.050 and R_2 = 0.061. A difference fourier synthesis revealed no peak exceeding 0.8 e A^{-3} and evidence for the phenyl H atoms and the H atom of the propanedionato ligand was observed. Up to this stage of refinement, those reflections with intensity greater than $3\sigma(I)$ had been employed. In subsequent cycles all reflections with intensities $I > 2\sigma(I)$ were employed. The 'p' value was adjusted to 0.014. Contributions from the phenyl H atoms were calculated assuming an idealized geometry with C-H = 1.00A and B = 4.0A^2. The position of HC(2), the H atom of the propanedionato ligand, was obtained from a difference fourier synthesis and included in the final cycles of refinement, though not refined, with B = 4.0A^2.

The conditions for the final cycle of refinement were

(i) 2328 observed ($>2\sigma(I)$) reflections with p = 0.014 and 115 variables.

(ii) the six non group atoms were allowed to vibrate anisotropically.

(iii) the phenyl ring atoms were refined as groups with individual temperature factors assigned to each carbon atom.

(iv) hydrogen atom contributions from the phenyl H atoms were included in the structure factor calculations.

(v) the position and temperature factor of HC(2) were not refined but included in the last cycle.

Under these conditions, refinement converged at $R_1 = 0.051$ and $R_2 = 0.063$. No evidence for extinction was observed. An examination of the observed and calculated structure factors, in terms of magnitude, $\lambda^{-1}\sin\theta$, indices and diffractometer setting angles (χ and ϕ) showed no unusual trends. A final difference fourier synthesis showed the largest residual peak to be 0.53(16)e A^{-3} at (-0.025, 0.0990, 0.4200), in the vicinity of 3C(5), a phenyl C atom. The standard deviation of an observation of unit weight is 0.99 electrons.

3. Results and Discussion

The structure consists of discrete monomers. The shortest intermolecular distance of approach is 2.42 Å between phenyl ring hydrogen atoms bonded to 1C(5) and 5C(5). The distance (3.80 Å) between phenyl carbon atoms 1C(1) and 2C(3) is the shortest non-hydrogen intermolecular distance.

Final positional parameters for the non-group atoms are given in Table 4.4. Group C atom positions are given in Table 4.5, and derived group hydrogen atoms in Table 4.6. The structure and

Table 4.4

Atomic and Group Positional and Thermal Parameters

Atom	x	y	z	U(1,1) or B	U(2,2)	U(3,3)	U(1,2)	U(1,3)	U(2,3)
Sn	.21697(5)	.35626(7)	.35640(3)	411(4)	414(4)	356(4)	45(4)	113(2)	-20(4)
O(1)	.3598(5)	.2396(8)	.3856(3)	537(41)	746(49)	482(43)	217(39)	-5(36)	-231(38)
O(2)	.2976(6)	.4385(8)	.4568(3)	588(45)	675(45)	422(39)	179(38)	2(36)	-95(37)
C(1)	.4377(7)	.2232(10)	.4382(4)	406(55)	436(55)	410(59)	-111(46)	111(48)	-26(47)
C(2)	.4474(8)	.2914(11)	.4937(4)	455(55)	557(59)	364(56)	18(51)	128(45)	-28(48)
C(3)	.3781(3)	.3962(9)	.5016(5)	428(57)	424(64)	398(55)	-37(45)	101(48)	1(43)
H	.525	.269	.530	4					

Group Parameters

Group	x_g	y_g	z_g	$\delta^{\dagger}$	ε	η
PH(1)	0.2163(3)	0.7153(5)	0.3060(2)	-0.569(10)	-1.991(4)	-2.113(10)
PH(2)	0.1641(3)	0.1993(5)	0.2039(2)	1.595(4)	-2.924(3)	-1.957(4)
PH(3)	0.0274(4)	0.2075(6)	0.4190(2)	-0.025(6)	-2.544(4)	2.280(6)
PH(4)	0.5988(3)	0.0260(5)	0.4269(2)	1.916(6)	2.229(4)	-2.526(6)
PH(5)	0.4119(3)	0.5351(5)	0.6220(2)	-2.165(4)	-2.971(3)	2.062(4)

† δ, ε and η are the group orientation angle in radians as defined in Ref. 27

Table 4.5

Phenyl Group Positional and Thermal Parameters

	x	y	z	B (A^2)
PH(1)				
1C(1)	0.2182(5)	0.5771(5)	0.3281(3)	3.5(2)
1C(2)	0.2384(5)	0.6901(6)	0.3705(2)	4.2(2)
1C(3)	0.2365(6)	0.8283(5)	0.3484(3)	4.9(2)
1C(4)	0.2145(6)	0.8534(5)	0.2839(3)	5.3(2)
1C(5)	0.1943(6)	0.7404(7)	0.2415(2)	5.0(2)
1C(6)	0.1961(6)	0.6023(6)	0.2636(3)	4.2(2)
PH(2)				
2C(1)	0.1855(4)	0.2555(7)	0.2642(2)	3.4(2)
2C(2)	0.0804(4)	0.2244(8)	0.2270(3)	4.4(2)
2C(3)	0.0590(4)	0.1682(8)	0.1665(3)	4.9(2)
2C(4)	0.1428(5)	0.1431(8)	0.1431(2)	5.2(2)
2C(5)	0.2479(4)	0.1742(7)	0.1803(3)	4.1(2)
2C(6)	0.2692(3)	0.2304(7)	0.2409(3)	3.4(2)
PH(3)				
3C(1)	0.1013(5)	0.2680(7)	0.3944(3)	3.7(2)
3C(2)	0.0663(6)	0.3433(6)	0.4375(4)	5.3(2)
3C(3)	-0.0076(7)	0.2828(9)	0.4620(4)	6.9(2)
3C(4)	-0.0469(7)	0.1469(9)	0.4436(4)	6.5(2)
3C(5)	-0.1151(6)	0.0717(7)	0.4005(4)	5.9(2)
3C(6)	0.0624(6)	0.1328(7)	0.3760(3)	4.8(2)
PH(4)				
4C(1)	0.5120(4)	0.1165(6)	0.4334(3)	3.0(2)
4C(2)	0.5037(4)	0.0448(7)	0.3765(2)	4.2(2)
4C(3)	0.5825(5)	-0.0457(7)	0.3700(3)	4.7(2)
4C(4)	0.6777(5)	-0.0646(7)	0.4204(3)	4.9(2)
4C(5)	0.6940(4)	0.0072(7)	0.4773(3)	4.4(2)
4C(6)	0.6151(5)	0.0977(7)	0.4838(2)	3.6(2)
PH(5)				
5C(1)	0.3963(5)	0.4652(6)	0.5648(2)	3.1(2)
5C(2)	0.4831(5)	0.4296(6)	0.6181(3)	3.9(2)
5C(3)	0.4987(5)	0.4995(7)	0.6753(2)	4.7(2)
5C(4)	0.4276(5)	0.6050(7)	0.6792(2)	4.8(2)
5C(5)	0.3407(5)	0.6405(7)	0.6259(3)	4.3(2)
5C(6)	0.3251(4)	0.5706(7)	0.5687(2)	3.9(2)

Table 4.6

Derived Phenyl Hydrogen Atom Positional Parameters

Atom	x	y	z	B(A^2)
H1C(2)	0.2547	0.6724	0.4167	4.0
H1C(3)	0.2512	0.9096	0.3785	4.0
H1C(4)	0.2130	0.9524	0.2677	4.0
H1C(5)	0.1783	0.7580	0.1951	4.0
H1C(6)	0.1818	0.5207	0.2333	4.0
H2C(2)	0.0218	0.2426	0.2436	4.0
H2C(3)	-0.0162	0.1452	0.1397	4.0
H2C(4)	0.1278	0.1017	0.0997	4.0
H2C(5)	0.3082	0.1555	0.1636	4.0
H2C(6)	0.3446	0.2530	0.2675	4.0
H3C(2)	0.0949	0.4409	0.4506	4.0
H3C(3)	-0.0332	0.3385	0.4923	4.0
H3C(4)	-0.1009	0.1056	0.4606	4.0
H3C(5)	-0.0405	-0.0249	0.3872	4.0
H3C(6)	0.0876	0.0775	0.3455	4.0
H4C(2)	0.4351	0.0589	0.3404	4.0
H4C(3)	0.5703	-0.0967	0.3288	4.0
H4C(4)	0.7338	-0.1297	0.4152	4.0
H4C(5)	0.7623	-0.0069	0.5130	4.0
H4C(6)	0.6271	0.1487	0.5246	4.0
H5C(2)	0.5344	0.3548	0.6153	4.0
H5C(3)	0.5608	0.4747	0.7137	4.0
H5C(4)	0.4383	0.6555	0.7203	4.0
H5C(5)	0.2894	0.7164	0.6287	4.0
H5C(6)	0.2630	0.5965	0.5303	4.0

Table 4.7

Selected Bond Distances (Å) and Angles (°)

a) Coordination about Sn

Atom	Distance (Å)	Atom	Angle (°)
Sn-O(2)	2.276(7)	3C(1)-Sn-O(1)	111.0(3)
Sn-O(1)	2.094(7)	3C(1)-Sn-1C(1)	124.1(2)
Sn-3C(1)	2.149(7)	1C(1)-Sn-O(1)	120.1(3)
Sn-2C(1)	2.180(6)	O(2)-Sn-2C(1)	163.7(3)
Sn-1C(1)	2.181(6)	O(2)-Sn-3C(1)	84.5(3)
		O(2)-Sn-O(1)	78.1(3)
		O(2)-Sn-1C(1)	85.0(3)
		2C(1)-Sn-1C(1)	99.3(2)
		2C(1)-Sn-O(1)	86.2(3)
		2C(1)-Sn-3C(1)	105.5(2)

b) The chelating ligand

O(2)-C(3)	1.260(11)	Sn-O(1)-C(1)	135.3(6)
C(3)-C(2)	1.399(13)	O(1)-C(1)-C(2)	125.3(9)
C(2)-C(1)	1.365(13)	C(1)-C(2)-C(3)	125.5(9)
C(1)-O(1)	1.290(11)	C(2)-C(3)-O(2)	122.6(9)
		C(3)-O(2)-Sn	132.1(6)
C(3)-5C(1)	1.499(11)	5C(1)-C(3)-C(2)	121.3(8)
C(1)-4C(1)	1.512(11)	5C(1)-C(3)-O(2)	116.1(8)
		4C(1)-C(1)-O(1)	112.9(8)
C(2)-HC(2)	1.09	4C(1)-C(1)-C(2)	121.8(8)
		C(3)-C(2)-HC(2)	122.3
		C(1)-C(2)-HC(2)	111.3

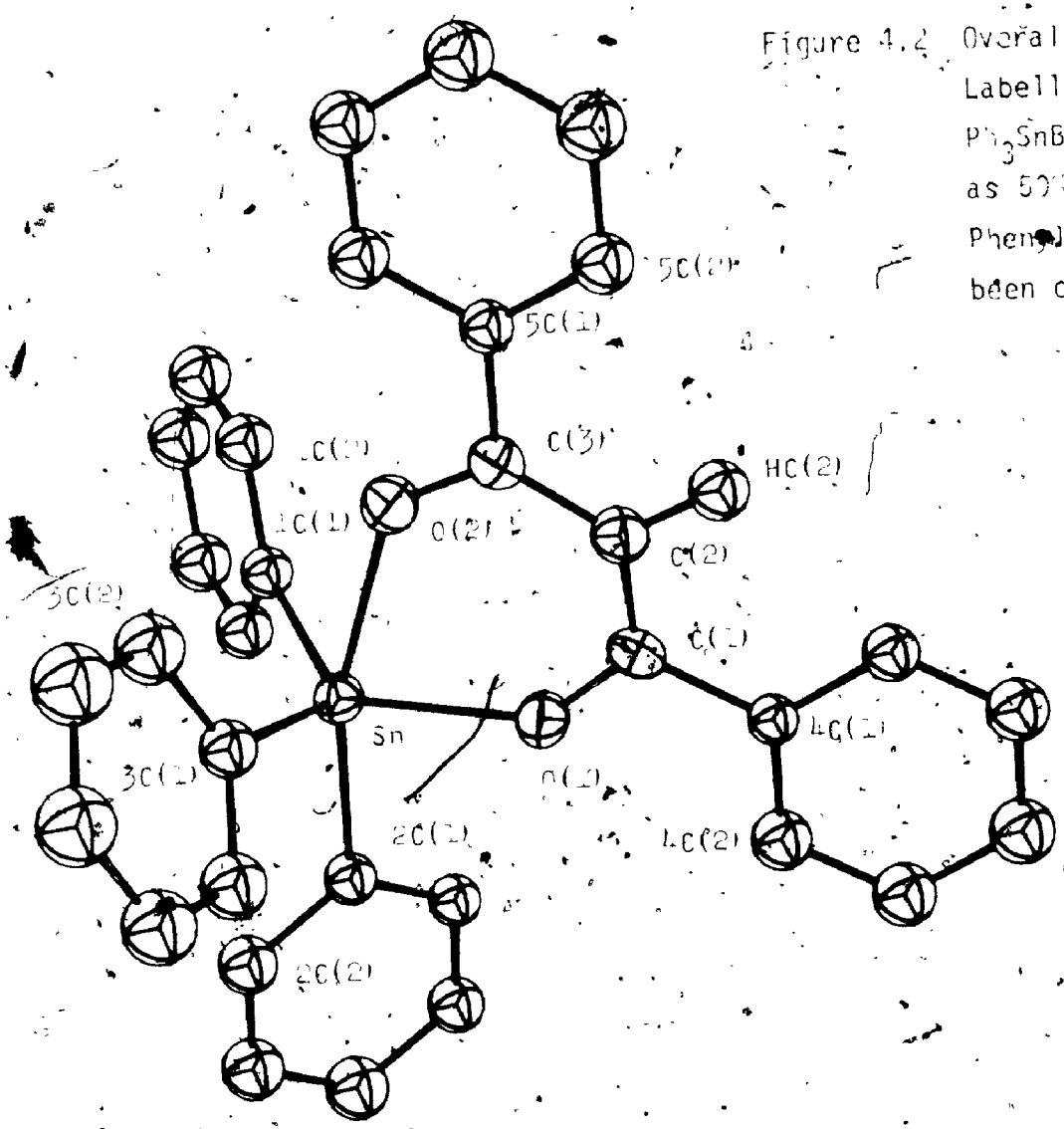

Figure 4.4 Overall View and the Labelling Scheme of $Ph_3SnBzBz$. Atoms are shown as 50% Probability Ellipsoids. Phenyl Ring H Atoms have been omitted.

2 OF/DE 2

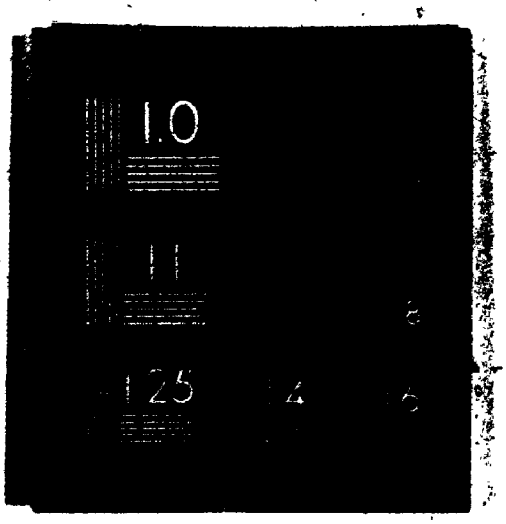

ARC - 274

labelling scheme of the atoms is shown in Figure 4.2. The coordination sphere of Sn, showing relevant bond distances and angles is shown in Figure 4.3. The structure of the chelating ligand is also shown in Figure 4.4. Selected bond distances and angles are given in Table 4.7 and some least-squares planes in Table 4.8.

The coordination about Sn is essentially trigonal bipyrimidal. O(2) and 2C(1) occupy axial positions, while 1C(1), 3C(1) and O(1) occupy equatorial positions (Figure 4.2). The most obvious departure from an ideal geometry is caused by the positions of the chelating oxygen atoms. The axial Sn-O(2) distance is 2.276(7) Å whilst the equatorial Sn-O(1) distance is 2.094(7) Å. These bond distances are significantly different. The axial oxygen-tin-axial phenyl angle, O(2)-Sn-2C(1), is 163.7(3)^{o} - far removed from the expected value of 180°; but equal to the sum of the O(1)-Sn-O(2) angle (78.1^{o}) and O(1)-Sn-2C(1) angle (86.2^{o}). The Sn-C distances to the phenyl rings are Sn-1C(1), 2.181(6); Sn-3C(1), 2.149(7) (both equatorial) and Sn-2C(1), 2.180(6) Å (axial). Although the two Sn-C (equatorial) distances are different, no chemical significance can be attached to this fact. Moreover, it is not conclusive that a lengthening of the Sn-C (axial) bond relative to the Sn-C (equatorial) bond occurs in this structure. However, along with other X-ray evidence [14,35] the difference (0.04 Å) between the axial Sn-C bond and the average equatorial Sn-C bond is probably significant. Details will be discussed in the next chapter.

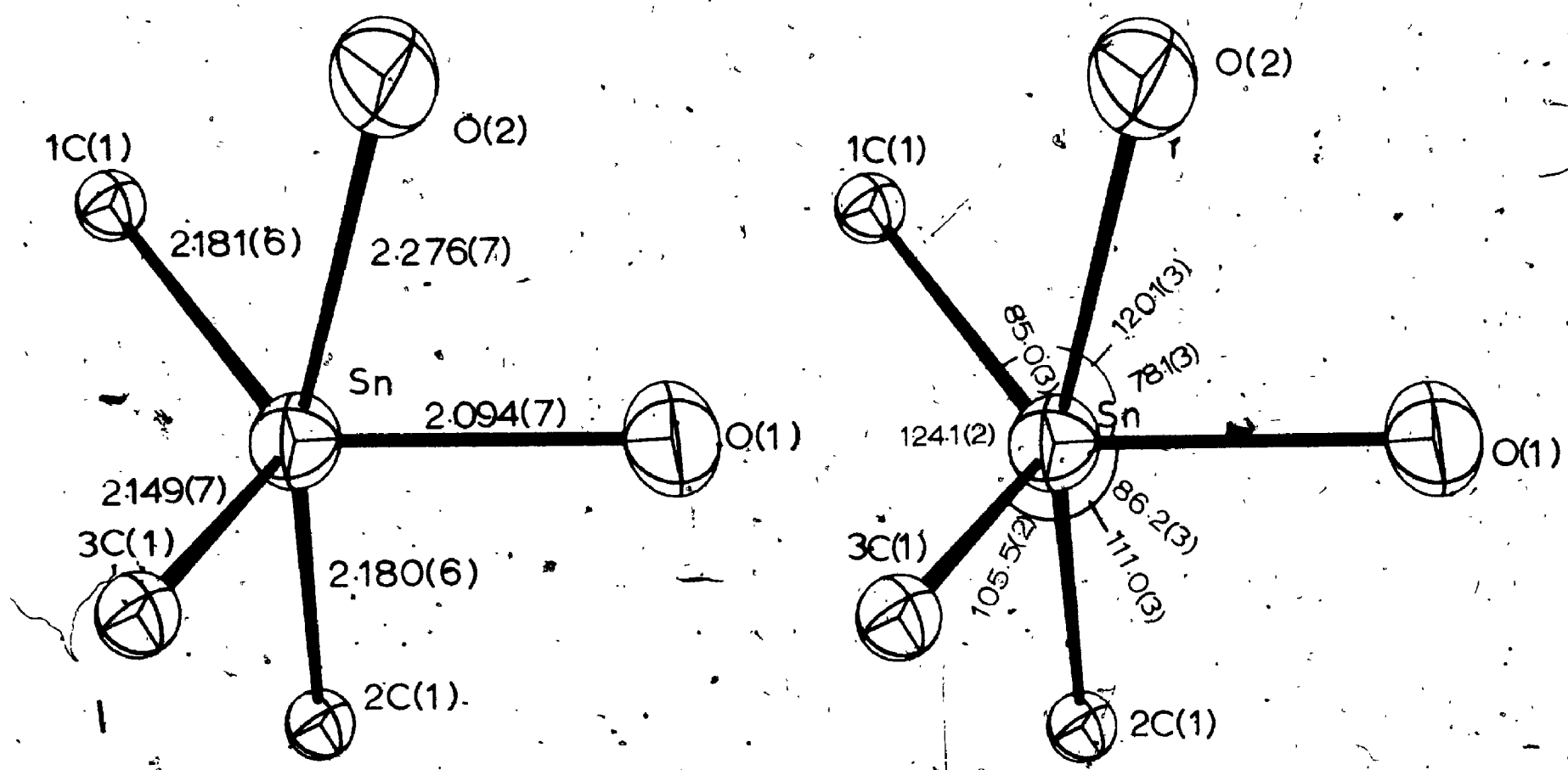

Figure 4.3

Coordination at Sn with Selected Bond Lengths and Bond-Angles

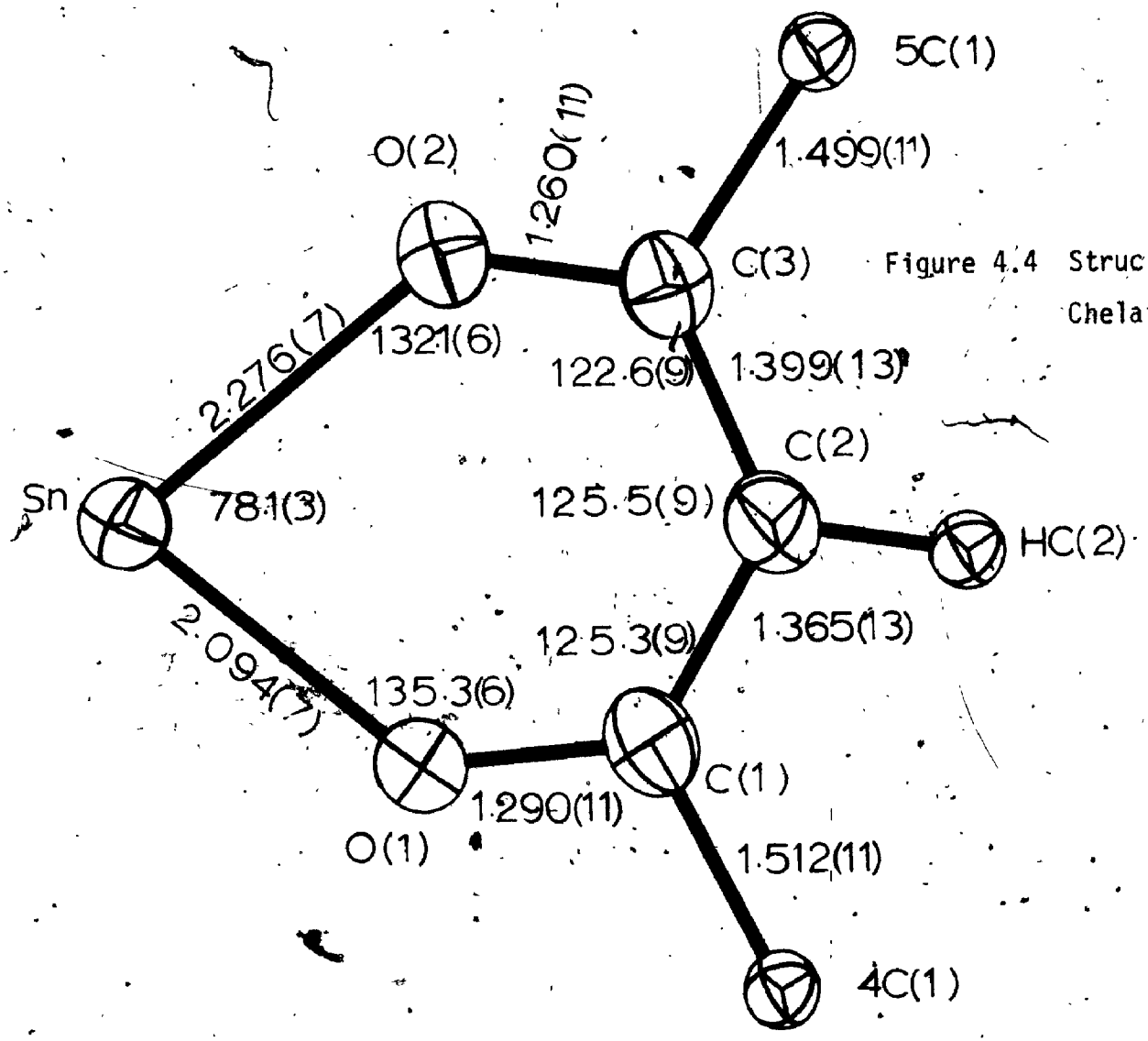

Figure 4.4 Structure of the Chelate Ligand

A series of least-square planes has been calculated and is shown in Table 4.8. The four atoms in the equatorial plane Sn 1C(1), 3C(1), and O(1) are situated such that the Sn atom is below the least-squares plane on the side of the axial phenyl ring, ring 3, by 0.20 A and the other three atoms, O(1), 3C(1) and 1C(1) are, respectively, 0.07, 0.07 and 0.07 A above the plane. A similar situation has been observed in $Ph_3SnPhNOCOPh$[14], whilst in $Me_2SnCl(S_2CNMe_2)$[12], the Sn atom is above the least-squares plane on the side of the axial S linkage. This result is in accord with the argument[37] that the Sn-C bond requires more 5S tin character. Thus, the presence of an axial phenyl group increases the S character in that bond and opens the C(axial)-Sn-C(equatorial) angle.

The bond distances and bond angles found in the 1,3-diphenyl-1,3-propanedionato ligand are comparable with those found in a series of solvated complexes of alkaline earth metals and chelating 1,3-diphenyl-1,3-propane-dione[38-40]. The ligand geometry is also not significantly different from the observed geometry of the uncoordinated ligand in the enolate form[41-42]. The two phenyl substituents, Ring 4 and Ring 5 are approximately coplanar with the plane of the chelating ligand, Ring 4 making an angle of 6.6° and Ring 3, 3.9° with this plane.

This is in contrast to the series of complexes studied by Zalkin et al[42] in these complexes the phenyl rings subtended angles from 5.6 to 47.6° with the plane of the β-diketone.

Table 4.8

a) Selected Least-Squares Planes

Plane	Atoms in Plane	Distance from Plane (A)	A	B	C	D
1	Sn	-0.061	8.454	6.705	-10.953	0.3800
	O(2)	0.073				
	C(1)	0.016				
	C(2)	-0.052				
	C(3)	-0.021				
	O(1)	0.044				
2	Sn	-0.205	1.041	3.650	18.17	8.423
	O(1)	0.066				
	3C(1)	0.067				
	1C(1)	0.072				

The equation of the plane is $Ax + By + Cz = D$

b) Planes through the phenyl rings†

Plane	Ring	A	B	C	D
3	1	13.086	-0.577	-4.703	0.9785
4	2	0.322	8.723	-8.220	0.117
5	3	6.976	-3.635	12.032	4.478
6	4	7.333	7.194	-11.1656	-0.188
7	5	9.021	6.479	-10.372	0.781

†calculated using the positions of atoms NC(1), NC(3), and NC(5) of ring N.

c) Interplanar angles

Planes	Angle
2, 3	80.21
2, 3	53.95
2, 4	89.51
3, 5	50.10
1, 6	6.14
1, 7	3.73

It is now possible to compare the structural features of the compounds of the type $R_2SnL_1L_2$[10, 13, 14] (Figure 4.5); since four X-ray structures are now available. A set of relevant structural parameters is given in Table 4.9 for comparison.

Several interesting features arise from these parameters. The most important ones are

1. that all the structures have essentially trigonalbipyramidal geometry (see Table 4.9, parameters 6, 8, 9, and 15).
2. that all the structures are distorted either axially or equatorially (see parameters 7, 13, 14, and 6).
3. that the equatorial distortion is reflected by the C-Sn-C angle in absence of steric constraints (as in $Me_2SnCl_3^-$) while axial distortions are imposed on the complexes by steric requirements of chelates, i.e., the smaller the bite (parameter 7) the larger the distortion (parameter 12).
4. that the Sn-L_1 (axial) bond is significantly longer than the Sn-L_2 (equatorial) bond (parameters 1, and 2) in contrast to the situation in $SnCl_5^-$ [43].

The above structural features are readily rationalized in terms of two factors, the steric requirement of the ligand; and the S character in the C-Sn bonds (Bent's rule).

In $Me_2SnCl_3^-$ [9] complex, no steric restriction is imposed on the ligands. The S character in C-Sn bonds tends to maximize by expanding the C-Sn-C angle. This is consistent with the observed angle (140°) and with the shorter Sn-Cl (eq) distance compared with the Sn-Cl (ax) distance. In $Me_2SnCl(S_2CNMe_2)$, the axial distortion due to the steric requirement of the ligand becomes apparent. The

Table 4.9

Selected Structural Parameters for $R_2SnL'L_1L_2$

Code	Selected Parameters	Me_2SnCl_3	$Me_2SnCldtc$	$Ph_3SnBzBz$	$Ph_3SnONPhCOPh$
1.	Sn-L_2	2.32(1)	2.48(1)	2.094(7)	2.091(5)
2.	Sn-L_1	2.55(2)	2.79(1)	2.276(7)	2.308(4)
3.	Sn-L'	2.53(2)	2.46(1)	2.180(6)	2.176(9)
4.	Sn-C_1	2.12(4)	2.20(5)	2.181(6)	2.142(9)
5.	Sn-C_2	2.11(5)	2.17(5)	2.149(7)	2.131(7)
6.	∠C_1-Sn-C_2	140. (2)	128. (2)	124.1 (2)	116.9 (3)
7.	∠L_1-Sn-L_2	90.5 (5)	68.2 (3)	78.1 (3)	71.3 (2)
8.	∠C_1-Sn-L_2	113 (1)	116 (1)	120.1 (3)	125.5 (2)
9.	∠C_2-Sn-L_2	107 (1)	113 (1)	111.0 (3)	110.9 (2)
10.	∠C_1-Sn-L'	92 (1)	99 (1)	105.[illegible] (7)	105.7 (3)
11.	∠C_2-Sn-L'	88 (1)	98 (1)	99.3 (2)	103.2 (3)
12.	∠L'-Sn-L_1	180	154.5 (4)	163.7 (3)	157.2 (2)
13.	∠L'-Sn-L_2	90 (5)	86.4 (4)	86.2 (3)	86.7 (2)
14.	(7. + 13.)	180.5	154.6	164.3	158.0
15.	(6. + 8. + 9.)	360	357	355.3	353.3
16.	∠C_1-Sn-L_1	88 (1)	93 (1)	85.0 (3)	83.1 (2)
17.	∠C_2-Sn-L_1	92 (1)	91 (1)	84.5 (3)	90.7 (2)

Figure 4.5

Structure of $R_2SnL_1L_2L'$

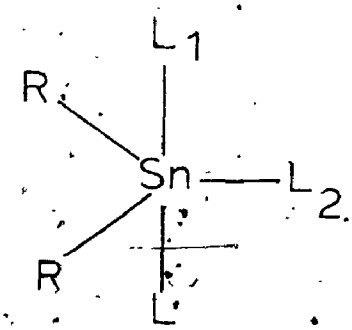

R = Me, Ph

L_1, L_2 = Cl- or ligands containing O, N, and S

L' = Ph, Cl

angle subtended at the Sn atom increases as the 'bite' becomes larger (i.e. from a four membered ring in $Me_2SnCl(S_2CNMe_2)$ to a six membered ring in $Ph_3SnBzBz$). The decrease in S character in the C-Sn bonds in $Me_2SnCl(S_2CNMe_2)$ is reflected by the C-Sn-C angle (128°) and a longer Sn-C distance (parameters 4, 5 Table 4.9). This is also consistent with the presence of the less electronegative sulfur (compared with Cl). The substantial lengthening of the axial Sn-S bond in $Me_2SnClS_2CNMe_2$ and the axial Sn-O bonds in triphenyl compounds is expected; since a direct overlap of the L_1 valence orbital with the valence hybrid of Sn is very unlikely[44].

The triphenyl compounds, $Ph_3SnBzBz$ and $Ph_3SnPhNOCOPh$, have an axial Ph-Sn bond which takes up some Sn S character and reduces the S character in the equatorial C-Sn bonds and eventually reduces the C_1-Sn-C_2 angle (Figure 4.5) to almost normal (120°). It is surprising that the C_1-Sn-C_2 angle in $Ph_3SnPhNOCOPh$ is less than 120°. This result is not readily rationalized. Crystal packing forces are perhaps one of the factors[14].

It is clear, that the steric requirements of the ligand and the S character in the Sn-ligand bond determine the structure of $R_2SnL'L_1L_2$ (Figure 4.5). The steric requirement determines the axial distortion while Bent's rule[37] governs the equatorial distortion. However, the present uncertainty is whether the substitution of a R group (i.e. L' = Me or Ph) would lead to a all-<u>cis</u> structure as in $Ph_3SnBzBz$, a <u>mer</u> structure as in $Me_3SnAcAc$, or a tetrahedral structure as in Me_3SnS_2CNMe[40].

D. Experimental

The six compounds in Table 1 were prepared under dry nitrogen using the thallous salt method[15] which has been previously described. The thallous salts of the acetylacetonates were prepared by established techniques[16, 17] and the purity of these reagents were checked by melting points. The organotin compounds were prepared by adding Ph_3SnCl and Me_3SnCl in dry benzene to the stoichiometric amount of the thallous salt in benzene. Thallium chloride precipitated immediately.

Except for $Me_3SnBzAc$, the solvent was removed from the filtrate under vacuum. For $Me_3SnBzAc$, solvent was removed by evaporating the benzene solution in a glove bag filled with N_2. The crude products were recrystallized in warm benzene with the addition of a small amount of petroleum spirit. The yield for all compounds was greater than 50%.

The preparation of $Ph_3SnBzBz$ is described here as an example since all the compounds are prepared by the same method.

(1,3-diphenyl-1,3-propanedionate)triphenyltin (IV) $Ph_3SnBzBz$. - 2.1 gm. of Ph_3SnCl was added to a 30 ml. benzene solution containing 2.46 gm. of TlBzBz. The solution was stirred for ~30 minutes. The white precipitate TlCl was discarded. Benzene was removed from the yellow solution under vacuum. Crystalline $Ph_3SnBzBz$ was obtained and recrystallized in benzene in presence of a small amount of petroleum ether. The yield was ~2.1 gm.

Physical data and chemical analyses for all the complexes are already given in Table 4.1.

Infrared spectra of nujol mulls were taken using a Perkin Elmer 621 spectrometer. N.m.r. spectra were taken in benzene at room temperature with TMS as standard using T60 and HA 100 spectrometers.

Mössbauer spectra were obtained using a 5 m Ci $BaSnO_3$ source at room temperature and an Austin Science Associates spectrometer. All absorbers were at 110K. Spectra were computed using standard procedures described in Chapter 1.

E. References

1. G. M. Bancroft and R. H. Platt, Adv. Inorg. Radiochem. 15, 59, (1972).

2. R. H. Herber, H. A. Stockler and W. T. Reichle, J. Chem. Phys. 42, 2447, (1965).

3. R. E. B. Garrod, R. H. Platt and J. R. Sams, Inorg. Chem. 10, 424, (1971).

4. B. Y. K. Ho and J. J. Zuckerman, Inorg. Chem. 12, 1552, (1973).

5. M. G. Clark, A. G. Maddock and R. H. Platt, J. Chem. Soc. (Dalton), 281, (1972).

6. B. Y. K. Ho and J. J. Zuckerman, J. Organomet. Chem. 49, 1 (1973).

7. R. C. Poller, Chemistry of Organotin Compounds, Table 7, Academic Press, (1970).

8. R. Hulme, J. Chem. Soc. 1524 (1963).

9. F. W. B. Einstein and B. R. Penfold, Chem. Comm. 780 (1966). and J. Chem. Soc. (A), 3019, (1968).

10. P. J. Vergamini, H. Vahrenkamp and L. F. Dahl, J. Amer. Chem. Soc. 93, 6327, (1971).

11. R. E. Drew and F. W. B. Einstein, Acta Cryst. B28, 345, (1972).

12. J. Buckle, P. G. Harrison, T. J. King and J. A. Richards, Chem. Comm. 1104, (1972).

13. K. Furue, T. Kimura, N. Yasmoka, N. Kasai and M. Kakudo, Bull. Chem. Soc. Japan 43, 1661, (1970).

14. T. J. King and P. G. Harrison, Chem. Comm. 815, (1972), and J. Chem. Soc. (Dalton), 2298, (1974).

15. W. H. Nelson, W. J. Randall and D. F. Martin, Inorg. Syn. 9, 52, (1967).

16. W. H. Nelson and D. F. Martin, J. Inorg. Nucl. Chem. 27, 89, (1965).

17. C. Z. Moore and W. H. Nelson, Inorg. Chem. 8, 138, (1969).

18. K. Kawakami and R. Okawara, J. Organomet. Chem. 6, 249, (1966).

19. P. W. Thompson and J. F. Lefelhoez, J. Organomet. Chem. 47, 103, (1973).

20. G. M. Bancroft and T. K. Sham, Can. J. Chem. 52, 1361, (1974).

21. M. M. McGrady and R. S. Tobias, J. Amer. Chem. Soc. 87, 1909, (1965).

22. V. G. Kumar Das and W. Kitching, J. Organomet. Chem. 13, 523, (1968); V. G. Kumar Das, to be published.

23. N. Serpone and R. Ishayek, Inorg. Chem. 13, 52, (1974).

24. G. A. Miller and E. O. Schlemper, Inorg. Chem. 12, 677 (1973).

25. G. M. Bancroft, M. G. Clark, V. G. Kumar Das and T. K. Sham, Chem. Comm. 236, (1974) and J. Chem. Soc. (Dalton) to be published.

26. G. M. Bancroft, K. D. Bulter, A. T. Rake and B. Dale, J. Chem. Soc. (Dalton), 2025 (1972).

27. International Tables for X-ray Crystallography, Kynock Press, Birmingham, England, 1962.

28. T. C. Furnas, Single Crystal Orienter instruction manual, General Electric Co., Milwaukee, Wis., 1957.

29. W. R. Busing and H. A. Levy, J. Chem. Phys. 26, 563, (1957).

30. The absorption correction trials used the analytical method of de Meulewoer and Tompa in the program AGNOST as modified by D. Cahen and J. A. Ibers, J. Appl. Crystallogr. 5, 298, (1972). Other programs used are local versions of the following: cell refinement and orientation matrix, PICKTT, based on Haillton's MODEL; Patterson and Fourier syntheses, Zalkin's FORDAP; least-squares refinement, Ibers' NUCLS; function and errors, Busing, Martin and Levy's ORFFE; crystal structure illustrations, Johnson's ORTEP. Computing was performed on the PDP-10 and CDC Cyber 73-14 at the University of Western Ontario.

31. D. T. Cromer and J. A. Waber, Acta Cryst. 18, 104, (1963).

32. R. F. Stewart, E. R. Davidson and W. T. Simpson, J. Chem. Phys. 42, 3175, (1965).

33. D. T. Cromer and D. Libermann, J. Chem. Phys. 53, 1891, (1970).

34. R. Eisenberg and J. A. Ibers, Inorg. Chem. 4, 773, (1965).

35. C. Brabant, B. Black et A. L. Beauchamp J. Organomet. Chem. 82, 231 (1975).

36. H. A. Bent. Inorg. Nucl. Chem., 19, 43, (1961).

37. R. F. Bryan, J. Am. Chem. Soc. 86, 733 (1964).

38. F. J. Hollander, D. H. Templeton and A. Zalkin, Acta Cryst. B29, 1289, (1973).

39. F. J. Hollander, D. H. Templeton and A. Zalkin, ibid. B29, 1295, (1973).

40. F. J. Hollander, D. H. Templeton and Z. Zalkin, ibid. B29 1303, (1973).

41. D. E. Williams, ibid. 21, 340, (1966).

42. D. H. Templeton and A. Zalkin, ibid. B29, 1552, (1973).

43. C. A. Coulson, 'Valence' Oxford Univ. Press, (1961).

44. G. M. Sheldrick and W. S. Sheldrick, J. Chem. Soc. (A), 490, (1970).

CHAPTER 5

ADDITIVE MODEL FOR MÖSSBAUER QUADRUPOLE SPLITTING IN FIVE COORDINATE ORGANOTIN COMPOUNDS

A. Introduction

Although the application of the additive model[1,2,3] outlined in Chapter 1 for ^{119}Sn Mössbauer quadrupole splittings has been demonstrated in Chapter 3 for four and six coordinate compounds, the discussion in Chapter 4 indicates that there are difficulties if one applies the same treatment for the quadrupole splittings in five coordinate organotin (IV) compounds. However, the Mössbauer data for five coordinate organotin acetylacetonates[4] and the recently reported quadrupole splittings for cationic organotin (IV) complexes[5,6] of the type $[R_3SnL_2]BPh_4$, and $[R_2SnL_4]BPh_4$, together with a regression analysis[7] enable one to overcome the difficulty in pqs assignments. In this chapter, the theory of the regression method[2] is discussed in detail. Also, pqs parameters for many commonly occurring ligands are derived and then applied to problems in five coordinate Sn (IV) stereochemistry.

Since the quadrupole coupling constant ratio for the ^{119}Sn and ^{121}Sb Mössbauer resonance in isoelectronic and isostructural compounds is well established[5,8], pqs parameters for the organoantimony (V) system can be easily deduced. These values are used

to discuss the structures of five coordinate organoantimony (V) compounds[9].

B. Regression Method

The quadrupole splittings discussed in this study are given in Table 5.1 where compounds (1) to (19) are six coordinate whereas compounds (101) to (108); (201) to (203) are their corresponding five coordinate analogues. These values are used for the regression analysis. The rest are used for derivation of pqs values. The structural assignments are given in Figure 5.1 together with R_2SnL_3 isomers and are supported by X-ray studies for isomers I[10] and II[4], and by other spectroscopic evidence for isomer III[4,6]. Magnetic Mössbauer spectra at 4.2K and 60 K gauss for all-cis-$Ph_3SnBzBz$, and mer-$[Me_3Sn(bipyo)]BPh_4$ (Figure 5.2) were taken and computed at the P.C.M.U., Harwell. The data (Table 5.1) give three regressions shown in Figure 5.3 and discussed below.

It is convenient that the ^{119}Sn Mössbauer quadrupole splittings $[\frac{1}{2} e^2Qq(1 + \frac{1}{3}\eta^2)^{1/2}$ in mm $s^{-1}]$ in trans-R_2SnL_4, equatorial-R_3SnL_2 (I in Fig. 5.1), all-cis-R_3SnL_2 (II), and mer-R_3SnL_2 (III) are denoted Δ_o, Δ_I, Δ_{II}, and Δ_{III} respectively. By use of the method introduced in Chapter 1 (Table 1.1, and eqs. (1.13) to (1.17), one correlates Δ_I with Δ_o and obtains eqs. (5.1) and (5.2):

Figure 5.1

Isomers of Five Coordinate R_3SnL_2 and R_2SnL_3

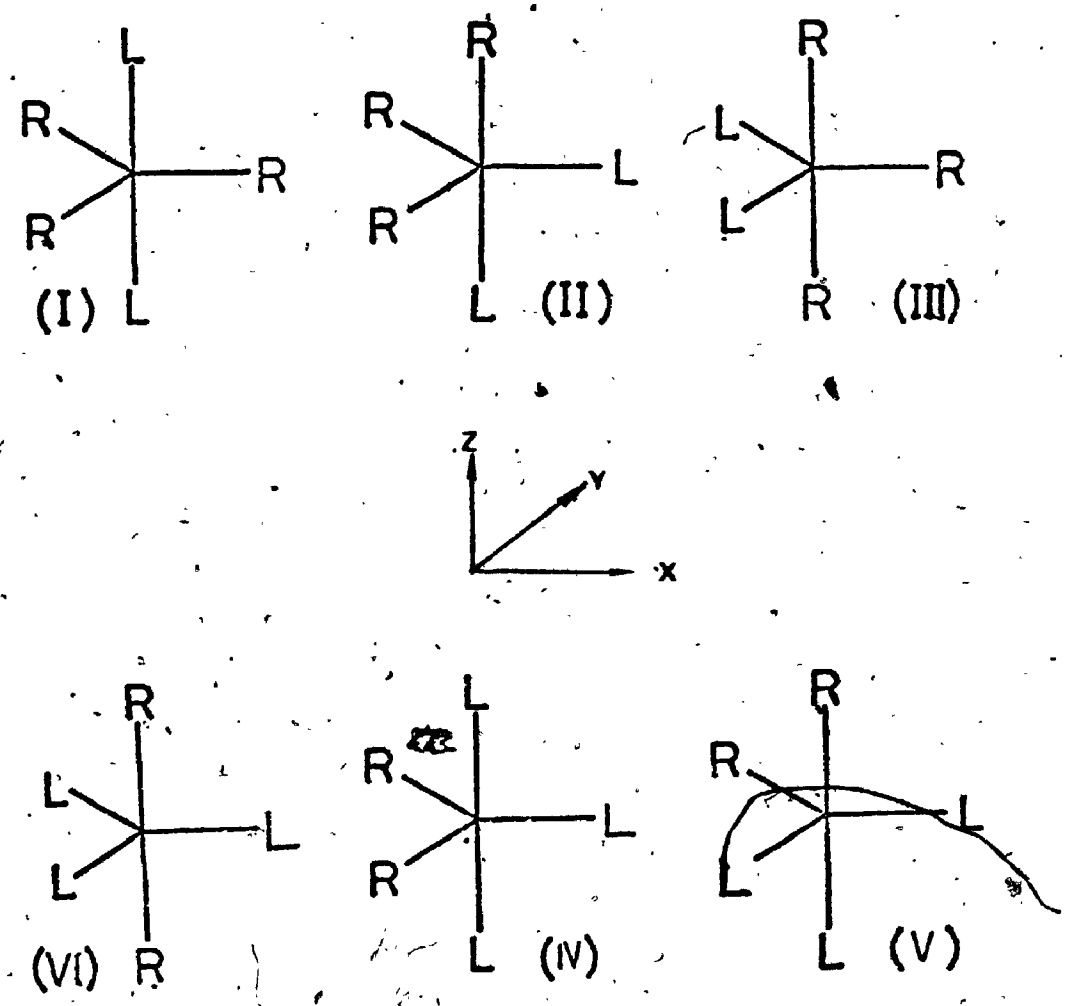

Table 5.1

^{119}Sn Mössbauer Data used in Regression Analysis and Calculation of pqs Parameters

Code no.†	Compound†	Structure†	Refs.	Obs. Q.S.‡
(1)	$[Me_2Sn(Ph_3PO)_4](BPh_4)_2$	trans-oct	a	(+)4.75
(2)	$[Me_2Sn(HMPA)_4](BPh_4)_2$	"	a	(+)4.58
(3)	$[Me_2Sn(DMSO)_4](BPh_4)_2$	"	a	(+)4.52
(4)	$[(alkyl)_2SnCl_4]^{2-}$	"	b	+ 4.12
(5)	$[Me_2Sn(Ph_3AsO)_4](BPh_4)_2$	"	a	(+)4.03
(6)	$[Ph_2Sn(DMSO)_4](BPh_4)_2$	"	a	(+)4.30
(7)	$(PyH)_2[Ph_2SnCl_4]$	"	c	(+)3.80
(8)	$[Me_2Sn(opo)_2](BPh_4)_2$	"	a	(+)4.50
(9)	$[Me_2Sn(diphosO)_2](BPh_4)_2$	"	a	(+)4.38
(10)	$[Me_2Sn(OAsO)_2](BPh_4)_2$	"	a	(+)4.08
(11)	$[Me_2Sn(bipyo)_2](BPh_4)_2$	"	a	(+)4.00
(12)	$Me_2Sn(AcAc)_2$	"	b,d	+ 4.02
(13)	$Me_2Sn(BzBz)_2$	"	d	+ 4.08
(14)	$Me_2Sn(BzAc)_2$	"	d	+ 3.87
(15)	$[Ph_2Sn(opo)_2](BPh_4)_2$	"	a	(+)3.78
(16)	$Ph_2Sn(oxin)_2$	cis-oct	o,p	+ 1.64
(17)	$Ph_2Sn(BzBz)_2$	"	d	(-)2.15
(18)	$Ph_2Sn(BzAc)_2$	"	d	(-)2.23
(19)	$(alkyl)_2Sn(oxin)_2$	"	o,p	+ 2.00
(101)	$[Me_3Sn(Ph_3PO)_2]BPh_4$	(I)	q	(-)3.87

Table 5.1 (cont'd.)

(102)	$[Me_3Sn(HMPA)_2]BPh_4$	"	q	(-)3.85
(103)	$[Me_3Sn(DMSO)_2]BPh_4$	"	q	(-)3.63
(104)	$[(alkyl)_3SnCl_2]^-$	"	b	- 3.31
(105)	$[Me_3Sn(Ph_3AsO)_2]BPh_4$	"	q	(-)3.29
(106)	$[Ph_3Sn(DMSO)_2]BPh_4$	"	q	(-)3.39
(107)	$[Ph_3SnCl_2]^-$	"	b	- 3.02
(108)	$[Ph_3Sn(HMPA)_2]BPh_4$	"	g	(-)3.51
(109)	$[Me_3Sn(DMF)_2]BPh_4$	"	q	(-)3.90
(110)	$[Me_3Sn(H_2O)_2]BPh_4$	"	h	(-)4.10
(111)	$Me_3SnCl(DMA)$	"	i	(-)3.69
(112)	$Me_3SnClPy$	"	o	(-)3.44
(113)	$Me_3SnBrPy$	"	j	(-)3.18
(114)	$Ph_3SnClPyO$	"	k	(-)2.94
(115)	$Ph_3Sn(NCS)PyO$	"	k	(-)3.14
(116)	Me_3SnF	"	b	(-)3.82
(117)	Me_3SnI	"	b	(-)3.05
(118)	Me_3SnOH	"	b,r,l	- 2.88
(119)	Me_3SnCN	"	b	(-)3.12
(120)	Me_3SnN_3	"	b,l	(-)3.52
(121)	$Ph_3SnNO_3(DMSO)$	"	g	(-)3.40
(122)	$Ph_3SnNO_3(HMPA)$	"	g	(-)3.33
(123)	$Me_3SnOCOCH_3$	"	m,s	- 3.68
(124)	$Me_3SnOCOCH_2I$	"	m	(-)3.83
(125)	$Me_3SnOCOCH_2Br$	"	m	(-)3.90

Table 5.1 (cont'd.)

(126)	$Me_3SnOCOCH_2Cl$	"	m	(-)3.89
(127)	$Me_3SnOCOCBr_3$	"	m	(-)4.13
(128)	$Me_3SnOCOCCl_3$	"	m	(-)4.15
(129)	$Me_3SnOCOCHCl_2$	"	m	(-)4.08
(130)	$Me_3SnOCOCF_3$	"	m	(-)4.22
(131)	$Me_3SnOCOH$	"	b	(-)3.55
(132)	$Me_3SnSO_3CF_3$	"	n	(-)4.57
(133)	$Me_3SnSO_3CH_3$	"	n	(-)4.21
(134)	$Me_3SnONOR$	"	t	(-)3.37
(135)	$Ph_3SnCl(pip)$	"	v	- 2.95
(201)	$Ph_3Sn(oxin)$	(II)	e,s	- 1.75
(202)	$Ph_3Sn(BzBz)$	"	f	- 2.25
(203)	$Ph_3Sn(BzAc)$	"	f	(+)2.25
(301)	$[Me_3Sn(opo)]BPh_4$	(III)	q	(-)4.10
(302)	$[Me_3Sn(diphoso)]BPh_4$	"	q	(-)3.90
(303)	$[Me_3Sn(OASO)]BPh_4$	"	q	(-)3.69
(304)	$[Me_3Sn(bipyo)BPh_4$	"	q	- 3.67
(305)	$Me_3Sn(AcAc)$	"	f	(-)3.81
(306)	$Me_3Sn(BzBz)$	"	f	(-)3.86
(307)	$Me_3Sn(BzAc)$	"	f	(-)3.69
(308)	$[Ph_3Sn(opo)]BPh_4$	"	q	(-)3.52

†(1) to (19) octahedral; (101) to (135), (201) to (203), and (301) to (308) trigonal-bipyramidal isomers (I), (II) and (III), respectively.

Table 5.1 continued...

$\pm 1/2e^2qQ(1+\frac{1}{3}\eta^2)^{\frac{1}{2}}$ in units of mms^{-1}. Values are unweighted averages, where appropriate, of measurements at ca 80°K. Where no measured sign is available, the additive-model predicted sign is given in parentheses.

a. Ref. 5 b. Average of values in Ref. 3 c. B.W.Fitzsimmons, N.J.Seeley and A.W.Smith, J.Chem.Soc.(A), 143, (1969).

d. G.M.Bancroft and T.K.Sham, Can.J.Chem. 52, 1361, (1974).

e. R.C.Poller and J.N.R.Ruddick, J.Chem.Soc.(A), 2273, (1969).

f. Ref. 4 g. G.M.Bancroft and V.G.Kumar Das unpublished results.

h. Ref 17. i. J.C.Hill, R.S.Drago, and R.H.Herber, J.Amer.Chem.Soc. 91, 1644, (1969). j. J.Nasielski, N.Sprecher, J de Vooght, and S Lejeune, J.Organomet.Chem. 8, 97, (1967). k. Ref. 19 and R.W.J.Wedd and J.R.Sams, Can.J.Chem., 48, 71, (1970). l. N.Bertazzi, G.Alonzo, R.Barbieri, and R.H.Herber, J.Organomet.Chem., 65, 23, (1974). m. C.Poder and J.R.Sams J.Organomet.Chem., 19, 67, (1969). n. J.R.Sams in MTP Internat. Rev Sci.Phys.Chem.Ser.1, Vol. 4(magnetic Resonance, ed. C.A. McDowell) p.85.

o. Average of values collected in P.J.Smith, Organomet.Chem.Rev.A 5, 373, (1970). p. Ref. 16. q. G.M.Bancroft, V.G.Kumar Das, T.K.Sham and M.G.Clark J.Chem.Soc.Dalton, submitted. r. B.A.Goodman and N.N. Greenwood, JChem.Soc.(A), 1862, (1971). s. Ref. 13. v. B.A.Goodman N.N.Greenwood, K.L.Jaura, and K.K.Sharma J.Chem.Soc. 1865, (1971).

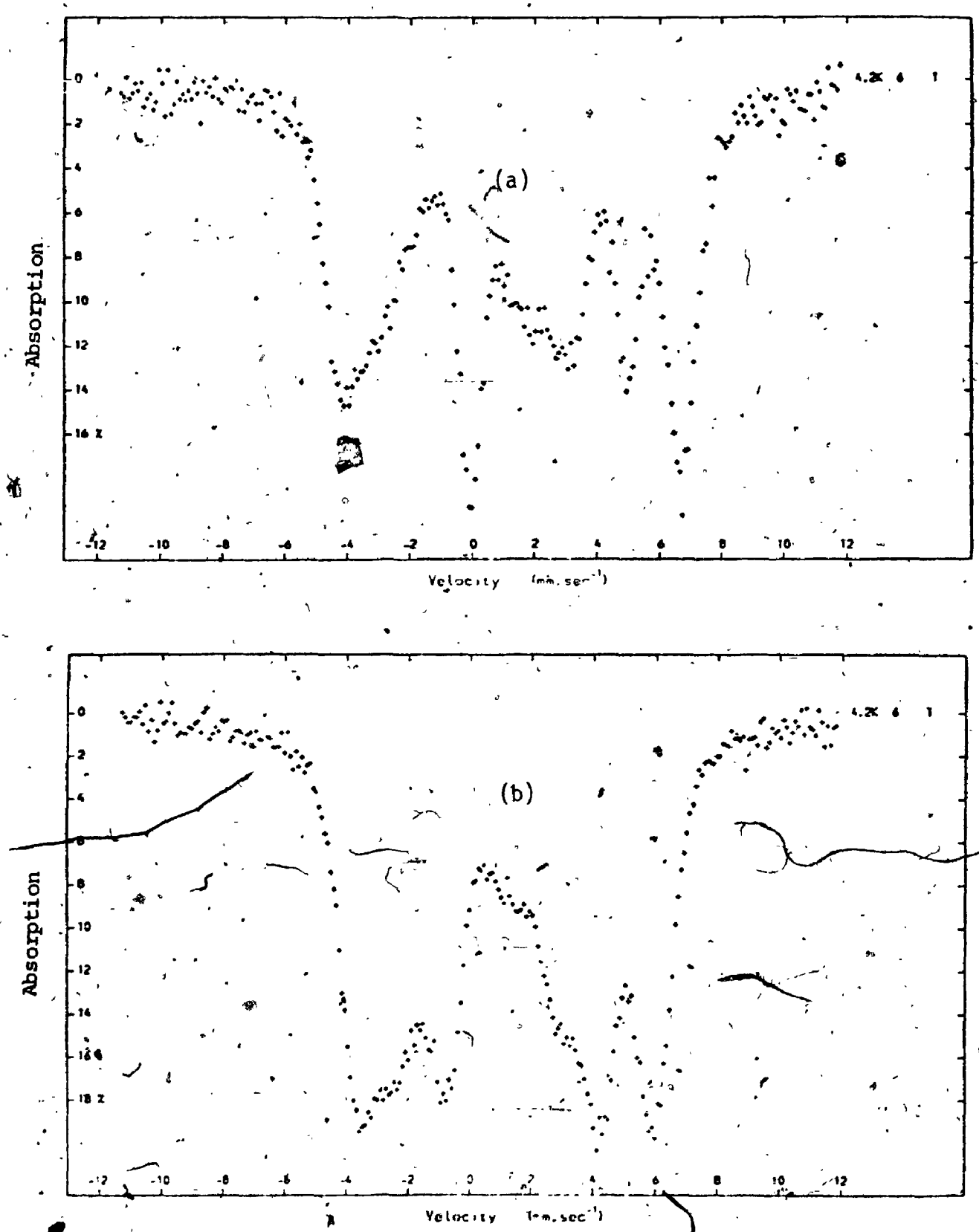

Figure 5.2 Mossbauer-Zeeman Spectra(4.2°K,6 tesla) of (a) $[Me_3Sn(bipyo)]BPh_4$ and (b) $Ph_3SnBzBz$

$$\Delta_I = -[(\{R\}^{tba} - \{L\}^{tba})/(\{R\}^{oct} - \{L\}^{oct})]\Delta_o + [4\{R\}^{tba} - 3\{R\}^{tbe}] \tag{5.1}$$

$$\Delta_I = -[(\sigma_R^{tba} - \sigma_L^{tba})/(\sigma_R^{oct} - \sigma_L^{oct})]\Delta_o - \frac{2}{5} e^2|Q|(1 - R) \langle r^{*3}\rangle_p (\sigma_R^{tba} - \sigma_R^{tbe}) \tag{5.2}$$

where {L}, and σ subscripted parameters etc, are defined by eqs (1.12) to (1.17). The derivation of (5.1) and (5.2) is described below:

Since

$$\Delta_I = 4\{L\}^{tba} - 3\{R\}^{tbe} \tag{5.3}$$

$$\Delta_o = 4\{R\}^{oct} - 4\{L\}^{oct} \tag{5.4}$$

eq. (5.3)/eq. (5.4) gives

$$\frac{\Delta_I}{\Delta_o} = \frac{4\{L\}^{tba} - 3\{R\}^{tbe}}{4\{R\}^{oct} - 4\{L\}^{oct}} \tag{5.5}$$

If we add and subtract $4\{R\}^{tba}$ to and from the numerator respectively, rearrange the terms and then multiply Δ_o to both sides, we then obtain eq. (5.1). Eq. (5.2) can be obtained by substitution of $\{R\}^{tbe}$ with $\frac{1}{2} e^2|Q|([R]^{tbe} - \frac{4}{3}[X]^{tba})$ etc., where $[R]^{tbe}$ etc. are defined by eqs. (1.14) to (1.17). For further discussion, eqs. (5.1) or (5.2) are best expressed as eq. (5.6) where m(R, L), Δ_R correspond to the proper terms in eq. (5.2)

$$\Delta_I = -m(R, L)\Delta_o + \Delta_R \qquad (5.6)$$

If R is fixed and L varied then, provided M(R, L) is roughly constant, there should be a linear regression between Δ_I and Δ_o. Thus, - m(R, L) corresponds to the slope whereas Δ_R is the intercept. The linear regression is confirmed for the seven points shown by filled circles in Figure 5.3. It is important to note that m(R, L) is approximately a constant only when $\sigma_R > \sigma_L$ (this is in fact the case); Δ_o is positive, and Δ_I is negative. The data fit a regression (eq. (5.7)) with correlation coefficient r = 0.977

$$\Delta_I = -0.932\ \Delta_o + 0.526\ \text{mm s}^{-1} \qquad (5.7)$$

It is not surprising that the ratio m(R, L) should be approximately constant, since h_z^{oct} and h_z^{tba} (Ref. 1) are similar in form, and become equal if θ in h_z^{tba} takes the value 54°44′ (eqs. (1.15), (1.16)).

The intercept (Δ_R) at Δ_o = 0 is the QS of the hypothetical species R_5Sn^-. Since the pqs due to Ph and alkyl are distinguishable[1], if the two points with R = Ph are removed, the regression becomes eq. (5.8) with correlation

$$\Delta_I = -\ 0.904\ \Delta_o + 0.387\ \text{mm s}^{-1} \qquad (5.8)$$

coefficient r = 0.972. It is apparent that the intercept is much more sensitive than the slope to small changes in the data since there is a change of only 3% in slope but about 30% in intercept.

To express Δ_{II}, Δ_{III} as a function of Δ_o is not an easy

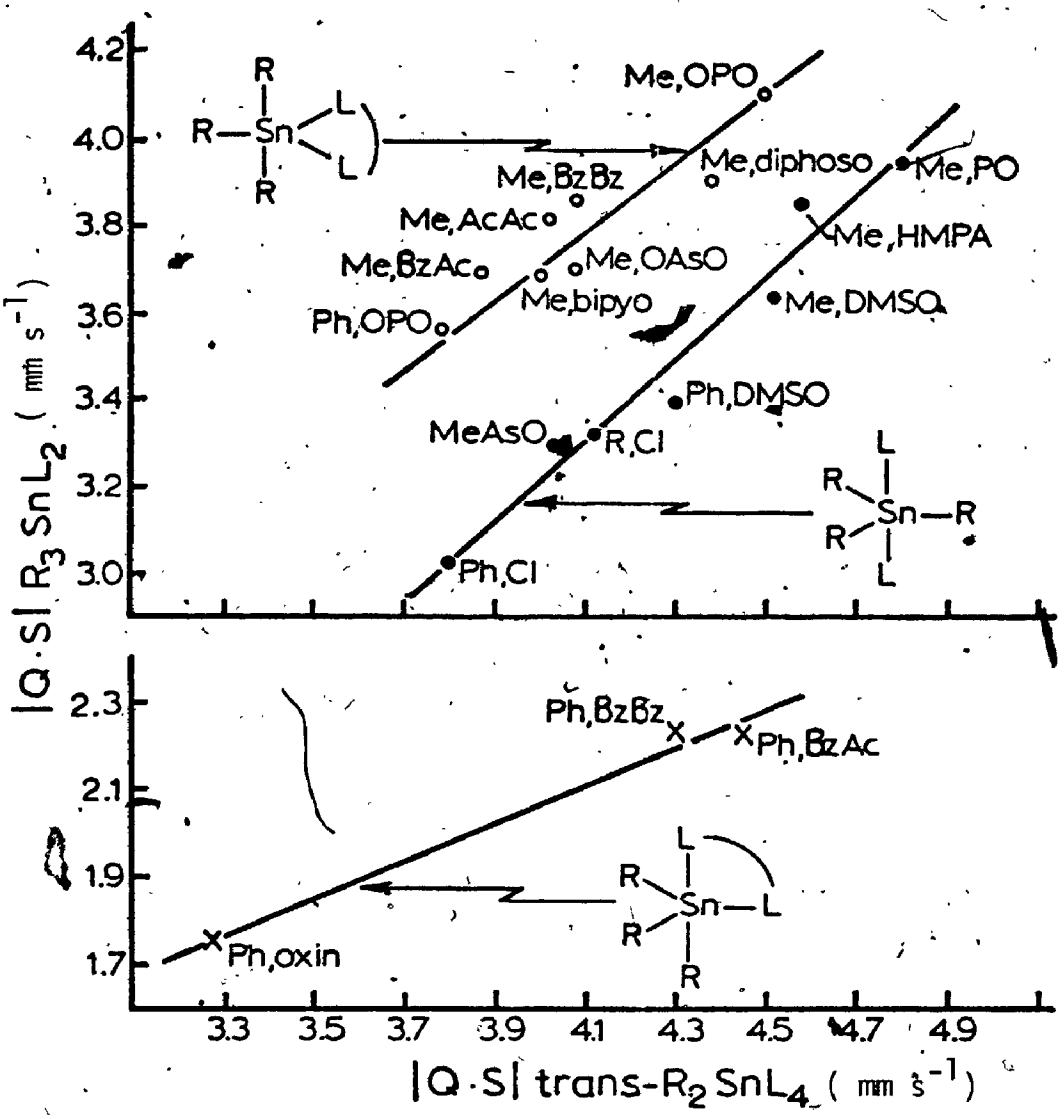

Figure 5.3 Plot of QS in R_3SnL_2 against Magnitude of QS in <u>trans</u>-R_2SnL_4 (or twice <u>cis</u>-R_2SnL_4)

matter, since $\eta \neq 0$ in these structures. The principal components of the EFG tensors[2, 11] for isomers (II) and (III) are given by eqs. (5.9) to (5.14).

$$V_{xx}^{II}/e = -[R]^{tba} - \frac{1}{2}[R]^{tbe} - [L]^{tba} + 2[L]^{tbe} \quad (5.9)$$

$$V_{yy}^{II}/e = -[R]^{tba} + \frac{5}{2}[R]^{tbe} - [L]^{tba} - [L]^{tbe} \quad (5.10)$$

$$V_{zz}^{II}/e = 2[R]^{tba} - 2[R]^{tbe} + 2[L]^{tba} - [L]^{tbe} \quad (5.11)$$

$$V_{xx}^{III}/e = -2[R]^{tba} + 2[R]^{tbe} - \frac{1}{2}[L]^{tbe} \quad (5.12)$$

$$V_{yy}^{III}/e = -2[R]^{tba} - [R]^{tbe} + \frac{5}{2}[L]^{tbe} \quad (5.13)$$

$$V_{zz}^{III}/e = 4[R]^{tba} - [R]^{tbe} - 2[L]^{tbe} \quad (5.14)$$

In general, Δ_{II}^2 and Δ_{III}^2 can be expressed as quadratic functions of Δ_o, Δ_R, and Δ_L where Δ_L, the QS of hypothetical $[SnL_5]$, is given by (5.15).

$$\Delta_L = -\frac{2}{5} e^2 Q(1 - R) \langle r^{-3} \rangle_p (\sigma_L^{tba} - \sigma_L^{tbe}) \quad (5.15)$$

However, all available data are such that $|\Delta_o|$ (~4 mm s^{-1}) is very much greater than $|\Delta_R|$ and $|\Delta_L|$ (~0.5 mm s^{-1}). Thus the exact expressions for Δ_{II} and Δ_{III} in terms of Δ_o, Δ_R, and Δ_L, calculated by symmetrized parameters (Chapter 1) and the following relations (eqs. (5.16a) to (5.16c)) are

$$\{R\}^{tba} = -\frac{1}{4} m(R, L) \Delta_o + \{L\}^{tba} \quad (5.16a)$$

$$\{R\}^{tbe} = \frac{1}{3}(\Delta_R - m\Delta_o) + \frac{4}{3}\{L\}^{tba} \quad (5.16b)$$

$$\{L\}^{tbe} = \frac{1}{3}\Delta_L + \frac{4}{3}\{L\}^{tba} \qquad (5.16c)$$

shown in eqs, (5.17a), and (5.18a). One must remember that $\{R\}^{tba} = \frac{1}{2}e^2Q([R]^{tba} - [X]^{tba})$ with $[X]^{tba}$ being zero converts field gradient to partial quadrupole splitting. To the first approximation eqs. (5.17a) and (5.18a) can be linearized by applying the binomial theorem and neglecting terms of second order in (Δ_R/Δ_o), (Δ_L/Δ_o), or $(\Delta_R\Delta_L/\Delta_o^2)^{1/2}$ to give eqs. (5.17b) and (5.18b). Therefore, the variation in Δ_L with the L encountered in practice is:

$$|\Delta_{II}| = \frac{1}{3}[\frac{13}{4}(m\ \Delta_o)^2 - 8m\Delta_o\Delta_R + 5m\Delta_o\Delta_L + 7\Delta_R^2 - 2\Delta_R\Delta_L + 4\Delta_L 2]^{1/2} \qquad (5.17a)$$

$$= \frac{\sqrt{13}}{6}m(R, L)|\Delta_o| - \frac{8}{3\sqrt{13}}\Delta_R + \frac{5}{3\sqrt{13}}\Delta_L \qquad (5.17b)$$

$$|\Delta_{III}| = \frac{1}{3}[7(m\ \Delta_o)^2 - 2m\Delta_o\Delta_R + 14m\Delta_o\Delta_L + 4\Delta_R^2 - 2\Delta_R\Delta_L + 7\Delta_L^2]^{1/2} \qquad (5.18a)$$

$$= \frac{\sqrt{7}}{3}m(R, L)|\Delta_o| - \frac{1}{3\sqrt{7}}\Delta_R + \frac{\sqrt{7}}{3}\Delta_L \qquad (5.18b)$$

too small to cause noticeable non-linearity in an R-fixed, L-variable regression.

Only the magnitudes $|\Delta_{II}|$ and $|\Delta_{III}|$ are considered because the signs of Δ_{II} and Δ_{III} cannot be firmly predicted when η is large, since then only a small change in the relative magnitudes of the principal components of the EFG may cause the principal axes to be permuted, leading to a change in the sign of the EFG. Changes of this kind arise, for example, because of distortions from ideal geometry. Thus whereas $[Me_3Sn(bipyo)]BPh_4$ has e^2qQ negative as predicted by the additive model, $Ph_3Sn(BzBz)$, $Ph_3SnPhNCOPh$,[12] and

$Ph_3Sn(oxin)$[13] all have negative e^2qQ, contrary to additive-model predictions.

Regression lines for compounds assigned to structure (II) (crosses in Fig. 5.3) and structure (III) (open circles) are given by eqs. (5.19) and (5.20) with correlation coefficients r = 0.992 and r = 0.914, respectively.

$$|\Delta_{II}| = 0.448\ |\Delta_o| + 0.283 \quad \text{mm s}^{-1} \qquad (5.19)$$

$$|\Delta_{III}| = 0.712\ |\Delta_o| + 0.868 \quad \text{mm s}^{-1} \qquad (5.20)$$

If the point (Ph, opo) is excluded from the regression for (III) it becomes eq. (5.21) with r = 0.881. From eqs. (5.18), (5.19), and (5.21) the

$$|\Delta_{III}| = 0.657\ |\Delta_o| + 1.103 \quad \text{mm s}^{-1} \qquad (5.21)$$

magnitudes of the observed slopes are in the ratio 1:0.50:0.73 in reasonable agreement with the theoretical values 1:0.60:0.88 given by eqs. (5.6), (5.17) and (5.18).

As mentioned above, the values for the intercepts at $\Delta_o = 0$ are rather less accurate than the slopes. Nevertheless, the regressions for (I) and (III) clearly imply that both Δ_R and Δ_L are positive. In the case of Δ_L this is contrary to previously-held opinion[8, 14] that $\Delta(SnCl_5^-)$ would prove to be negative. However, pqs values deduced on the asuumption that Δ_L is positive lead to a consistent interpretion of ^{119}Sn quadrupole coupling constants.

Finally, it must be pointed out that Δ_I, Δ_{II}, Δ_{III} and Δ_0 have associated with them experimental errors and errors from deficiencies in the additive model. The total errors are regarded as pseudo-random and are assumed to be the same for all variables, and the regression lines calculated above are orthogonal regression lines[15]. Detailed error analysis treated elsewhere[6] supports the validity of these correlations.

C. Partial Quadrupole Splittings for Five Coordinate ^{119}Sn (IV)

The partial quadrupole splittings can now be derived for ligands based on measurements of either (scheme A) eqs. (5.22), (5.23) or (scheme B) eqs. (5.24) and (5.25), where X is a fixed reference ligand. In agreement with Ref. 9, we favor scheme A with X = Cl, Br: and $[X]^{tba} = 0$.

$$\{L\}^{tba} = \frac{1}{2} e^2|Q|([L]^{tba} - [X]^{tba}) \quad (5.22)$$

$$\{L\}^{tbe} = \frac{1}{2} e^2|Q|([L]^{tbe} - \frac{4}{3}[X]^{tba}) \quad (5.23)$$

$$\{L\}^{tba} = \frac{1}{2} e^2|Q|([L]^{tba} - \frac{3}{4}[X]^{tbe}) \quad (5.24)$$

$$\{L\}^{tbe} = \frac{1}{2} e^2|Q|([L]^{tbe} - [X]^{tbe}) \quad (5.25)$$

The importance of establishing representative pqs values for the key frequently-occuring alkyl, phenyl, and halogen ligands has already been emphasized[1]. Since $\{X\}^{tba} = \{Cl\}^{tba} = \{Br\}^{tba} = 0$ by definition, we have to determine values of $\{R\}^{tba}$, $\{R\}^{tbe}$, (R = alkyl and Ph) and $\{X\}^{tbe}$. Mössbauer data are available for

$(alkyl)_nSnX_{5-n}^-$ with n = 0, 1, 2, and 3. In all cases the alkyl groups occupy equatorial positions[10]. Thus good representative values for $\{alkyl\}^{tbe}$ and $\{X\}^{tbe}$, together with 'errors' measuring the discrepancies between theory and observation, may be obtained by calculating the best least-squares solution of eqs (5.26) to (5.29). The left-hand sides of eqs (5.26) - (5.29) are additive-model

$$-3\{R\}^{tbe} = +3.39 \qquad (5.26)$$

$$\sqrt{7}\{R\}^{tbe} - \frac{1}{\sqrt{7}}\{X\}^{tbe} = -3.45 \qquad (5.27)$$

$$2\{R\}^{tbe} - \frac{1}{2}\{X\}^{tbe} = -1.82 \qquad (5.28)$$

$$-3\{X\}^{tbe} = -0.63 \qquad (5.29)$$

predictions for minus the quadrupole splittings (Q is negative) in $R_3SnX_2^-$, $R_2SnX_3^-$, $RSnX_4^-$, and SnX_5^-, respectively, linearized if $\eta \neq 0$ by neglecting terms of second order in $\{X\}^{tbe}/\{R\}^{tbe}$. The right-hand sides are unweighted averages in units of mm s^{-1} of all literature values available to us,[14, 16, 17] with the sign (of V_{zz}) for SnX_5^- chosen negative following the regression analysis above.

The least-squares solution[18] of eqs (5.26) - (5.29) are

$$\{R\}^{tbe} = -1.13 \pm 0.11 \quad \text{mm s}^{-1}$$

$$\{X\}^{tbe} = +0.20 \pm 0.15 \quad \text{mm s}^{-1}$$

These values are almost exactly the same as those derived from eqs. (5.26), (5.27) independently. The errors indicate that the rough tolerance limit of 0.4 mm s^{-1} suggested[1] for application of the additive model to tetrahedral and octahedral organotin (IV) compounds is suitable for trigonal-bipyramidal systems too.

Since the above procedure treats data from four different structures it should minimize the effect of any bias of the type exemplified by the $ASnX_3$ and A_2SnX_2 systems[19].

Next, we derive additive-model expressions for Δ_{II} and Δ_{III} (R_3SnL_2 compounds) and Δ_I for R_3SnLL' compounds. The required expressions[20, 21] calculated by use of S_{02} parameters are given in eqs. (5.30) to (5.32), where eqs. (5.31) and (5.32) are linearized under the same approximations as eqs (5.17b) and (5.18b).

$$|\Delta_I(R_3SnLL')| = |2\{L\}^{tba} + 2\{L'\}^{tba} - 3\{R\}^{tbe}| \quad (5.30)$$

$$|\Delta_{III}(R_3SnL_2)| \simeq [-8\{R\}^{tba} - \{R\}^{tbe} + 7\{L\}^{tbe}]/\sqrt{7} \quad (5.31)$$

$$|\Delta_{II}(R_3SnL_2)| \simeq [2\{R\}^{tbe} + 2\{L\}^{tba} + 5\{L\}^{tbe}]/\sqrt{13} \quad (5.32)$$

A value for $\{R\}^{tba}$ may now be calculated by use of eq. (5.31), the previously derived values of $\{R\}^{tbe}$ and $\{X\}^{tbe}$, and an estimate of the quadrupole splitting in hypothetical <u>mer</u>-R_3SnX_2 obtained by interpolating in the regression of Δ_{III} against Δ_0 at $\Delta_0 = 4.12$ mm s^{-1}, the averaged value[1] for <u>trans</u>-R_2SnX_4. The interpolation gives $|\Delta_{III}(R_3SnX_2)| = 3.80$ mm s^{-1}. Since the point concerned lies near the centre of gravity of the data on structure (III) (Fig. 5.3), the interpolated value is virtually independent of the choice of data base, giving confidence that the estimate

$$\{R\}^{tba} = -0.94 \pm 0.13 \quad \text{mm s}^{-1}$$

obtained from this quadrupole splitting and eq. (5.31) is a good representative value of $\{R\}^{tba}$. The error quoted reflects only the errors given above for $\{R\}^{tbe}$ and $\{X\}^{tbe}$. It is encouraging that the value of $\{R\}^{tba}$ calculated from $m(R, X) = (\{R\}^{tba}/\{R\}^{oct}) = +0.904$[see eqs. (5.1) and (5.8)] is -0.93 mm s^{-1}; and from $\Delta_R = 0.387$ is -0.94 mm s^{-1}.

The available data on phenyl derivatives is more limited. The average of the ^{119}Sn quadrupole splittings[14, 19] in $(Me_4N)(Ph_3SnCl_2)$ and $(Ph_3PC_{10}H_{21})(Ph_3SnCl_2)$ [both structures (I)] gives

$$\{Ph\}^{tbe} = -0.98 \quad \text{mm s}^{-1}$$

Interpolation in the regression of Δ_{III} against Δ_o, as described above gives

$$\{Ph\}^{tba} = -0.89 \quad \text{mm s}^{-1}$$

There is not sufficient evidence for 'errors' to be assigned to these values individually, but the discussion above indicates that ca. 0.15 mm s^{-1} would be a sensible guess.

Notice that the derived values for $\{R\}^{tbe}$ and $\{R\}^{tba}$, and the positive quadrupole splitting for R_5Sn^-, are consistent with theoretical predictions. The theoretical ratio, $\{R\}^{tba}/\{R\}^{tbe}$ is equal to $3/4[(\sigma_R^{tba} - \sigma_X^{tba})/(\sigma_R^{tbe} - \sigma_X^{tba})]$ compared to the calculated values of 0.83 and 0.91 for R = alkyl, and Ph respectively. Since results in Chapter 3 indicate that $\{R\}^{oct}/\{R\}^{tet} = 2/3[(\sigma_R^{oct} - \sigma_X^{oct})/(\sigma_R^{tet} - \sigma_X^{tet})]$ compared with the calculated value of 0.75,

one expects that $[(\sigma_R^{tba} - \sigma_X^{tba})/(\sigma_R^{tbe} - \sigma_X^{tba})] \sim 1$ and $\{R\}^{tba}/\{R\}^{tbe} \sim 3/4$. Thus the values of 0.83 and 0.91 seem entirely reasonable. If $(\{R\}^{tba}/\{R\}^{tbe}) > 1$, then $(\sigma_R^{tba} - \sigma_X^{tba})$ would have to be more than 33% greater than $(\sigma_R^{tbe} - \sigma_X^{tbe})$, (eq. 5.2) and this does not appear likely. Our value for $\{R\}^{tba}/\{R\}^{tbe}$ implies that $\Delta(R_5Sn^-) > 0$, whereas $\Delta(R_5Sn^-)$ negative would require $0.75 > (\{R\}^{tba}/\{R\}^{tbe}) \gtrsim 0.5$, which is not consistent with our results.

It is also possible to compare the parameters in Table 5.2 with their corresponding $\{L\}^{oct}$ values. We note that the ordering of $-\{L\}^{tba}$ ($\propto \sigma_L^{tba}$) values is very close to that observed[1,3,5] for $-\{L\}^{oct}$:

oct: R > Ph > I > Py > PyO ~ Ph_3AsO > pip ~ Cl > DMF > NCS > DMSO ~ ~ HMPA > Ph_3PO

tba: R > Ph > I > Py ~ Ph_3AsO ~ PyO ~ Cl ~ pip > NCS ~ DMSO > Ph_3PO ~ ~ DMF ~ HMPA

where ~ is used for differences in pqs of less than 0.03 mm s^{-1}. This indicates that the donor strength of common ligands (as measured by σ_L) behaves consistently in trigonal-bipyramidal-axial and octahedral coordination, and confirms the validity of the additive-model treatment used above.

Available experimental data are such that pqs parameters for other ligands L must be derived by special procedures based on one or two compounds believed to be reasonably close to ideal geometry. We have calculated values for ligands commonly occurring in 5-coordination by use of quadrupole splittings observed (Table 5.2) in

either R_3SnL_2 (equatorial, cis, or mer) or equatorial-R_3SnLL'. For equatorial (I) and mer (III) isomers, $\{L\}^{tba}$ and $\{L\}^{tbe}$, respectively, are readily obtained by equating the observed splittings to the additive model expressions given in eqs (5.30) and (5.31). The cis isomer (II) [eq. (5.32)] yields either $\{L\}^{tba}$ or $\{L\}^{tbe}$ if the other is known. However, since the coefficient of $\{L\}^{tba}$ in the last part of eq. (5.32) is rather small, any error in $|\Delta_{II}|$ will be magnified, and (assuming isomer (I) is not available) it is preferable to determine $\{L\}^{tba}$ from $\Delta_I(R_3SnL_2)$ obtained by interpolation into the regression of Δ_I against Δ_o at the measured value of Δ_o(trans-R_2SnL_4) (or twice $|\Delta$(cis-$R_2SnL_4)|$, if necessary). Indeed, this is the only method for bidentate chelates L_2 not available in both cis and mer structures.

Apical parameters for all chelates listed in Table 5.2 were obtained by this interpolation procedure. For example, the value $\Delta_o = +4.02$ mm s^{-1} for trans-$Me_2Sn(AcAc)_2$ (Table 5.2, compound (12)) was inserted into eq. (5.8) to give $\Delta_I = -3.25$ mm s^{-1} for hypothetical equatorial-$Me_3Sn(AcAc)$, and $\{AcAc\}^{tba}$ was then calculated by use of eq. (5.30). The other values listed were obtained in a similar way, taking $\Delta_o = 2|\Delta$[cis-oct.-$(alkyl)_2Sn(oxin)_2$]$|$ in the case of oxin. Equatorial parameters were obtained by use of eq. (5.31), or (for oxin only) eq. (5.32), and data from Table 5.1 as noted. The remaining monodentate ligands are usually found only in the axial position, and values of $\{L\}^{tba}$ were obtained by applying eq. (5.30) to the compounds noted. If required, equatorial parameters for these ligands could be estimated by transforming from Δ_I to Δ_{III}.

Table 5.2

Estimated Partial Quadrupole Splitting Parameters for Trigonal-Bipyramidal Organotin(IV) Compounds

Ligand	$\{L\}^{tba}$† (mm s^{-1})	Data used‡	$\{L\}^{tbe}$† (mm s^{-1})	Data used‡
Cl, Br	0	by definition	+ 0.20	see text
alkyl	- 0.94	see text	- 1.13	see text
Ph	- 0.89	see text	- 0.98	see text
oxin	- 0.05	§ (19)	+ 0.04	(201)
AcAc	- 0.03	§ (12)	+ 0.20	(305)
BzAc	- 0.07	§ (14)	+ 0.15	(307)
BzBz	- 0.02	§ (13)	+ 0.22	(306)
opo	+ 0.075	§ (8)	+ 0.31	(301)
diphoso	+ 0.05	§ (9)	+ 0.24	(302)
OAsO	- 0.02	§ (10)	+ 0.16	(303)
bipyo	- 0.04	§ (11)	+ 0.15	(304)
Ph_3PO	+ 0.12	(101)		
Ph_3AsO	- 0.02	(105)		
HMPA	+ 0.13	(102),(108)		
DMSO	+ 0.09	(103),(106)		
DMF	+ 0.13	(109)		
DMA	+ 0.16	(111)		
Py	- 0.035	(112),(113)		
PyO	0.00	(114)		
NCS	+ 0.065	(115)		
F	+ 0.11	(116)		

Table 5.2 (cont'd.)

I	- 0.08	(117)
OH	- 0.13	(118)
H_2O	+ 0.18	(110)
N_3	+ 0.03	(120)
pip	+ 0.01	(135)
CN	- 0.065	(119)
NO_2R	0.00	(134)
NO_3	+ 0.11	(121),(122)
OCOH	+ 0.04	(131)
$OCOCH_3$	+ 0.075	(123)
$OCOCH_2I$	+ 0.11	(124)
$OCOCH_2Br$	+ 0.13	(125)
$OCOCH_2Cl$	+ 0.13	(126)
$OCOCBr_3$	+ 0.19	(127)
$OCOCCl_3$	+ 0.19	(128)
$OCOCHCl_2$	+ 0.175	(129)
$OCOCF_3$	+ 0.21	(130)
SO_3CF_3	+ 0.30	(132)
SO_3CH_3	+ 0.21	(133)

† $\{L\}^{tba}$ and $\{L\}^{tbe}$ are defined in eqs. (5.22) and (5.23). All values may be assigned nominal standard errors of ca 0.15 mm s^{-1}.

‡ Code numbers refer to Table 5.1.

§ Calculated after interpolation into eq. (8) with data from compounds noted; details are given in the text.

D. Discussion and Application of ^{119}Sn (IV) pqs Parameters.

The quadrupole splittings predicted for a large number of R_3SnL_2, R_3SnLL', and R_2SnL_2L' compounds by use of values given in Table 5.2 are shown in Table 5.3, and are compared with the quadrupole splittings observed for these compounds. The structural assignments noted are based on the agreement between predicted and observed values, and in many cases are supported by the systematics of organotin (IV) structural chemistry[10]. Only $Me_3SnPyNO_3$ (compound (11)) shows a discrepancy greater than the tolerance limit of 0.4 mm s^{-1}, indicating that the tin atom in this compound is not five-coordinate.

The three isomers of R_2SnL_3 (Fig. 51) are often readily distinguished when {L}/{R} is small, since then for given R and L we have from[20,21] eqs. (5.33) to (5.35) that $|\Delta_{VI}| > |\Delta_{IV}| > |\Delta_V|$ with differences $\geq$ 0.4 mm s^{-1}.

$$|\Delta_{IV}| \simeq (-7\{R\}^{tbe} + 8\{L\}^{tba} + \{L\}^{tbe})/\sqrt{7} \qquad (5.33)$$

$$|\Delta_V| \simeq (-2\{R\}^{tba} - 5\{R\}^{tbe} - 2\{L\}^{tba} + 8\{L\}^{tbe})/\sqrt{13} \qquad (5.34)$$

$$|\Delta_{VI}| = -4\{R\}^{tba} + 3\{L\}^{tbe} \qquad (5.35)$$

For example, if R = alkyl and L = Cl, $|\Delta_{VI}|$ = 4.36 mm s^{-1}, $|\Delta_{IV}|$ = 3.07 mm s^{-1}, $|\Delta_V|$ = 2.53 mm s^{-1}. In Table 5.3 the agreement between observed and predicted quadrupole splittings strongly suggests that compounds (33) - (41) have structure (IV). With {L'} ≠ {L} in

Table 5.3

Observed and Calculated Quadrupole Splittings for Some Organotin(IV) Compounds

Compound	Refs.	Obs. Q.S.[‡]	Calc. Q.S.[§]	Structure
(1) $Me_3SnCl(DMA)$	a	3.69	- 3.69	(I)
(2) $Me_3SnCl(HMPA)$	a	3.52	- 3.65	"
(3) $Me_3SnCl(PMPO)$	a	3.45	- 3.38	"
(4) $Me_3SnCl(Ph_3PO)$	a	3.49	- 3.63	"
(5) $Me_3SnNCS[(pip)_3PO]$	b	3.82	- 3.77	"
(6) $Me_3SnBr[(morph)_3PO]$	b	3.63	- 3.64	"
(7) $Me_3SnBr(quinoline)$	c	3.20	- 3.31	"
(8) Me_3SnCl	d	3.44	- 3.39	"
(9) Me_3SnNO_3	f	4.14	- 3.82	"
(10) $(Me_3Sn)_2(OH)N_3$	e	3.25	- 3.18	"
(11) $Me_3SnPyNO_3$	f	4.20	- 3.52	"
(12) $Ph_3SnCl(DMSO)$	b	3.19	- 3.11	(I)
(13) $Ph_3SnBr(Ph_3PO)$	b	3.20	- 3.18	"
(14) $Ph_3SnBr(DMSO)$	b	3.22	- 3.11	"
(15) $Ph_3SnCl(Ph_3PO)$	b	3.23	- 3.18	"
(16) $Ph_3SnNCS(DMSO)$	b	3.33	- 3.24	"
(17) Ph_3SnNCS	b	3.54	- 3.19	"
(18) $Ph_3SnNCS(Ph_3PO)$	b	3.48	- 3.30	"
(19) $Ph_3SnOCOCH_3$	g,o	3.32	- 3.23	"
(20) $Ph_3SnOCOCH_2I$	g	3.59	- 3.38	"
(21) $Ph_3SnOCOCH_2Cl$	g,o	3.50	- 3.45	"

Table 5.3 (cont'd.)

(22) $Ph_3SnOCOCH_2Br$	g	3.51	- 3.45	"
(23) $Ph_3SnOCOCHCl_2$	g,o	3.77	- 3.63	"
(24) $Ph_3SnOCOCCl_3$	g	3.97	- 3.69	"
(25) $Ph_3SnOCOCF_3$	g	4.00	- 3.77	"
(26) Ph_3SnF	d	3.58	- 3.37	"
(27) Ph_3SnOH	d	2.73	- 2.41	"
(28) Ph_3SnN_3	d	3.19	- 3.05	"
(29) $Ph_3SnCl(Ph_3AsO)$	p	3.09	- 2.89	"
(30) $[Ph_3Sn(opo)]BPh_4$	h	3.52	- 3.88	(III)
(31) $[Ph_3Sn(diphoso)]BPh_4$	h	3.56	- 3.70	(III)
(32) $Ph_3Sn(BzBz)$	h	- 2.25	+ 1.98	(II)
(33) $(alkyl)_2SnCl(oxin)$	j,q	- 3.12	+ 2.92	(IV)
(34) $Et_2SnI(oxin)$	j	2.85	+ 2.80	(IV)
(35) $Et_2SnNCS(oxin)$	j	3.07	+ 3.02	(IV)
(36) $Ph_2SnCl(oxin)$	j,q	+ 2.40	+ 2.53	(IV)
(37) $[Et_4N][Ph_2SnCl_3]$	k	2.62	+ 2.59	(IV)
(38) $Ph_2SnCl_2(Ph_3PO)$	l	2.98	+ 2.77	(IV)††
(39) $Ph_2SnCl_2(Ph_3AsO)$	l	2.83	+ 2.57	(IV)‡‡
(40) $Ph_2SnCl(BzBz)$	h	2.61	+ 2.65	(IV)
(41) $Ph_2SnCl_2[(alkyl)_2SO]$	n	3.05	+ 2.73	(IV)††

‡ $\frac{1}{2} e^2qQ(1 + \frac{1}{3}\eta^2)$ in units of mm s^{-1}. Values are unweighted averages, where appropriate, of measurements at or below 80 K. Signs are explicitly stated only when an experimental determination is known to us.

Table 5.3 (cont'd.)

§ Calculated for the structure noted by use of the parameters in Table 5.2, with the additional assumptions: $\{PMPO\}^{tba} = \{PyO\}^{tba}$, $\{(pip)_3PO\}^{tba} = \{HMPA\}^{tba} = \{(morph)_3PO\}^{tba}$, $\{quinoline\}^{tba} = \{Py\}^{tba}$, and $\{(alkyl)_2SO\}^{tba} = \{DMSO\}^{tba}$.

See Figs. 5.1 and 5.4.

¶ Discrepancy between observed and calculated values indicates that compound is not trigonal-bipyramidal.

†† Axial Ph_3PO and $(alkyl)_2SO$ give slightly better fit than equatorial.

‡‡ Axial and equatorial Ph_3AsO indistinguishable.

a J.C. Hill, R.S. Drago and R.H. Herber, J. Am. Chem. Soc., 91, 1644, (1969).

b Ref. 19.

c J. Nasielski, N. Sprecher, J. de Vooght and S. Lejeune, J. Organomet. Chem., 8, 97, (1967).

d Average of values collected in Ref. 3.

e N. Bertazzi, G. Alonzo, R. Barbieri and R.H. Herber, J. Organomet. Chem., 65, 23, (1974).

f D. Potts, H.D. Sharma, A.J. Carty and A. Walker, Inorg. Chem., 13, 1205, (1974).

g B.F.E. Ford and J.R. Sams, J. Organomet. Chem., 31, 47, (1971).

h This work.

j R.C. Poller and J.N.R. Ruddick, J. Chem. Soc. (A), 2273, (1969).

k Ref. 17.

l F.P. Mullins, Can. J. Chem., 49, 2719, (1971).

Table 5.3 (cont'd.)

n R.S. Randell, R.W.J. Wedd and J.R. Sams, J. Organomet. Chem., 30, C19, (1971).

o Average of values collected by P.J. Smith, Organomet. Chem. Rev. A, 5, 373, (1970).

p R.W.J. Wedd and J.R. Sams, Can. J. Chem., 48, 71, (1970).

q Ref. 13.

R_2SnL_2L', structures (IV) and (V) have two isomers, namely L' axial and L' equatorial. However, with {L} being small the quadrupole splittings of the two structures are scarcely distinguishable.

Compounds (32) and (33) in Table 5.3 illustrate that the predicted additive-model prediction of sign is unreliable when η is large. Here, as in cis-octahedral systems[16], the discrepancies may be attributed to distortions from ideal geometry[13].

When compound (11) is excluded the agreement in Table 5.3 is generally very good, the observed and calculated values of $|QS|$ having a correlation coefficient $r = 0.94$. However, close inspection reveals that the calculated magnitudes tend to underestimate slightly the observed ones, on average by about 0.09 mm s^{-1}. This would indicate that a slight revision of the parameters in Table 5.2 may be advisable. In particular the pqs parameters for Ph were based on rather limited data, yet $\{Ph\}^{tbe}$ especially is quite severely tested in Table 5.2 since many of the compounds contain this ligand in an equatorial position.

Quadrupole splittings involving less-common ligands not listed in Table 5.2 may often be rationalized by self-consistent methods. Consider, for example, the $RSn[(OC_2H_4)_2N]$ and $R_2Sn[(OC_2H_4)_2NR']$ species[22] shown in Table 5.4. The geometrical requirements of the ligand ensure that in $RSn[(OC_2H_4)_3N]$ R and N occupy the axial positions. Thus, setting $\{R'_3N\}^{tba} = \{pip\}^{tba}$, compounds (1) to (4) in Table 5.4 give $\{-C_2H_4O\}^{tbe} = -0.06$ mm s^{-1}. The quadrupole splitting then predicted for $R_2Sn[(OC_2H_4)_2NR']$ with structure (V) is 1.95 mm s^{-1}, in agreement

Table 5.4

^{119}Sn Mössbauer Data of $RSn[(OC_2H_4)_3N]$ and $R_2Sn[(OC_2H_4)_2NR']$ Species*

	Compound	Centre shift† (mm s^{-1})	Quad.split (mm s^{-1})	ρ = QS/CS
(1)	$CH_3Sn[(OC_2H_4)_3N]$	1.04	1.64	1.58
(2)	$C_2H_5Sn[(OC_2H_4)_3N]$	1.20	1.72	1.43
(3)	$(n\text{-}C_4H_9)Sn[(OC_2H_4)_3N]$	0.91	1.74	1.91
(4)	$C_6H_5Sn[(OC_2H_4)_3N]$	0.94	1.66	1.77
(5)	$(n\text{-}C_4H_9)_2Sn[(OC_2H_4)_3NH]$	0.91	2.20	2.42
(6)	$(n\text{-}C_4H_9)_2Sn[(OC_2H_4)_2N(C_6H_4CH_3)]$	0.85	2.23	2.62
(7)	$(C_2H_5)_2Sn[(OC_2H_4)_2NC_2H_5]$	0.96	2.16	2.25

* Taken from Ref. 22. † Relative to $BaSnO_3$

Table 5.5

Observed and Calculated Quadrupole Splittings in $[Ph_2Sn(OCOR)]_2$ Dimers

	Compound	Obs.QS*	Calc.QS*
(1)	$Ph_4Sn_2(OCOCH_3)_2$	3.70	≠
(2)	$Ph_4Sn_2(OCOCH_2Cl)_2$	3.85	3.92
(3)	$Ph_4Sn_2(OCOCCl_3)_2$	4.10	4.16
(4)	$Ph_4Sn_2(OCOCF_3)_2$	4.35	4.24
(5)	$Ph_4Sn_2(OCOC_6H_5)_2$	3.50	3.33#

* Units are mm s^{-1}; observed values taken from Ref. 23.

≠ This compound used to derive $\{SnL_2R_2^{\circ}\}^{tbe}$ = - 1.38 mm s^{-1}.

\# Assume $pqs^{tba} \cong BzBz^{tba}$

with observation for compounds (5) to (7).

Another interesting example is provided by the $[Ph_2SnO_2CR]_2$ dimers (Table 5.5), which are five-co-ordinate with an equatorial Sn-Sn bond and bidentate RCO_2^- ligands bridging axial positions[23]. Thus each moiety is an R_2SnL_2M system with quadrupole splitting given by[20, 21] eq. (5.36), where for the compounds in Table 5.5, R ≡ Ph, M = SnL_2R_2,

$$|\Delta| = [7\{R\}^{tbe\,2} - 2\{R\}^{tbe}\{M\}^{tbe} + 4\{M\}^{tbe\,2} - 16\{R\}^{tbe}\{L\}^{tba} - 8\{M\}^{tbe}\{L\}^{tba} + 16\{L\}^{tba\,2}]^{1/2} \qquad (5.36)$$

and L = CH_3CO_2, CH_2ClCO_2, CCl_3CO_2, CF_3CO_2, or $C_6H_5CO_2$. From compound (1) we get $\{SnL_2R_2\}^{tbe}$ = - 1.38 mm s^{-1}. The splittings calculated by use of this value for compounds (2) to (5) are consistent with observation.

Many other systems could be illustrated. For example, in the $R_2SnCl(S_2CNR'_2)$ compounds[24] the observed quadrupole splittings of ca. 3 mm s^{-1} for R = alkyl and ca. 2.3 mm s^{-1} for R = Ph are clearly consistent with the equatorial R_2SnL_3 structure (IV), in agreement with an X-ray study[25] of $Me_2SnCl(S_2CNMe_2)$.

Notice that throughout the data discussed in this study there is little correlation between the quadrupole splittings and centre shifts. Values of the ratio (ρ) of quadrupole splitting to centre shift relative to SnO_2 are listed in Tables 4.5, 5.5 and 5.6, assuming that $BaSnO_3$ has zero shift relative to SnO_2. The ratio ρ

Table 5.6

ρ Values for Some Five-coordinate R_3SnL_2 Compounds

Compound	Ref.	Quad.split‡	Centre shift§	ρ=QS/CS
Ph_3Sn(oxin)	a	1.75	1.07	1.64
Ph_3Sn(BzBz)	b	2.25	1.13	1.99
Ph_3Sn(BzAc)	b	2.25	1.08	2.08
Ph_3Sn(ONPhCOPh)	c	1.94	1.26	1.54
Pr_3Sn(ONPHCOPh)	c	2.65	1.50	1.77
Me_3Sn(ONPhCOPh)	c	2.36	1.34	1.76
Me_3Sn(ONhCOPh)	c	2.74	1.37	2.00
$(Et_3NH)[Ph_3Sn(ONCOPh)]$	c	1.74	1.23	1.41

‡ Units are mm s^{-1}.

§ Units are mm s^{-1}; relative to SnO_2 with $BaSnO_3$ assumed to have zero shift.

a Ref. 6 and R.C. Poller and J.N.R. Ruddick, J. Chem. Soc. (A), 2273, (1969).

b This work.

c P.G. Harrison, Inorg. Chem., 12, 1545, (1973).

has been suggested[26] as a criteria of coordination number, with $\rho >$ ca. 2.1 characteristic of coordination numbers greater than four. However, the data show that ρ varies above and below 2.1 even in closely related compounds.

E. Partial Quadrupole Splittings for Five Coordinate ^{121}Sb (V)

The quadrupole coupling constant (e^2qQ) in ^{121}Sb compounds may be observed by the 37.15 Kev $\frac{5+}{2} \leftrightarrow \frac{7+}{2}$ Mössbauer resonance. The partial quadrupole splittings for ^{121}Sb (V) are defined by eqs. (5.37), (5.38) in mm s^{-1}. It is important to realize that 'pqs' for ^{121}Sb (V) in fact measures the 'partial quadrupole coupling constant'.

$$\{L\}^{tba} = e^2|Q|([L]^{tba} - [X]^{tba}) \qquad (5.37)$$

$$\{L\}^{tbe} = e^2|Q|([L]^{tbe} - \tfrac{4}{3}[X]^{tba}) \qquad (5.38)$$

Studies of isoelectronic isostructural Sn (IV) and Sb (V) compounds show that ^{121}Sb (V) coupling constants are +6.76 times the corresponding ^{119}Sn quadrupole splittings[5,8]. In Table 5.7 pqs values obtained by use of this multiplying factor are compared with values previously derived by ad hoc methods[9]. With the exception of $\{Ph\}^{tba}$, the two procedures are in good agreement, with the results presented here resolving the sign of $\{Cl\}^{tbe}$.

In Table 5.8, coupling constants calculated by use of ^{119}Sn - derived pqs are compared with observed values[9,27] for a number of trigonal-bipyramidal Sb (V) compounds. The agreement

Table 5.7

Estimated Partial Quadrupole Splitting Parameters for Trigonal-Bipyramidal Organoantimony(V) Compounds*

Ligand	$\{L\}^{tba}$ This work†	(mm s^{-1}) Ref. 9	$\{L\}^{tbe}$ This work†	(mm s^{-1}) Ref. 9
Cl	0 ‡	0 ‡	+ 1.34‡	± 0.9
Br	0 ‡	- 0.2	+ 1.34‡	
alkyl	- 6.37		- 7.62	- 8.0
Ph	- 6.00	- 7.2	- 6.62	- 6.9
F	+ 0.75	+ 0.3		
I	- 0.54	- 0.7		
NO_3	+ 0.75	+ 0.2		
NCS	+ 0.44	- 0.1		
OCOMe	+ 0.51			
OH	- 0.87	- 0.3		

* $\{L\}^{tba}$ and $\{L\}^{tbe}$ for ^{121}Sb are defined in eqs. (5.37) and (5.38). For the ^{121}Sb 37.15 keV Mössbauer resonance 1 mm s^{-1} = 29.96 MHz.

† 6.76 × [^{119}Sn pqs parameter given in Table 5.2].

‡ Here and in Ref. 9 $\{Cl\}^{tba}$ = 0 by definition; we also take $\{Br\} \equiv \{Cl\}$ for both tba and tbe.

Table 5.8

Observed and Calculated Quadrupole Coupling Constants for Some Organoantimony(V) Compounds

Compound	Obs. $[e^2qQ]$ (mm s^{-1})[a]	Calc. $[e^2qQ]$ (mm s^{-1})[a] This work	Ref. 9
(1) Ph_3SbF_2	- 22.0	- 22.8	b
(2) Ph_3SbCl_2	- 20.6	- 19.9	b
(3) Ph_3SbBr_2	- 19.8	- 19.9	b
(4) Ph_3SbI_2	- 18.1	- 17.7	b
(5) $Ph_3Sb(NO_3)_2$	- 21.3	- 22.8	b
(6) $Ph_3Sb(NCS)_2$	- 20.4	- 21.6	b
(7) $Ph_3Sb(OCOMe)_2$	- 20.9[a]	- 21.9	
(8) Me_3SbCl_2	- 24.0	- 22.9	b
(9) Me_3SbBr_2	- 22.1	- 22.9	- 23.2
(10) Ph_4SbF	- 7.2	- 9.4	- 6.9
(11) Ph_4SbCl	- 6.2	- 7.9	b
(12) Ph_4SbBr	- 6.8	- 7.9	- 5.9
(13) Ph_4SbNO_3	- 6.4	- 9.4	- 6.7
(14) Ph_4SbOH	- 5.3	- 6.1	b
(15) Ph_4SbNCS	- 6.4	- 8.7	- 6.1 b

a. Assuming ideal trigonal-bipyramidal geometry with electronegative ligands apical.

b In Ref. 9 these coupling constants were used to calculate pqs parameters.

for R_3SbL_2 species is good. However, the calculated values for Ph_4SbL species are always larger than the observed values (by up to ~3 mm s^{-1}). This discrepancy is probably due to a smaller $|\{Ph\}^{tba}|$ value (6.00 mm s^{-1}) compared with previously derived value (7.2 mm s^{-1}). However, the ^{119}Sn data discussed above indicates that $|\{Ph\}^{tba}| < |\{Ph\}^{tbe}|$. Thus it seems that Ph_4SbL and the unknown Ph_4SnL may not be strictly comparable, even though X-ray structure of $Ph_5Sb.C_6H_{12}$ is consistent with $\{R\}^{tba}/\{R\}^{tbe} < 1$ in terms of a literal point charge model.

Table 5.9 shows the relevant bond lengths for related Sn (IV) and Sb (V) structures. It is apparent that the difference between axial and equatorial Sb-C distances at ca. 0.09 Å is larger than that (0.03 Å) observed for the two Sn (IV) compounds. The (perhaps unexpected) possibility that, for a given ligand A, larger σ_A values seem to be associated with longer bonds also follows from the positive ($\sigma_A^{tba} - \sigma_A^{tbe}$) values, since axial Sn-ligand bonds tend to be longer than equatorial ones[10]. However, it is very difficult to assess the validity of this point because the relationship of bond length to partial field gradients is complicated by other factors.

Finally, six coordinate structure may be assigned to Ph_2SbCl_3 by the methods used in this Section. From Table 5.4 the calculated coupling constant for a trigonal-bipyramidal structure with equatorial phenyls is + 17.9 mm s^{-1}, whereas the coupling constant for a trans-phenyl octahedral structure with bridging chlorine is + 25.7 mm s^{-1}. The observed value[7] of + 25.9 mm s^{-1} is consistent with the octahedral structure.

Table 5.9

Metal-Ligand Bond Lengths in Some Trigonal-Bipyramidal Sn(IV) and Sb(V) Compounds

Compound†	Ref.	Metal-carbon Distances*		Metal-oxygen*
		equatorial‡	axial	axial
Ph_4SbOH	a	2.128	2.218	2.048
Ph_4SbOCH_3	b	2.118	2.199	2.061
$Ph_3Sb(OCH_3)_2$	b	2.120		2.033
Ph_5Sb, C_6H_{12}	e	2.14	2.24	
$Ph_3Sn(BzBz)$	c	2.165	2.180	2.276
$Ph_3Sn(ONPhCOPh)$	d	2.14	2.18	2.31

* Units are Å

† For abbreviations

‡ Averaged where appropriate

a A.L. Beauchamp, M.J. Bennett and F.A. Cotton, J. Am. Chem. Soc., 91, 297 (1969).

b K-W. Shen, W.E. McEwen, S.J. LaPlaca, W.C. Hamilton and A.P. Wolf, J. Am. Chem. Soc., 90, 1718 (1968). c Ref. 4. d T.J. King and P.G. Harrison, Chem. Commun., 815 (1972). e C. Brabant, B. Blanck and A. Beauchamp, J. Organomet. Chem., 82, 231 (1974).

F. Conclusion

This study essentially completes the additive treatment of ^{119}Sn Mössbauer quadrupole splittings in terms of the molecular orbital model previously developed by Clark et al[1]. The 'working values' of different pqs parameters for tetrahedral, trigonal-bipyramidal, and octahedral structures seem to give a very consistent description of the relationship between quadrupole splittings and structures of organotin (IV) compounds in spite of distortion. The calculated ratio of pqs parameters is in good agreement with that predicted by theory. For example, the predicted ratio for R, $\{R\}^{tet} : \{R\}^{oct} : \{R\}^{tba} : \{R\}^{tbe}$ = 1.5:1:1:1.33 is compared with the calculated ratio 1:45:1.10:1:1.20 respectively. This consistency thus gives us some insight into the structure and bonding of organotin chemistry. These pqs values can also lead to synthesis of new compounds. From Fig. 5.3 it is seen that quadrupole splittings in R_3SnL_2 span almost the entire range of splittings observed in tetrahedral R_3SnL and octahedral R_2SnL_4 species. It would appear that in general a particular range of quadrupole splittings cannot be uniquely associated with a particular coordination, and that reliable structural information can only be deduced by use of either unbiassed pqs values or a regression method of the type outlined in this chapter.

Finally, the advantages of using S_{02} parameters[20,21] in the QS calculations for low symmetry structures become evident.

G. References

1. M. G. Clark, A. G. Maddock, and R. H. Platt, J. Chem. Soc. Dalton, 281; (1972).

2. M. G. Clark, in 'Molecular Structure and Properties' ed. A. D. Buckingham, MTP International Review of Science, Physical Chemistry Series 2, Vol. 2, Butterworths, London, in the press.

3. G. M. Bancroft and R. H. Platt, Advan. Inorg. Chem. Radiochem. 15, 59, (1972).

4. G. M. Bancroft, B. W. Davis, N. C. Payne, and T. K. Sham, J. Chem. Soc. Dalton, in press.

5. G. M. Bancroft, V. G. Kumar Das, and K. D. Butler, J. Chem. Soc. Dalton, 2355, (1974).

6. G. M. Bancroft, V. G. K. Das, T. K. Sham, and M. G. Clark, J. Chem. Soc. Dalton, submitted.

7. G. M. Bancroft, V. G. Kumar Das, T. K. Sham, and M. G. Clark, J. Chem. Soc. Chem. Commun., 236, (1974).

8. G. M. Bancroft, K. D. Butler, and E. T. Libbey, J. Chem. Soc. Dalton, 2643 (1972).

9. J. N. R. Ruddick, J. R. Sams, and J. C. Scott, Inorg. Chem. 13, 1503 (1974).

10. B. Y. K. Ho and J. J. Zuckerman, J. Organomet. Chem., 49, 1 (1973).

11. For the basic theory of electric field gradient tensors see M. H. Cohen and F. Reif, Solid State Phys., 5, 321 (1957).

12. P. G. Harrison and T. J. King, J. Chem. Soc. Dalton, 2298 (1974).

13. J. N. R. Ruddick and J. R. Sams, J. Chem. Soc. Dalton, 470, (1974).

14. R. V. Parish and R. H. Platt, Inorg. Chim. Acta, 4, 65 (1970).

15. H. Cramer, 'Mathematical Methods of Statistics', University Press, Princeton, 1946, Sec. 21.6.

16. R. V. Parish and C. E. Johnson, J. Chem. Soc. (A), 1906 (1971).

17. N. W. G. Debye, E. Rosenberg, and J. J. Zuckerman, J. Am. Chem. Soc. 90, 3234 (1968).

18. J. Topping, 'Errors of Observation and their Treatment', Institute of Physics and Physical Society, London, 1962.

19. J. Ensling, Ph.Gutlich, K. M. Hassellbach, and B. W. Fitzsimmons, J. Chem. Soc. (A), 1940 (1971).

20. M. G. Clark, J. Chem. Phys., 54, 697 (1971), and Molec. Phys. 20, 257 (1971).

21. Exact expressions were obtained by calculating the symmetrized parameter S_{02} (Ref. 20) and linearized approximations followed by expansion. A useful check on the linearized expressions follows from eqs (22) and (23): the algebraic sum of the coefficients of $\{\ \}^{tba}$ terms and 4/3 x coefficients of $\{\ \}^{tbe}$ terms must be zero, provided that if apical X is present $\{X\}^{tba}$ must be explicitly included in the expression even though $\{X\}^{tba} = 0$.

22. A. Tzschach, K. Ponicke, L. Korecz, K. Burger, J. Organomet. Chem. 59, 199 (1973).

23. M. Delmas, J. C. Maire and Y. Richard, J. Organomet. Chem., 30, C101, (1971).

24. B. W. Fitzsimmons and A. C. Sawbridge, J. Chem. Soc. Dalton, 1678 (1972).

25. K. Furue, T. Kimura, N. Yasuoka, N. Kasai, and M. Kakudo, Bull. Chem. Soc. Jap. 43, 1661 (1970).

26. R. H. Herber, H A. Stockler, and W. T. Reichle, J. Chem. Phys., 42, 2447 (1965).

27. G. G. Long, J. G. Stevens, R. J. Tullbane, and L. H. Bowen, J. Am. Chem. Soc., 92, 4230 (1970).

CHAPTER 6

Mössbauer Effect Study of Electron Spin Relaxation and Radiolytic Effects in Tris(acetylacetonato)Fe(III) Diluted in Tris-(acetylacetonato)Al(III) and in Tris(acetylacetonato)Ga(III)

A. Introduction

The application of Mössbauer spectroscopy to the studies of electron spin relaxation and ^{60}Co γ ray irradiation effects in diluted tris(acetylacetonato) Iron(III), $[Fe(AcAc)_3]$, systems are discussed in this chapter.

It has been known for some time that the fluctuating hyperfine fields felt by the nucleus in a paramagnetic ion can influence the nuclear transitions markedly.[1] This phenomenon has been successfully shown by the use of the Mössbauer effect in recent years.[2-6] For example, Wignall[2] has reported Mössbauer line broadening in Fe(III) high spin systems; and actually observed a partially resolved paramagnetic hyperfine pattern in a frozen solution spectrum of magnetically diluted $Fe(AcAc)_3$ at low temperature. These results have been attributed to the spin-spin relaxation of the paramagnetic electronic states, since the observed line broadening does not in general depend upon the temperature, but depends upon the Fe-Fe distances. Wertheim et al[3] have observed the paramagnetic hyperfine splitting (mainly due to $|\pm\frac{5}{2}>$ and $|\pm\frac{3}{2}>$) in the Mössbauer spectrum of $^{57}Fe^{3+}$ in corundum. Moreover Wickman et al[4,5] have investigated the temperature, concentration and external magnetic field dependent hyperfine structures in the Mössbauer spectrum of metalloprotein A and discussed the possible mechanisms[5] which account

for the observed patterns. Blume[6] has also proposed a simple relaxation model in terms of fluctuating electromagnetic fields.

The paramagnetic hyperfine structures[5] so far observed are typified by the change of Mössbauer line shape. This shape depends rather critically upon the rate of electronic relaxation responsible for the magnetic hyperfine fields felt by the nucleus. As mentioned in Chapter 1, the theory of this phenomenon is very complicated except in two extreme cases. First, a very slow electron spin relaxation rate of an electronic state (e.g. $| \pm \frac{5}{2} >$) will give a six line pattern, provided that the effective field approximation is valid; and second, a very rapid relaxation will give a doublet or singlet pattern. Several models have been proposed for the interpretation of the relaxation effect[5,6]. Theoretical details can be found in two papers[7] by Blume and Tjon, and will not be discussed in this context. The objective of the spin-relaxation experiment, described in this chapter, is an attempt to resolve the Mössbauer paramagnetic hyperfine structures in $Fe(AcAc)_3$ by diluting $Fe(AcAc)_3$ in a diamagnetic matrix such as $Ga(AcAc)_3$ and $Al(AcAc)_3$ which have similar molecular structures. If spin spin relaxation is important to the change of line shapes, the Mössbauer line widths of the diluted $Fe(AcAc)_3$ are expected to broaden and eventually split into six lines, as the concentration of $Fe(AcAc)_3$ decreases. If, on the other hand, the spin-lattice relaxation is important, the widths are expected to become more narrow as the temperature increases.

The Mössbauer effect also plays an important role in studies of radiation effects[9] in solids, and of some other closely related areas of chemical physics, such as EC (electron capture)[9]- decay and high

pressure effects[11]. If these effects are studied in a solid containing a Mössbauer nucleus, their physical and chemical consequences can sometimes be conjectured from the additional features in their Mössbauer spectra. Thus Bancroft et al[12] have obtained narrow line widths and resolved the QS in Mössbauer spectra of $Fe(AcAc)_3$ by ^{60}Co γ-irradiation ($\sim 10^8$ rad). Sano et al[13] have found that the Mössbauer absorption spectra of $Fe(AcAc)_3$ irradiated with ^{60}Co γ rays ($\sim 10^9$ rad) are the same as the emission spectra of a ^{57}Co-labelled $Co(AcAc)_3$ source after E-C (both spectra indicate the presence of Fe(II) species), whereas Friedt et al[14] have observed the same phenomenon by electron radiation (2 Mev). Drickamer et al[11] have also observed Fe(II) species in the Mössbauer spectra of $Fe(AcAc)_3$ under high pressure.

In section B, the Mössbauer spectra of $Fe(AcAc)_3$ diluted in $Al(AcAc)_3$ and in $Ga(AcAc)_3$, as a function of $Fe(AcAc)_3$ concentration and temperature are discussed. At constant temperature, the Mössbauer absorption peak broadens as the concentration of $Fe(AcAc)_3$ decreases. However, the spectra of the diluted samples also show temperature dependent effects. Moreover, the paramagnetic hyperfine structures are resolved at low temperature (4.2 °K) and low $Fe(AcAc)_3$ concentration (1%).

The studies of the effect of γ irradiation on diluted $Fe(AcAc)_3$ solids are reported in section C. The comparatively narrow line widths of the irradiated $Fe(AcAc)_3$ diluted in $Al(AcAc)_3$ matrix are consistent with previous results.[12] At low concentrations, Fe(II) species were detected in $(Fe{\cdot}Al)(AcAc)_3$ systems. The $(Ga{\cdot}Fe)(AcAc)_3$ solid samples, however, showed high radiation stability.

B. Electron Spin Relaxation Effects in Mössbauer Spectra: ^{57}Fe in $Fe(AcAc)_3$ Diluted in $Al(AcAc)_3$ and in $Ga(AcAc)_3$

1. Experimental Results

The velocity spectra obtained at 110°K with $Fe(AcAc)_3$ diluted in $Al(AcAc)_3$ are shown in Fig. 6.1. Mössbauer parameters recorded at 110°K and room temperature are given in Table 6.1. The neat $Fe(AcAc)_3$ spectrum shows a broad line of half-widths $\Gamma = 1.97 \pm 0.02$ and 1.72 ± 0.02 mm s^{-1} at 110°K and room temperature respectively. A centre shift of 0.80 ± 0.01 observed at 110°K is consistent with previous results[2]. As the concentration was decreased, a continuous broadening of the line width occurred. At a concentration of 3.3% $Fe(AcAc)_3$, the line width of 13.97 ± 1.83 mm s^{-1} was observed, whereas at a concentration of 1% $Fe(AcAc)_3$ (99% Fe enriched sample), some hyperfine features began to show (Fig. 6.2).

To demonstrate that a large portion of the $Fe(AcAc)_3$ were effectively separated in the host matrix, several independent experiments have been performed. The esr spectra of these samples at 10 GC sec^{-1} were measured at room temperature. Line width narrowing effects characteristic of spin-spin relaxation[15] were observed, as the $Fe(AcAc)_3$ concentration was decreased. This result is consistent with previous esr experiments[16].

Mössbauer spectra of samples prepared by grinding $Fe(AcAc)_3$ and $Al(AcAc)_3$ in proportion were obtained at 110°K. However, no line width broadening was observed, even at a concentration of 10% $Fe(AcAc)_3$ ($\Gamma = 1.80$ mm s^{-1}). This indicates that the observed

Table 6.1

^{57}Fe Mössbauer Parameters[a] of $(Fe.Al)(AcAc)_3$ at 110 ± 5°K and Room Temperature

%wt $Fe(AcAc)_3$	CS(110°K)	CS(R.T.)	Γ (110°K)	Γ(R.T.)
100	0.80	0.73	1.97	1.72
50	0.85	0.76	2.89	2.24 ± 0.12
30	0.86	0.80	3.71	2.78 ± 0.08
20	0.86	0.87 ± 0.11	4.48 ± 0.10	3.11 ± 0.27
15	0.78	0.72 ± 0.19	5.30 ± 0.10	3.53 ± 0.50
10	0.69 ± 0.12	0.60 ± 0.21	7.84 ± 0.44	4.78 ± 0.60
5.5[b]	0.89 ± 0.09	0.88 ± 0.13	9.23 ± 0.38	5.97 ± 0.38
3.3[b]	0.94 ± 0.29	---	13.97 ± 1.83	---
1[b,c]	0.98	---	14.8 ± 0.29	---

a. Errors ≤ |0.05| mm s^{-1}, except specified. Reproducibility for concentration < 15% are ± 0.3 mm s^{-1}. All samples are enriched with ~10% ^{57}Fe except specified. CS are relative to sodium nitroprusside.

b. χ^2 are substantially greater than 500.

c. ~90% ^{57}Fe enriched.

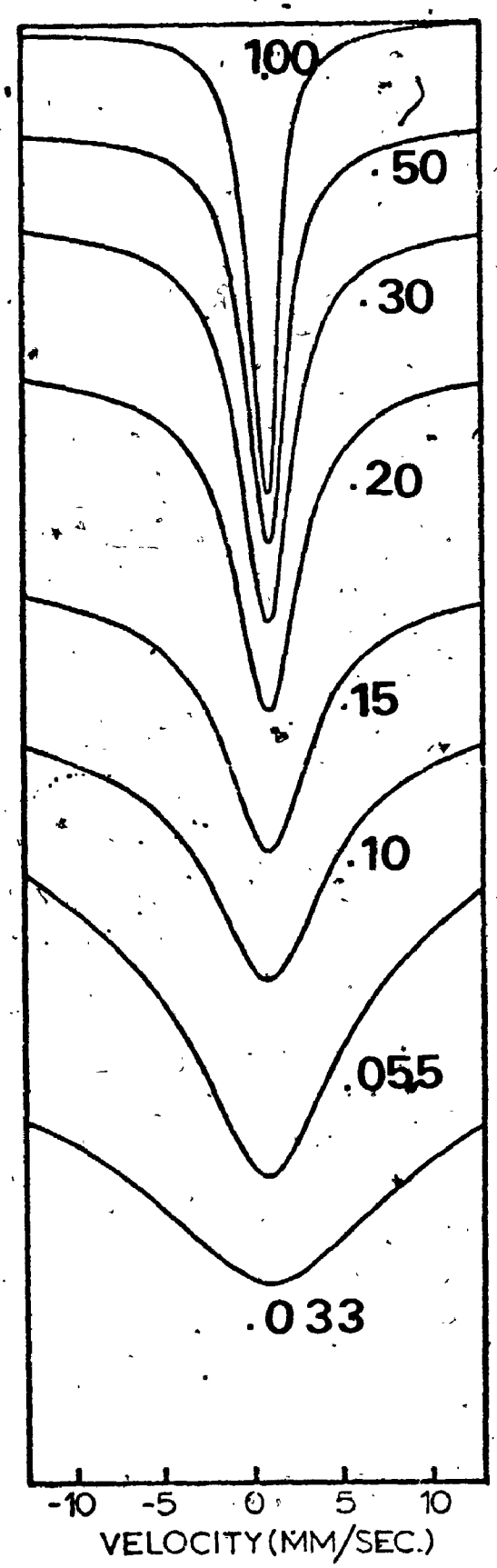

Figure 6.1 Mössbauer Spectra(110°K) of $Fe(AcAc)_3$ Diluted in $Al(AcAc)_3$

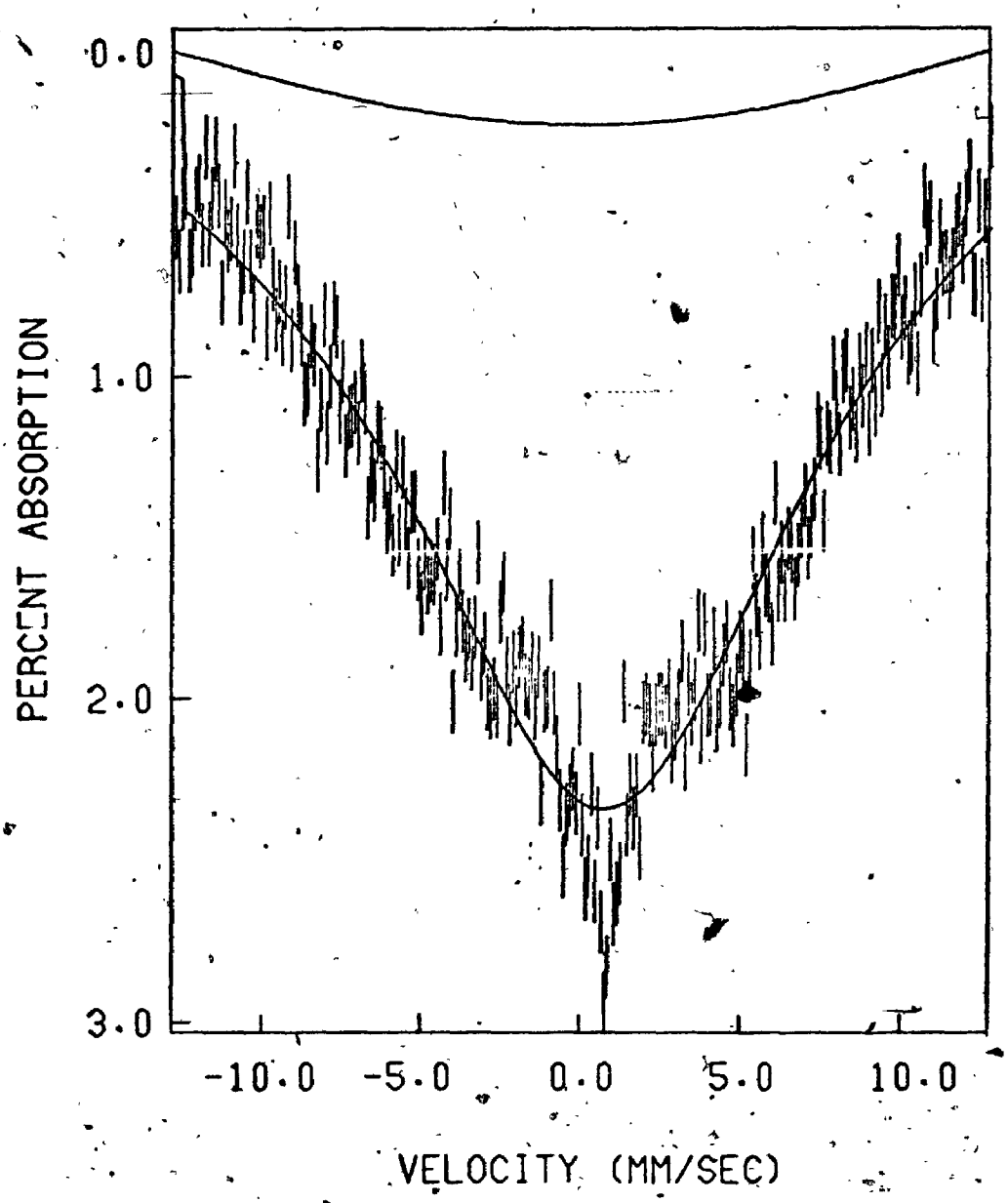

Figure 6.2 Mössbauer Spectrum of the 1% (Fe·Al)$(AcAc)_3$ Sample taken at 110°K

broadening (Fig. 6.1) is mainly due to an effective Fe-Fe separation. It is believed that $Fe(AcAc)_3$ and $M(AcAc)_3$ form a solid solution at a concentration of lower than 10% $Fe(AcAc)_3$[13].

$K_3Fe(C_2O_4)_3.3H_2O$ and $K_3Al(C_2O_4)_3.3H_2O$ are known to form solid solutions[16]. Mössbauer spectra were obtained for solid solution samples of $K_3Fe(C_2O_4)_3.3H_2O.K_3Al(C_2O_4)_3.3H_2O$. At 110°K, a broad single line of half width $\Gamma = 2.95 \pm 0.16$ was observed for the neat $K_3Fe(C_2O_4)_3.3H_2O$. As the concentration was decreased, half widths of 4.1 ± 0.4 and 8.4 ± 0.9 mm s^{-1} were observed respectively for concentrations of 0.3 and 0.2 mole fraction of $K_3Fe(C_2O_4)_3.3H_2O$. Note that the half width of neat $K_3Fe(C_2O_4)_3.3H_2O$ reported here is significantly larger than 2.22 ± 0.05 mm s^{-1} reported previously[17]. This indicates that a high velocity scan is necessary for Mössbauer line width studies of paramagnetic systems, which give broad lines.

Similar line broadenings were also observed in the $(Ga.Fe)(AcAc)_3$ system. The results are given in Table 6.2.

The room temperature spectra of $(Fe.M)(AcAc)_3$ (M = Al. or Ga) gave substantially narrow line widths than these 110°K spectra. These results are expected for effectively diluted samples, since the line widths of neat $Fe(AcAc)_3$ and samples prepared by grinding $Fe(AcAc)_3$ and $Al(AcAc)_3$ are practically temperature independent.

Finally, good fits (χ^2 ~500) were always obtained for concentrations higher than 10%; eventhough the line shapes became less Lorentzian as the concentration was decreased. The reproducibility is in general good ($\pm$ 0.2 mm s^{-1} and in the worst cases, $\pm$ 0.5 mm s^{-1} for broader lines).

Table 6.2

^{57}Fe Mössbauer Parameters of $(Fe,Ga)(AcAc)_3$ at 110 ± 5°K

%wt $Fe(AcAc)_3$	CS (110°K)	Γ (110°K)
100	0.80	1.97
90	0.76	2.02
80	0.78	2.10
70	0.76	2.32 ± 0.09
60	0.70	2.39 ± 0.08
50	0.89 ± 0.09	2.94 ± 0.22
40	0.[illegible]0 ± 0.05	2.34 ± 0.11
30	0.60 ± 0.26	3.51 ± 0.26
20[b]	0.75 ± 0.11	4.86 ± 0.32
10[b]	0.78 ± 0.12	7.22 ± 0.46

a. Errors are ± 0.04 mm s^{-1} except specified. The 10% sample is enriched with ~10% ^{57}Fe. CS are relative to sodium nitropruiside.

b. χ^2 are substantially greater than 500.

The Mössbauer spectrum of the 1% $(Fe.Al)(AcAc)_3$ sample at $4.2^{o}K$ was run at PCMU, Harewell. The hyperfine pattern was well resolved in this spectrum Fig. 6.3). The largest internal field observed (corresponding to $S_z = \pm \frac{5}{2}$) is 550 ± 4 KOe, typical of Fe^{3+}[5]. The estimated quadrupole splitting is close to zero.

2. Discussion

As discussed in Chapter 1, two mechanisms are always responsible for line broadening[5]. The spin-spin relaxation which varies as a function of the separation of the paramagnetic centres becomes slower as the $Fe(AcAc)_3$ molecules are farther apart. The effect on the Mössbauer spectra is the continuous broadening of the single line, and eventually the appearance of the hyperfine structures.

The spin-lattice relaxation is in general unimportant to line broadening in cases of zero orbital momentum such as in Fe^{3+} iron. This has been confirmed by a previous Mössbauer study of the neat $Fe(AcAc)_3$ at different temperatures[2]. If spin-lattice relaxation is important to the Mössbauer line shape, the single broad line would become narrower as the temperature increases (faster relaxation rate).

The line broadening shown in Fig. 6.1 can now be readily rationalized. It has been shown[2] that other broadening mechanisms can only account for a small portion of the broad line observed in $Fe(AcAc)_3$ and that spin relaxation (either spin-spin or spin-lattice)

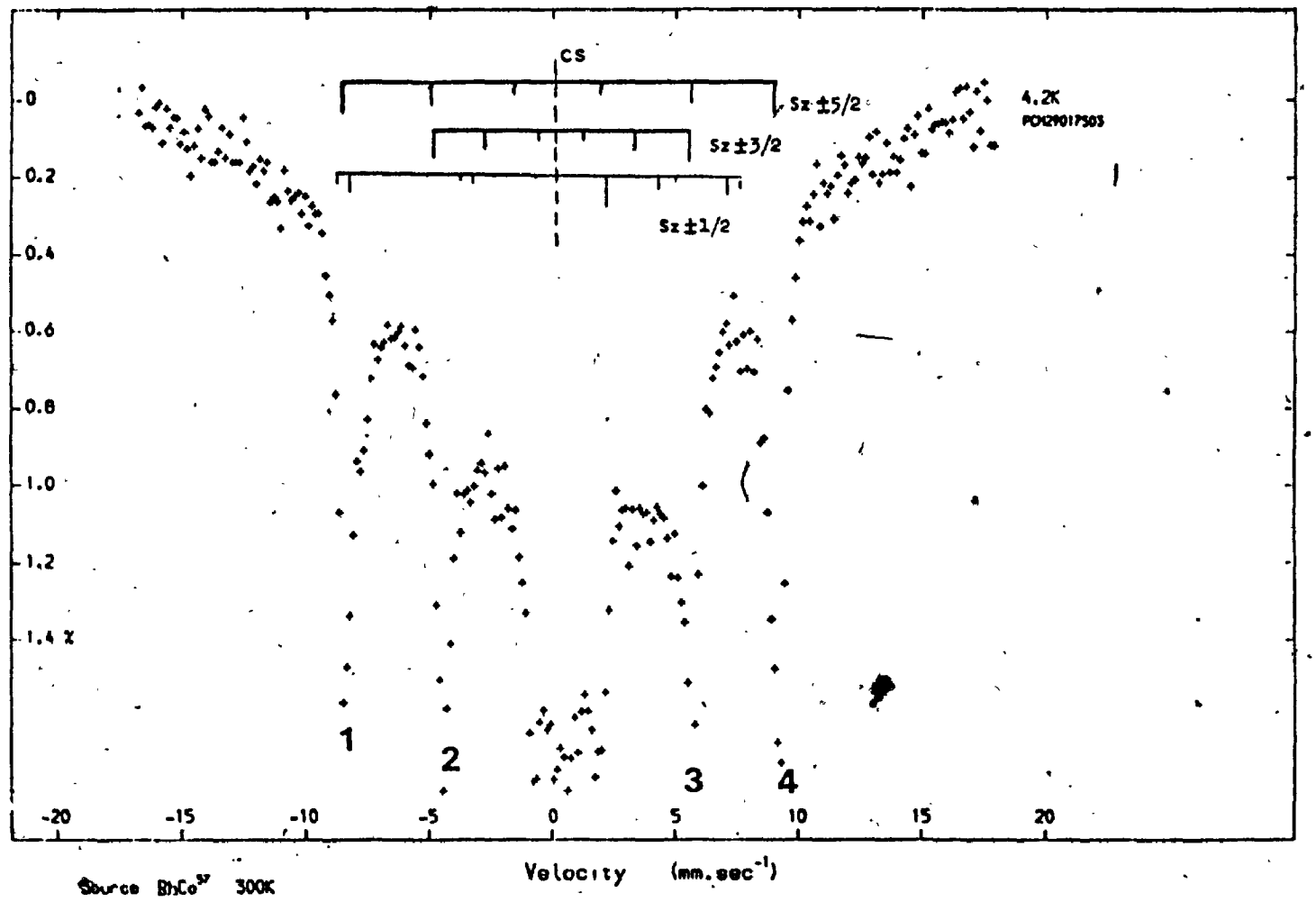

Figure 6.3 Theorectical (isotropic hyperfine) and 4.2°K Spectra of the 1% $(Fe^{\cdot}Al)(AcAc)_3$ Sample. $A = -2.58$ mm s^{-1} was used for the Calculation.

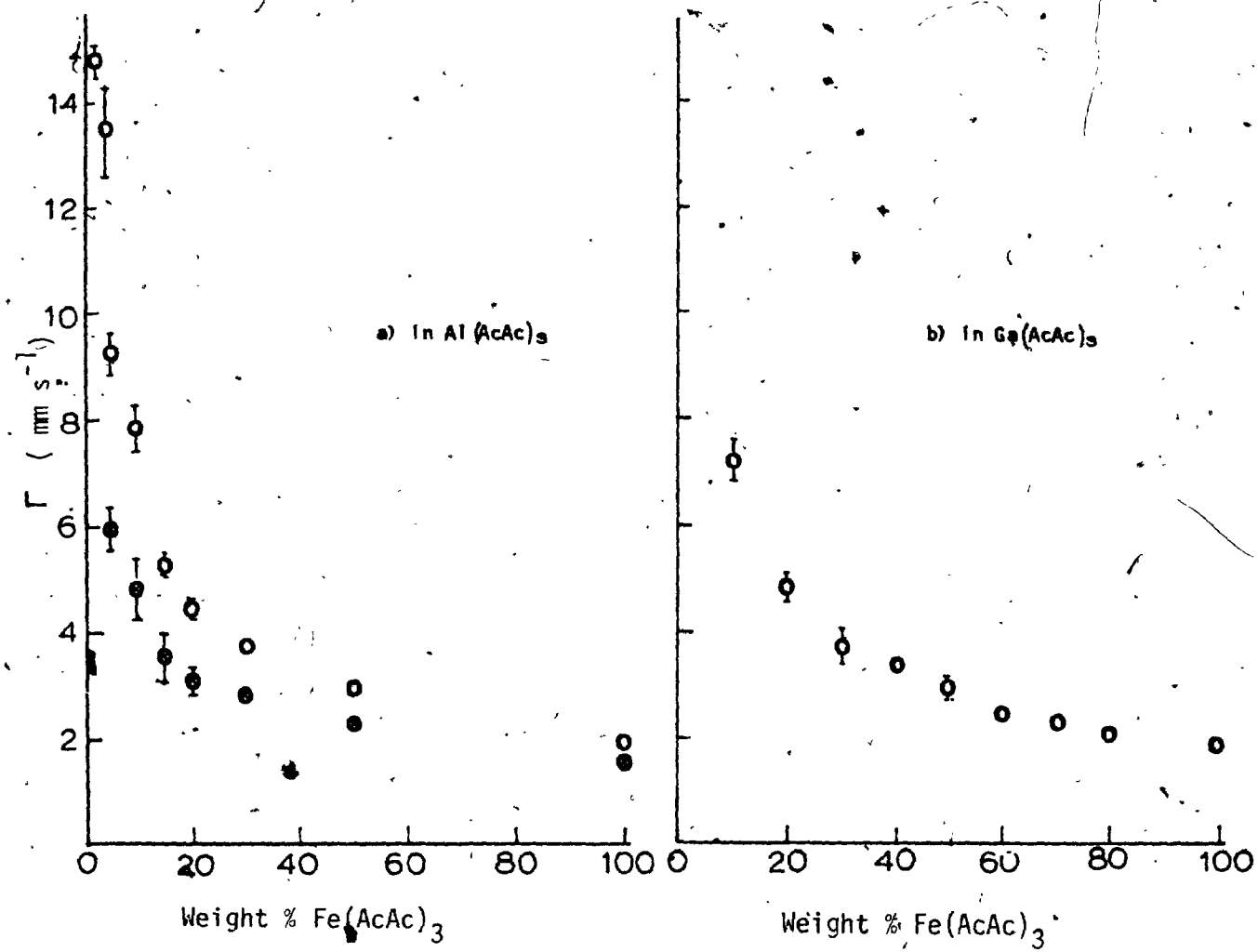

Figure 6.4 Plots of Mössbauer Line Widths vs. % Concentration of $Fe(AcAc)_3$ in (a) $Al(AcAc)_3$ (b) $Ga(AcAc)_3$

is most important. Fig. 6.4a is a plot of half widths (Γ) of $(Fe.Al)(AcAc)_3$ versus the weight % of $Fe(AcAc)_3$ at 110°K and room temperature; whereas Fig. 6.4b is a similar plot for $(Fe.Ga)(AcAc)_3$ at 110°K. From these figures, it is apparent that Γ broadens markedly as the $Fe(AcAc)_3$ concentration decreases. This is, of course, expected on the basis of electron spin-spin relaxation; since dilution reduces the relaxation rate. Similar effects have been observed in other Fe^{3+} systems studied previously[2,19].

Another striking feature is the temperature dependence of the line widths shown in Fig. 6.4a. The line widths observed at room temperature are significantly narrower than those observed at 110°K. Also, the difference in widths ($\Gamma_{110°K} - \Gamma_{R.T.}$) increases as the concentration decreases. These results are characteristic of spin lattice relaxation and thus indicate that the spin-lattice relaxation is as important as spin-spin relaxation at these temperatures. A similar trend was also observed in the $(Ga.Fe)(AcAc)_3$ system. For example, the room temperature spectrum of the 40% sample has a width of ~1.5 mm s^{-1}, which is narrower than that observed for the undiluted sample. This result consistently accounts for the narrow half widths observed in the $Ga(AcAc)_3$ matrix. It is perhaps surprising that spin-lattice relaxation is observed in a system containing an S state ion with $\langle L \rangle = 0$[5]. Although the relaxation mechanisms may be those described by Blume and Orbach[20] or by Leushin[21]; the real picture is not clearly understood at the present time.

It is evident that the paramagnetic hyperfine cannot be resolved at high temperatures such as from 110°K to room temperature.

The 1% spectrum taken at 110°K (Fig. 6.2) is obscured by spin-lattice relaxation, even though the spin-spin relaxation is sufficiently reduced in this sample. At low temperature (4.2°K), the spin-lattice relaxation is minimized and the hyperfine structures are clearly seen (Fig. 6.3).

Figure 6.3 is very similar to the frozen spectra of $Fe(AcAc)_3$[2] and spectra of some magnetically diluted Fe (III) high spin compounds[19]. There are at least four well resolved peaks (Fig. 6.3, 1 to 4). The field obtained from the outmost peaks is 550 ± 4 KOe, a value characteristic of $S_z = \pm 5/2$ states of Fe^{3+} with cubic symmetry[5]. However, the inner peaks (Fig. 6.3, 2 and 3) are broader and almost twice as intense as the outer peaks ($I_2 \simeq I_3 \simeq 2I_1 \simeq 2I_2$). In contrast to the frozen solution spectra, this intensity ratio immediately indicates that the $S_z = \pm \frac{3}{2}$ state is also resolved under this condition, whereas in the frozen solution spectra, only the $S_z = \pm \frac{5}{2}$ gives rise to resolved hyperfine structures. One must notice that the separation between the Kramers doublets in $Fe(AcAc)_3$ is less than 1°K[16]; and all the three Kramers doublets are well populated even at 4.2°K.

A better understanding of this spectrum can be achieved by considering the "Spin Hamiltonian"[5] expressed (for isotropic interaction) as

$$\mathcal{H} = A[I_z S_z + \tfrac{1}{2}(S_+ I_- + S_- I_+) + e^2 Qq[I_z^2 - 3I(I+1)] + CS \qquad (6.1)$$

This Hamiltonian represents the hyperfine interaction between the Kramer doublets and the nucleus ($I_{gr} = \frac{1}{2}$, $I_{ex} = \frac{3}{2}$) in absence of an external field and relaxation. A theoretical spectrum has been calculated according to eq. (6.1). This spectrum is also shown in Fig. 6.3, assuming H_{eff} = 550 KOe for $S_z = \pm\frac{5}{2}$, $e^2qQ \sim 0$, and a constant A for all Kramer doublets. It is important to realize that the calculations for $S_z = \pm\frac{3}{2}, \pm\frac{5}{2}$ by use of eq. (6.1) give results identical to those of the effective field approximation (AI_zS_z is the only hyperfine term involving the electron spin operator), whereas those for $S_z = \pm\frac{1}{2}$ are entirely different, since the second term $[\frac{1}{2} A(S_+I_- + S_-I_+)]$ of the Hamiltonian does not effect $S_z = \pm\frac{3}{2}$ and $\pm\frac{5}{2}$ in Mössbauer transitions. The $S_z = \pm\frac{1}{2}$ states, however, split into more energy levels than might be expected on the basis of the effective field Hamiltonian $[AI_zS_z]$. Thus more than six transitions result (Fig. 6.3) for $S_z = \pm\frac{1}{2}$. It is then apparent that the observed outer peaks (1 and 4) in Fig. 6.3. are mainly due to the transitions arising from $S_z = \pm\frac{5}{2}$; while the inner peaks (2 and 3) are due to the overlaps of the transitions arising from $S_z = \pm\frac{3}{2}$ and $S_z = \pm\frac{5}{2}$. The broader line width and higher intensity of peaks 2 and 3 compared with those of peaks 1 and 4 are entirely consistent with the calculated spectrum and with the previously observed ^{57}Fe doped α Al_2O_3 spectra[3]. The calculated lines shown for $S_z = \pm\frac{1}{2}$ are, however, not clearly seen indicating that spin-spin relaxation due to $S_z = \pm\frac{1}{2}$ is still sufficiently rapid. Thus, the central portion of the spectrum is attributed to the overlapping of a broad line arising from $S_z = \pm\frac{1}{2}$ and the central lines from $S_z = \pm\frac{3}{2}, \pm\frac{5}{2}$.

Figure 6.5

(taken from ref. 5)

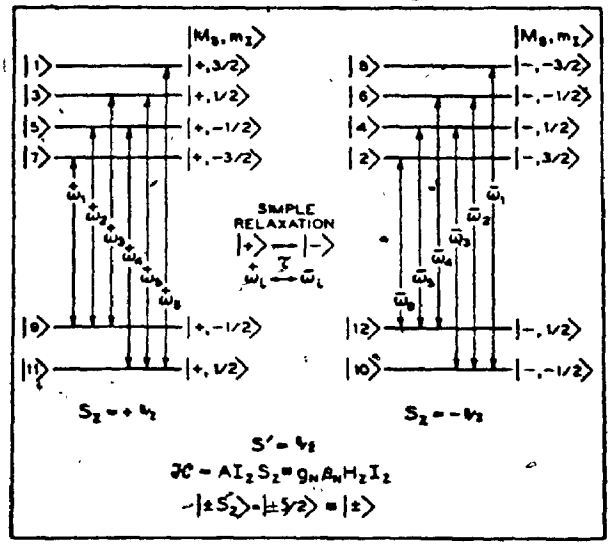

(a) Simple Relaxation Model for Mössbauer Transitions in $^{57}Fe^{3+}$ with $S_z = \pm \frac{5}{2}$

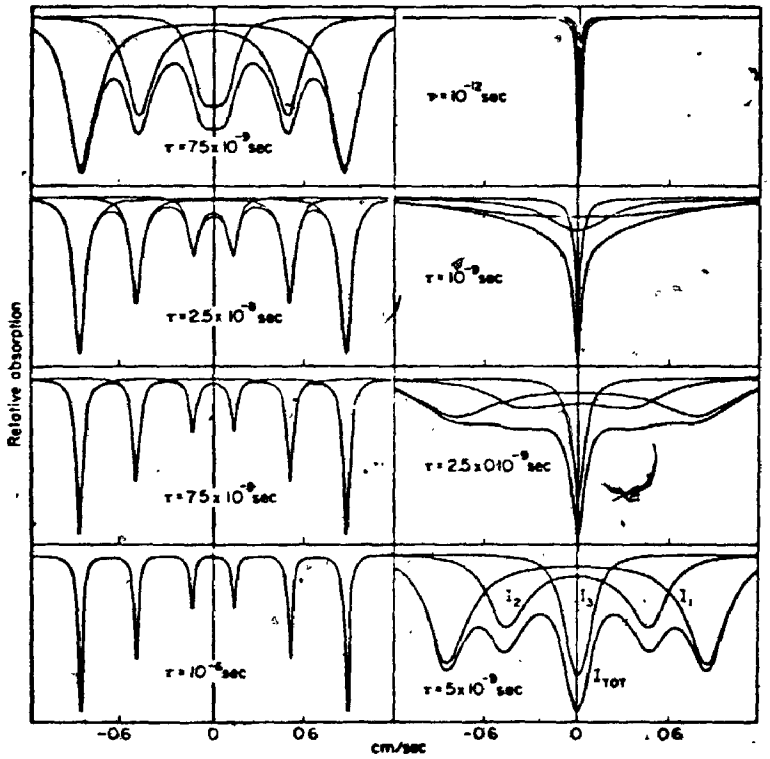

(b) Relaxation Spectra for ^{57}Fe with indicated τ Values and A Doublet, $S_z = \pm \frac{5}{2}$, with $H_{eff} = \pm 550$ KOe

The spin-spin relaxation time for the 1% (Fe.Al)(AcAc)$_3$ sample can now be estimated by comparing the observed spectrum with those (Fig. 6.5) computed by use of a spin-spin relaxation model proposed by Wickman et al[4,5]. In their model, relaxation is characterized by a relaxation time τ. For example, considering the $S_z = \pm \frac{5}{2}$ doublet (Fig. 6.5a), Mössbauer transitions $|+\frac{5}{2}, \frac{1}{2}> \rightarrow |+\frac{5}{2}, +\frac{3}{2}>$ and $|-\frac{5}{2}, +\frac{3}{2}> \rightarrow |-\frac{5}{2} + \frac{3}{2}>$ are characterized by frequences ω_6^+ and ω_6^- respectively. When the spin flips, a spin-spin relaxation, $|M_s = +\frac{5}{2}> \xrightarrow{\tau} |M_s = -\frac{5}{2}>$ occurs and the rate of this relaxtion (τ) influences the line shape. This is demonstrated in Fig. 6.5b with different τ values. This situation is analogous to proton exchange in solution and can be rationalized readily. Thus ω_6^+ and ω_6^- are analogous to ω_A and ω_B in nmr studies. The average line width of the outmost peaks in Fig. 6.3 is ca. 1 mm s^{-1} characteristic of a relaxation time $2.5 \times 10^{-8} < \tau_{\pm\frac{5}{2}} < 7.5 \times 10^{-9}$ sec; since the corresponding line widths for the theoretically calculated spectra (Fig. 6.5b) with $\tau = 2.5 \times 10^{-8}$ and $\tau = 7.5 \times 10^{-9}$ are 0.7 and 1.9 mm s^{-1} respectively. The relaxation time of the $S_z = \pm\frac{3}{2}, \pm\frac{1}{2}$ doublets cannot be easily obtained. However, it is reasonable to conjecture that $\tau_{\pm\frac{3}{2}}$ is comparable to $\tau_{\pm\frac{5}{2}}$, whereas $\tau_{\pm\frac{1}{2}}$ is faster than the other two. The complex features in the $\pm$ 2 mm s^{-1} region in Fig. 6.3 are consistent with rapid spin relaxation arising from $S_z = \pm\frac{1}{2}$.

The spectra observed at higher temperatures are best understood in terms of Blume's model[6] regardless of the origin of the relaxation which produces a fluctuating field at the nucleus. As the

temperature increases, the spin-lattice relaxation increases the rate of flipping of spin states. Thus line broadening occurs.

C. The Effect of ^{60}Co γ-Irradiation on $Fe(AcAc)_3$ and $Fe(AcAc)_3$-Diluted in $Al(AcAc)_3$ and $Ga(AcAc)_3$.

1. Results

The samples prepared for the relaxation study were irradiated at room temperature in an Atomic Canada ^{60}Co Gamma Cell 220 2.4×10^4 curies unit giving a dose rate of 1.2×10^6, 1.0×10^6, and 7.7×10^5 rads per hour during the experiment. Total doses deposited on the samples were in a range of 2.7×10^8 rads to 4.5×10^8 rads.

The Mössbauer half widths of the irradiated (Fe.Al)$(AcAc)_3$ and (Fe.Ga)$(AcAc)_3$ solids are given in Table 6.3. Both line width narrowing and radiolytic decomposition occurred in the irradiated (Fe.Al)$(AcAc)_3$ systems, whereas only line width narrowing was observed in (Ga.Fe)$(AcAc)_3$ systems at low concentrations.

The Mössbauer data of the irradiated $Fe(AcAc)_3$ (neat) are given in Table 6.4. It is interesting to note that the spectra taken six months after irradiation are similar to that taken immediately after irradiation, and that the recrystallized material is also similar to the above spectra.

The infrared spectra of all the irradiated samples were practically the same as the unirradiated samples. Also, no drastic

Table 6.3.

Fe(III) Mössbauer Parameters of γ-Irradiated (Fe.M)(AcAc)$_3$[a]

M = Al (Dose: 3.45 x 10^8 rads)

%wt Fe(AcAc)$_3$	CS (110°K)[b]	Γ (110°K)[b]
100	0.80	0.80
50	0.71	2.10 ± 0.11
30	0.79	2.93 ± 0.07
20	0.81	3.59 ± 0.09
15	0.86	4.75 ± 0.12
10[c]	0.77 ± 0.07	1.70 ± 0.10
5.5[c]	0.72 ± 0.07	1.54 ± 0.10
3.3[c]	0.80 ± 0.06	2.24 ± 0.21

M = Ga (Dose: 2.7 x 10^8 rads)

%wt Fe(AcAc)$_3$	CS (110°K)[b]	Γ (110°K)[b]
90	0.77	2.06 ± 0.11
80	0.78	2.11 ± 0.01
70	0.78	2.18 ± 0.11
60	0.82 ± 0.07	2.50 ± 0.17
50	0.88 ± 0.14	2.64 ± 0.33
40	0.64 ± 0.12	3.53 ± 0.39
30	0.82 ± 0.11	3.70 ± 0.29
20	0.91 ± 0.15	3.27 ± 0.33
10	0.82 ± 0.10	5.91 ± 0.40

a. Samples were irradiated at room temperature. Mössbauer spectra were taken shortly after irradiation.

b. Errors are ≤ |0.04| mm s^{-1} except specified.

c. Fe(II) species were also detected, see Table 6.5.

change was observed in the mass spectra of some representative samples before and after irradiation. These observations indicate that most of the compounds remained essentially unchanged after the irradiation described in this study.

Neat samples of $Fe(AcAc)_3$, $Al(AcAc)_3$ and $Ga(AcAc)_3$ were also irradiated. The X-ray powder photographs suggested that a very small amount of $Al(AcAc)_3$ might have decomposed, whereas $Fe(AcAc)_3$ and $Ga(AcAc)_3$ remained unchanged.

The mechanically mixed $Fe(AcAc)_3.Al(AcAc)_3$ samples (prepared by grinding) were irradiated. The resultant spectra were similar to those of the irradiated pure $Fe(AcAc)_3$.

The Fe^{2+} contents in the irradiated $(Fe.Al)AcAc_3$ samples were measured by use of U.V.[19]; since Fe^{2+} complexes with 1-10-phenanthroline give an absorption band at 315 mμ. The results are shown in Fig. 6.6. The Fe^{2+} contents detected are consistent with the observation of Fe (II) in the Mössbauer spectra. A typical spectrum of the irradiated 10% sample is shown in Fig. 6.7 and the Mössbauer data in Table 6.5. These results are compared with $[Fe(AcAc)_2]_n$[22] indicating that all the observed Fe (II) species are high spin.

No H. radical was detected in the esr spectra of $(Fe.Al)(AcAc)_3$ taken at 78°K immediately after irradiation. However, in some cases (low concentrations), unidentified organic radicals were observed. In addition no weight loss was observed for the irradiated samples.

Table 6.4

^{57}Fe Mössbauer Parameters *(110°K) of γ-Irradiated $Fe(AcAc)_3$

$Fe(AcAc)_3$	CS	QS	Γ_{ave}
Sample 1[a]	0.76	0.83	0.83
Sample 2[b]	0.84	0.73	1.07 ± 0.07
Sample 3[c]	0.75	0.74	0.88 ± 0.03

* Units in mm s^{-1}; errors are ± 0.02 mm s^{-1} except noted.

a. Right after irradiation (3.45 x 10^8 rads).

b. Sample 1 standing for six months.

c. Sample 2 recrystallized in $CHCl_3$.

Table 6.5

Fe(II) Mössbauer Data* of γ-Irradiated $(Fe,Al)(AcAc)_3$

Sample	CS	QS	Γ_{ave}	$I(Fe^{2+})/I(Fe^{3+})$
10%	1.65	3.07	0.33	0.6 ± 0.05
55%	1.69	2.84	0.31	0.2 ± 0.1
33%[a]	1.24	2.35	0.41	0.2 ± 0.1
$Fe(AcAc)_2$[b]	1.59	2.74	---	---
	1.49	2.40	---	---

*. Errors are ± 0.02 mm s^{-1}. Units in mm s^{-1}.

a. Good fits were not obtained. Errors in the parameters are relatively large.

b. Ref. 21.

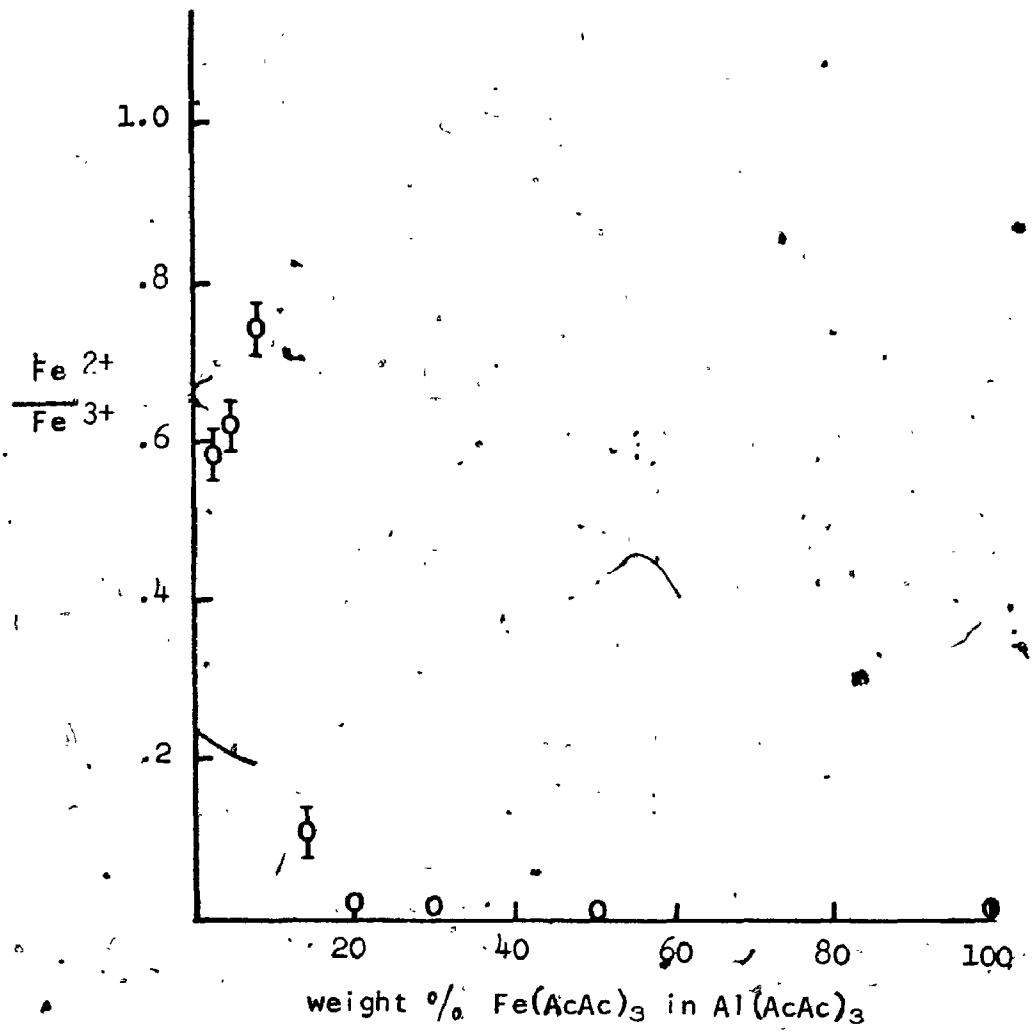

Figure 6.6 Plot of $\frac{Fe^{2+}}{Fe^{3+}}$ Ratio by Weight(from U.V. Spectra of the irradiated $(Fe^{\cdot}Al)(AcAc)_3$ Samples) vs. the Weight % Concentration of $Fe(AcAc)_3$ in $Al(AcAc)_3$

2. Discussion

The effect of γ irradiation on the Mössbauer spectra of $Fe(AcAc)_3$ has been studied previously under different conditions[12,13]. Line width narrowing and resolved QS have been observed[12] when $Fe(AcAc)_3$ was irradiated with 3×10^8 rads and at room temperature; whereas Mössbauer resonance due to Fe (II) species has been observed in spectra of $Fe(AcAc)_3$ irradiated with $\sim 10^9$ rads under 1 torr helium[13]. The former observation has been attributed to a motional narrowing mechanism and the latter has been attributed to an internal autoradiolysis simultated by irradiation with an external radiation source; since Fe (II) species has also been detected in Mössbauer spectra of high energy electron irradiated $Fe(AcAc)_3$ at 160^oC[23]. It is believed[23] that the conditions of irradiation are important and that high dose and low temperature may favor the Fe (II) formation.

All the irradiations described in this study were performed under a low dose ($2.7 - 4.5 \times 10^8$ rads), and room temperature condition. The Mössbauer results (Table 6.3) of the irradiated $(Fe.Al)(AcAc)_3$ samples are in general consistent with the line width narrowing effects observed in $Fe(AcAc)_3$; since the line widths of the irradiated $(Fe.Al)(AcAc)_3$ are appreciably narrower than those of of unirradiated samples. The $(Ga.Fe)(AcAc)_3$ samples, however, are almost insensitive to γ irradiation. To illustrate this, the widths of the unirradiated samples are compared with those of the irradiated samples (Fig. 6.8). The drastic change of the line widths in the 0 - 10% region in Fig. 6.8a is due to the formation of Fe (II) and Fe (III) species which are not

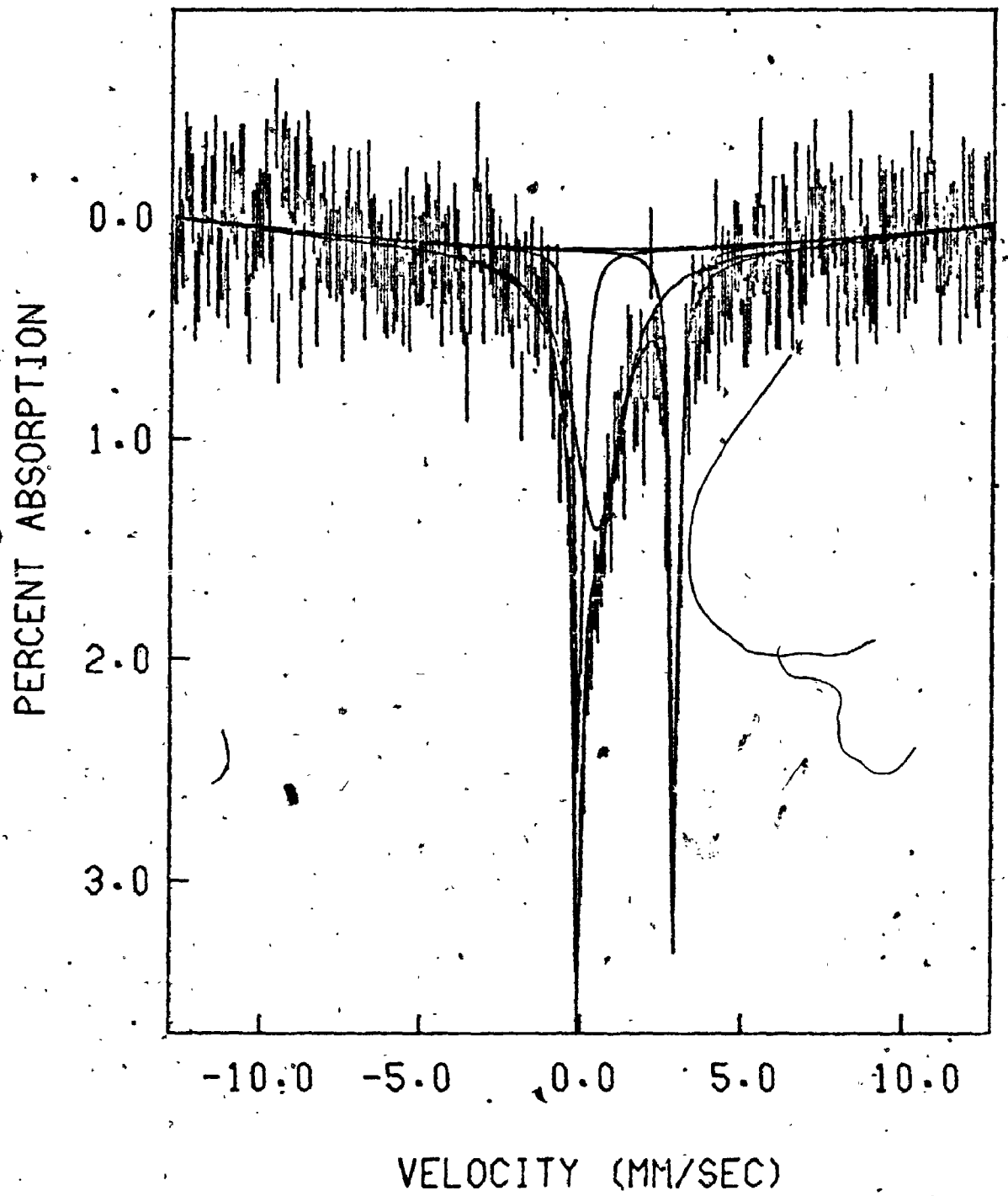

Figure 6.7 Mössbauer Spectrum of the irradiated 10% $Fe(AcAc)_3$ in $Al(AcAc)_3$ Sample (3.45×10^8 rads)

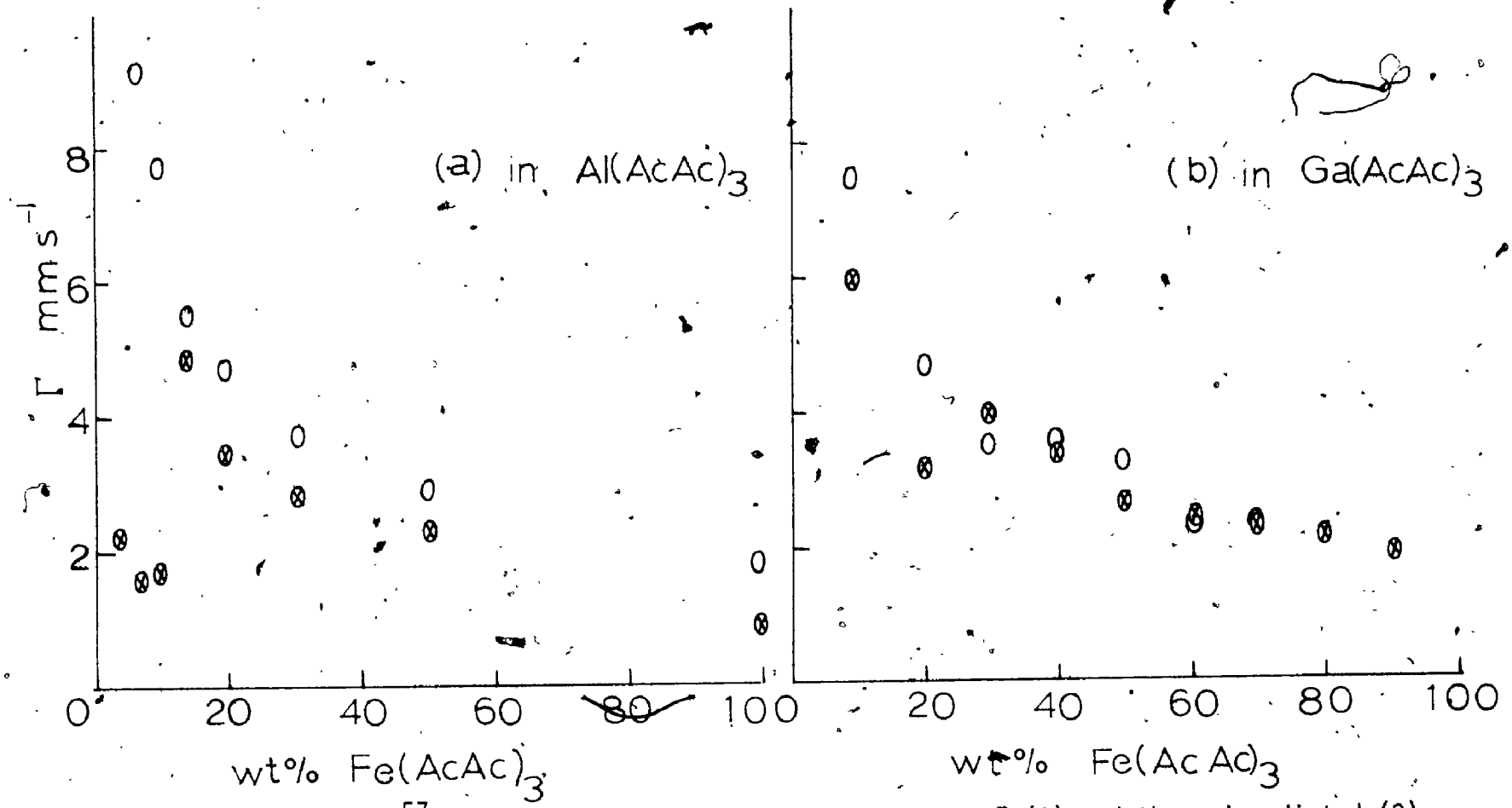

Figure 6.8 Plots of ^{57}Fe Mossbauer Line Withs of the irradiated (⊗) and the unirradiated (O) Samples vs. the % Concentration of $Fe(AcAc)_3$ in (a) $Al(AcAc)_3$ (b) $Ga(AcAc)_3$

necessarily $Fe(AcAc)_3$. To demonstrate that the formation of Fe (II) only occurred in diluted $Fe(AcAc)_3$ which is effectively separated or surrounded by $Al(AcAc)_3$, the mechanically mixed 10% $Fe(AcAc)_3$ in $Al(AcAc)_3$ sample was also irradiated under similar conditions. However, no appreciable change in the spectrum was observed after irradiation except line width narrowing. It is apparent that the local environment of the $Fe(AcAc)_3$ in the host matrix effects the radiolytic decomposition. The Mössbauer results of the irradiated $(Fe.Ga)(AcAc)_3$ support this arguments for the radiolytic sensitivity of the neat $M(AcAc)_3$ is in the order of $Al(AcAc)_3 > Fe(AcAc)_3 \gtrsim Ga(AcAc)_3$.

The comparatively narrow line widths observed in irradiated $(Fe.Al)(AcAc)_3$ compounds can be qualitatively described in terms of the motional narrowing mechanism[12] in which the γ-ray converts a small amount of $Fe(AcAc)_3$ into $FeAcAc_3^-$ or other Fe (II) compounds. The extra electron could then jump easily from one complex to the next, providing an efficient relaxation mechanism. The jumping rate can be estimated from

$$\Gamma = \frac{QS^2}{f\,\nu e} \qquad (6.2)$$

where: Γ is the observed line width, QS is the quadrupole splitting of a d-electron in absence of any relaxation, f is the mole fraction of Fe (II) and νe the jumping rate of one electron. The observation of Fe (II) species in the 10% $Fe(AcAc)_3$ region supports this argument. An alternative interpretation is that the radiation damages the crystal lattice or the extra electrons induced by the γ-rays facilitates.

the spin-lattice relaxation.

The Fe^{2+} contents in irradiated (Al.Fe)$AcAc_3$ samples are illustrated in Fig. 6.6 as a function of $Fe(AcAc)_3$ concentration. The Fe^{2+}/Fe^{3+} ratio (by weight, determined by U.V.) for the 10%, 5.5%, and 3.3% are in accord with the Mössbauer results where Fe^{2+} peaks can be actually seen in the spectra (Table 6.5). The spectrum in Fig. 6.7 is typical of Fe (III) and Fe (II) high spin. Attempts to identify these species have not yet been successful. However, the results are in a great degree consistent with a recently proposed internal autoradiolysis mechanism[23] stimulated by irradiation.

It is known that free organic ligands such as acetylacetone are radiosensitive[23, 24]. Esr experiments showed that the most important primary step in the radiolysis involves the H. radical which is very mobile in a solid[23,24]. When these ligands are complexed to a transition metal, the radiolysis is inhibited by the metal cation through oxidation-reduction radiolytic protection mechanism[25]. Thus, the high radiation stability of a series of ligands complexed to metals has been attributed to the fast annihiliation of free radicals by the oxidation-reduction mechanism[23-25].

According to Baggio-Saitovitch et al[22], the following mechanism ($Fe^{III}RH^2$=$Fe(AcAc)_3$ etc.) is proposed for the γ-irradiation study of (Al.Fe)$(AcAc)_3$.

$$Fe^{III}RH \xrightarrow{\gamma} Fe^{III}R. + H. \text{ (primary} \qquad (6.3)$$

$$Al^{III}RH \xrightarrow{\gamma} Al^{III}R. + H. \text{ step)} \qquad (6.4)$$

$$Fe^{III}RH + H. \rightarrow Fe^{II}RH^- + H^+ \text{ (reduction)} \qquad (6.5)$$

$$Fe^{III}R. + H. \rightarrow Fe^{III}RH \qquad (6.6)$$

$$Al^{III}R. + H. \rightarrow Al^{III}RH \qquad (6.7)$$

These equations by no means represent the real mechanism but rather qualitatively illustrate the results obtained. Eqs. (6.3) to (6.7) are probably the most important processes occurring during the chemical stage of the radiolysis. At higher $Fe(AcAc)_3$ concentrations, eq. (6.5) is probably not effective. Thus the small amount of $Fe^{II}RH$) produced (in this case $Fe(AcAc)_3^-$) leads to a motional narrowing mechanism. At lower concentrations, eq. (6.4) tends to facilitate the reduction process, eq. (6.5), which may lead to stable $Fe^{(II)}$ products. Furthermore, the following degradation processes are also possible:

$$Al^{III}R. \rightarrow Al^{III} + R. \qquad (6.8)$$

$$Fe^{III}R. \rightarrow Fe^{III} + R. \qquad (6.9)$$

$$Fe^{II}R. \rightarrow Fe^{II} + R. \qquad (6.10)$$

The esr evidence of unidentified organic radicals indicates these possibilities. The irreversibility of the Fe(II) spectra (remained unchanged after six months) and the esr results for $(Al.Fe)AcAc_3$ are consistent with the radiolysis of $[Fe^{III}(dipy)_3]ClO_4$ which was characterized by organic radicals as well as irreversible Fe(II) spectra.

It is apparent that the radiolysis of the impurity, $Fe(AcAc)_3$ in host matrices, $Ga(AcAc)_3$ or $Al(AcAc)_3$, depends on the nature of the matrix material and the characteristics of the "solid solution"

which has not been fully investigated. It is very likely that a host matrix [$Ga(AcAc)_3$] which has higher radiation stability than the impurity [$Fe(AcAc)_3$] tends to inhibit the impurity molecules from radiolysis, whereas a matrix [$Al(AcAc)_3$] with lower radiation stability tends to facilitate the radiolysis.

D. Experimental

The metal acetylacetonates were prepared by use of standard procedure described in the literature[26] except $Ga(AcAc)_3$ which was prepared from $Ga(NO_3)_3$ and acetylacetone in presence of sodium acetate in aqueous solution.

The "solid solution" samples of $(Fe.M)(AcAc)_3$ were prepared by dissolving appropriate amounts of $Fe(AcAc)_3$ and the corresponding host matrix material in chloroform. The solution was evaporated slowly at room temperature and under atmospheric pressure. $K_3(Al.Fe)(C_2O_4)_3$ was prepared by a similar method in aqueous solution[14].

The irradiation was performed in a 2.4×10^4 curies Atomic Energy Canada Gammacell 220 unit assembly at the Cancer Research Centre of the University of Western Ontario. All the irradiations were done under the following conditions (all at room temperature):

a. In polythene vials with no access to air under nitrogen.

b. In glass tubes with pinholes with restricted access to air.

Results obtained under above conditions are practically the same. Three dose rates were used for the irradiation.

a. 1.2×10^6 rads per hour and 1.0×10^6 rads per hour were used for

the irradiation of $(Fe.Al)(AcAc)_3$ and related samples.

b. 7.7×10^5 rads per hour was used for the irradiation of $(Fe.Ga)(AcAc)_3$.

The total dose deposited on the samples are 3.5×10^8 rads to 4.5×10^8 rads for the $(Fe.Al)(AcAc)_3$ solids and 2.7×10^8 rads for the $(Ga.Fe)(AcAc)_3$ solids.

Mössbauer spectra were obtained by standard methods described in Chapter 1 with an energy scan of $\pm$ ~12 mm s^{-1}. A 50 mCi ^{57}Co (Cu) radiation source was kept at room temperature. The 90% enriched 1% sample was run at PUMC Harwell. All the samples in the $(Fe.Al)(AcAc)_3$ series were enriched with ^{57}Fe to ~10% ^{57}Fe content except the 1%. In the Ga.Fe series, only the 10% sample was enriched to this level.

Other spectroscopic experiments (U.V., nmr, IR) were done by use of the routine techniques available in the Chemistry Department, U.W.O., whereas the esr spectra and X-ray powder photographs were taken in the esr and X-ray laboratories in the Chemistry Department, U.W.O. respectively.

E. References

1. A Abragam, and R. V. Pound, Phys. Rev. 92, 943 (1953).
2. J. W. G. Wignall, J. Chem. Phys. 44, 2462 (1966).
3. G. K. Wertheim, and J. P. Remeika Phys. Lett. 10, 14, (1964).
4. H. H. Wickman, M. P. Klein, and D. A. Shirley, Phys. Rev. 152, 345 (1966).
5. H. H. Wickman, and G. K. Wertheim in "Chemical Application of Mössbauer Spectroscopy", ed. V. I. Goldanskii and R. H. Herber. Academic Press, N. Y. and London, 1968.
6. M. Blume, Phys. Rev. Lett. 14, 96 (1965).
7. M. Blume, and J. A. Tjon, Phys. Rev, 165, 456 (1968).
8. H. S. Jarrett, J. Chem. Phys. 6, 1298 (1957). Table I.
9. D. Schroeer, R. L. Lambe, and C. D. Spencer in "Mössbauer Effect Methodology" 7, ed. I. J. Gruverman, Plenum Press, N. Y. 1971.
10. G. K. Werthiem, W. R. Kingston, and R. H. Herber, J. Chem. Phys. 37, 687 (1962).
11. A. R. Champion, R. W. Vaughan and H. G. Drickamer, J. Chem. Phys. 47, 2583, (1967).
12. G. M. Bancroft, K. G. Dharmawardena, and A. J. Stone, Chem. Comm. 6, (1971).
13. H. Sano, and H. Iwagami, Chem. Comm. 1637, (1971).
14. J. M. Friedt, E. Baggio - Saitovitch and J. Danon, Chem. Phys. Lett. 7, 603 (1970).
15. Private Communication with Dr. J. Bolton.
16. H. F. Symmons, and G. S. Bogle; Proc. Phys. Soc., 82, 412 (1963).
17. K. G. Dharmawardena, Ph.D. Thesis, University of Cambridge, 1970.
18. K. G. Dharmawardena, and G. M. Bancroft, J. Chem. Soc., (A), 2655, (1968).
19. S. F. Krzeminski and D. R. Straub, J. Chem. Phys. 58, 1086, (1973).
20. M. Blume, and R. Orbach, Phys. Rev. 127, 1587, (1962).

21. A. M. Leushin, Soviet Phys.-Solid State (English Trans). 5, 440 (1963).

22. J. L. K. F. de Vries, J. M. Trooster, and E. de Boer, J. Chem. Soc. Dalton, 1771 (1974).

23. E. Baggio-Saitovitch, J. M. Friedt, and J. Darren, J. Chem. Phys. 56, 1269 (1972).

24. B. Smaller and M. S. Matheson, J. Chem. Phys. 28; 1169 (1958).

25. K. Tsuji, S. Tazuke, K. Hayashi, and S. Okamura, J. Phys. Chem. 73, 2345 (1969).

26. F. C. Fernelius, Inorg. Syn. 2, 25, (1946).

APPENDIX I

Room Temperature Spectra of trans $Me_2Sn(AcAc)_2$

As discussed in Chapter 2, the Goldanskii - Karyagin asymmetry can be used to calculate the anisotropy of the thermal motion of the Sn atom. This asymmetry, often expressed by the deviation of the intensity ratio from unity, can then be compared directly with X-ray crystallographic thermal ellipsoids, provided that both measurements were carried out at the same temperature.

A room temperature X-ray study of trans $Me_2SnAcAc_2$ has been reported[1]. It is necessary to obtain room temperature spectra of trans $Me_2SnAcAc_2$ to make the comparison possible. Figure A.1 is a typical RT spectrum of unassociated trans $Me_2SnAcAc_2$. The observation of room temperature spectra[2] strongly indicates that intramolecular interactions are more important in determining both f factor and Goldanskii asymmetry than previously assumed[3].

The Goldanskii - Karyagin asymmetry observed at room temperature can now be used to derive the difference in mean square vibrational amplitudes of the Sn atom parallel and perpendicular to the Z EFG axes; since the M[illegible]n-Me axis is unambiguously the Z EFG axis. This difference derived from room temperature can then be compared directly with that derived from X-ray data.

The area ratio (A) of the 3/2 and 1/2 lines can be expressed as[4]:

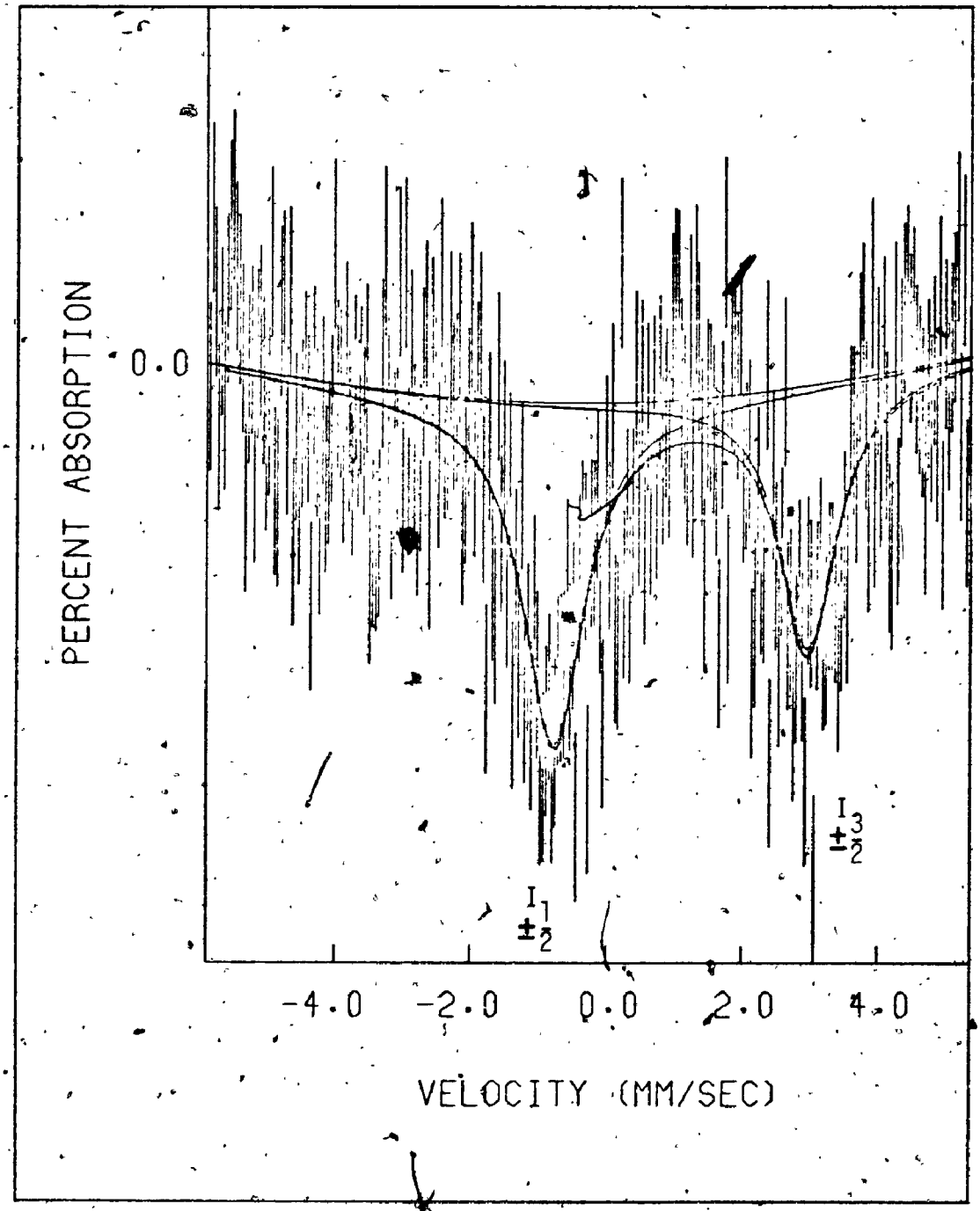

Figure A1.1 Room Temperature Spectrum of <u>trans</u> $Me_2Sn(AcAc)_2$

$$A = \frac{I_{\frac{3}{2}}}{I_{\frac{1}{2}}} = \frac{\int_0^1 (1+\mu)^2 e^{-\varepsilon\mu^2} d\mu}{\int_0^1 (\frac{5}{3} - \mu^2) e^{-\varepsilon\mu^2} d\mu} \qquad (A1.1)$$

where $\varepsilon = (\langle X_{11}^2 \rangle - \langle X_{\perp}^2 \rangle)$

and $\mu = \cos\theta$

The sign of e^2qQ for $Me_2Sn(AcAc)_2$[5] is positive indicating that the observed A value in eq(A.1) is 0.72 ± 0.02. Numerical solutions to eq.(A1.1) gives $\varepsilon = 4.1 \pm 0.8$. Taking $E_\gamma = 23.9$ Kev, this values leads to $\langle X_{11}^2 \rangle - \langle X_{\perp}^2 \rangle = 2.8\ (\pm 0.6) \times 10^{-18}\ cm^2$, in good agreement with the value of $2.92 \times 10^{-18}\ cm^2$ calculated from X-ray data[1] assuming that the arithmetic mean of axis 1 and 2 could be used for $\langle X_{\perp}^2 \rangle$. It is important to note that ε is very sensitive to small changes in A, and the deviation in $\langle X_{11}^2 \rangle - \langle X_{\perp} \rangle^2$ is large. Unless A can be measured (and this is not easy to do with room temperature spectra), the Mössbauer determined $\langle X_{11}^2 \rangle - \langle X_{\perp}^2 \rangle$ will have a large uncertainty.

References:

1. G. A. Miller and E. O. Schlemper, Inorg. Chem. 12, 677, (1973).
2. G. M. Bancroft, K. D. Butler, and T. K. Sham, J. Chem. Soc.(Dalton), in press.
3. R. C. Poller, J. N. R. Ruddick, B. Taylor and D. L. B. Toley, J. Organomet. Chem. 24, 341 (1970).
4. P. Flinn , S. L. Ruby, and W. L. Kehl, Science 143, 1434 (1964).
5. G. M. Bancroft and R. H. Platt, Adv. Inorg. Radiochem. 15, 59, (1973).

APPENDIX II

^{119}Sn Mössbauer Quadrupole Splittings for Distorted Me_2Sn^{IV} Structures

The additive model[1,2] so far discussed is based on the assumption that all molecules have the ideal geometry. Although extensive results have been successfully interpreted on this basis, this model does not give a chemically realistic picture when surprising structural situation arises. For example, the unambiguous assigned six coordinate structures of $Me_2Sn(oxin)_2$[3], $Me_2Sn[S_2CNMe_2]_3$[4] and $Me_2Sn(salen)$[5] have C-Sn-C bond angles varying from 110° to 136° to 160° respectively. These angles are significantly deviated from the expected 90° and 180° for cis R_2SnL_4 and trans R_2SnL_4 respectively. An alternative description of the unusual structural situation occurred in Me_2SnL_2 (L_2 are anisobidentate[6] ligands in most cases) is given below.

The literal point charge model is used for the interpretation in conjunction with a further assumption that the quadrupole splitting is set up just by the Me_2Sn unit. This assumption is reasonable in most cases; since for octahedral compounds containing oxygen, nitrogen and halide ligands, the pqs values of these ligands[7] are nearly all $\pm$ 0.10 mm s^{-1}, compared with the Me value[2] of - 1.03 mm s^{-1}. Any contribution to the QS from such ligands then should be small.

The axis system given in Fig. A2.1 is used for the Me_2Sn unit.

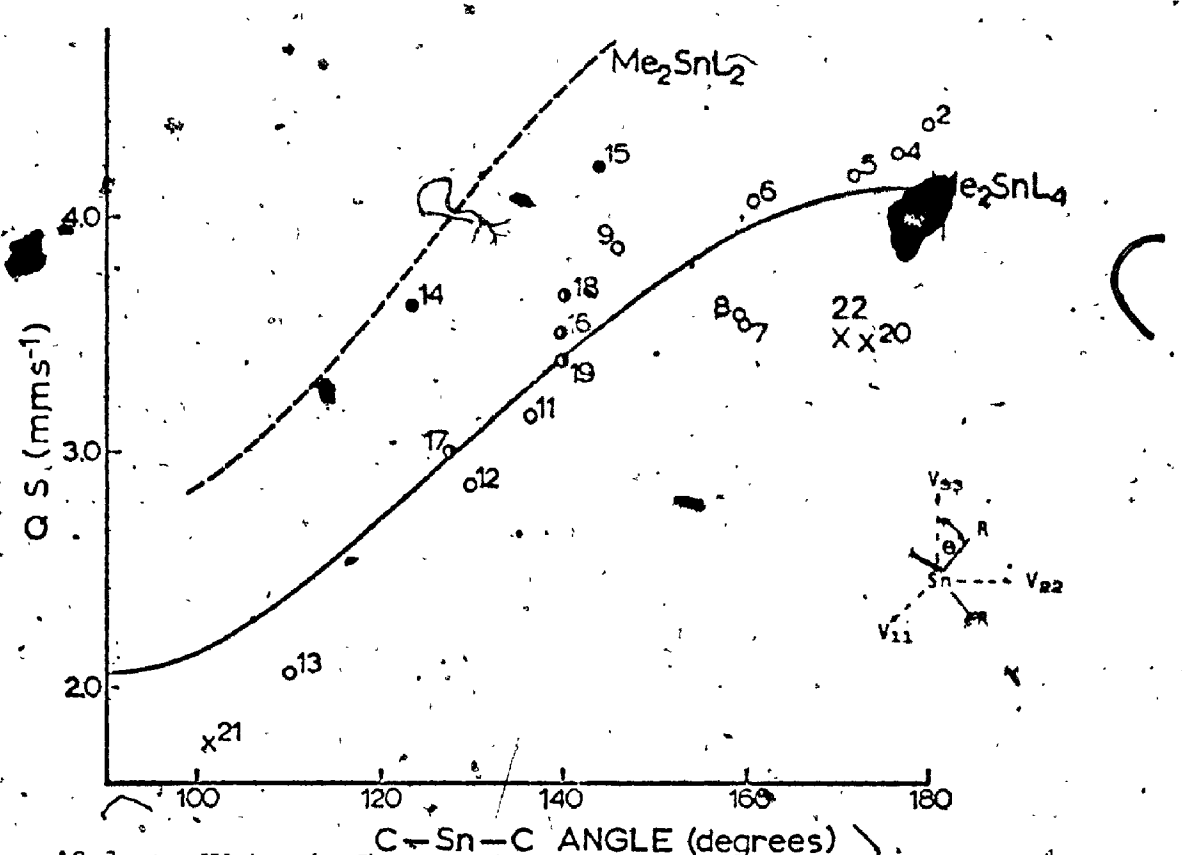

Figure A2.1 EFG Axes for The R_2Sn Unit and Plot of Observed QS versus Observed C-Sn-C Angle in Me_2Sn Compounds (● and ○). The Numbers Refer to The Compounds In Table A2.1. Ph_2Sn Parameters (x) Are Given in The Text. The Curves Are Those Calculated for Six (—) and Four (---) Coordinate Me_2Sn Compounds Respectively.

The EFG expressions are:

$$V_{11} = -2\,[Me] \qquad (A2.1a)$$

$$V_{22} = 2\,[Me]\,(3\sin^2\theta - 1) \qquad (A2.1b)$$

$$V_{33} = 2\,[Me]\,(3\cos^2\theta - 1) \qquad (A2.1c)$$

V_{11} is perpendicular to the RSnR plane, while V_{22}, V_{33} are coplanar with RSnR.

By use of the symmetrized parameters introduced by Clark[8], the QS is expressed as:

$$QS = 4\,\{Me\}\,[1 - 3\sin^2\theta\cos^2\theta]^{1/2} \qquad (A2.2)$$

where $\{Me\} = 1/2\,e^2Q\,[Me]$

The QS as a function of C-Sn-C angle (180-2θ) can be readily calculated using $\{Me\}^{oct} = -1.03$ mm s^{-1} (Fig. A2.1, solid line). The sign of the QS is positive from 180° to 109.5° where it changes sign.

Nineteen crystal structures of Me_2Sn^{IV} compounds with known QS (except $Me_2Sn(CN)_2$) are now available (Table A2.1). Compounds (1-13) and (17-19) have been unambiguously assigned as six and five coordinate structures respectively, where as Me_2SnCl_2 and $Me_2Sn(NO_3)_2$ have been classed as either distorted tetrahedral or octahedral structures.

In Fig. A2.1, the observed QS are plotted against the Me-Sn-Me angle for these compounds. The agreement between the predicted and the observed values is good considering the gross assumptions: only for Me_2SnCl_2 and $Me_2Sn(NO_3)_2$, the deviation is significant (by more than 0.4 mm s^{-1}).

The {Me} value for five coordinate structures is taken as the average value of $\{Me\}^{tba}$ (-0.94 mm s^{-1}) and $\{Me\}^{tbe}$ (-1.13 mm s^{-1}) derived in Chapter 5. It turns out that this average value is identical to $\{Me\}^{oct}$.

The three Ph_2Sn^{IV} six coordinate structures shown in Fig. A2.1 also give the same trend. Thus, $Ph_2SnCl_2(bipy)$[9] (20 in Fig. A2.1), $Ph_2SnCl_2(DMSO)_2$[10], (22 in Fig A2.1) have C-Sn-C angles of 173.5° and 169.7° and QS of 3.45 mm s^{-1} and 3.54 mm s^{-1} respectively; while $Ph_2Sn(S_2CNEt_2)_2$[11] (21 in Fig. A2.1) has a C-Sn-C angle of 101.4° and a QS of 1.76 mm s^{-1}[12].

The good agreement between predicted and observed values in Fig. A2.1 (with the exception of Me_2SnCl_2 and $Me_2Sn(NO_3)_2$) implies that $\{Me\}^{oct}$ = - 1.03 mm s^{-1} is a good working value. However, $\{Me\}^{oct}$ value cannot be constant, since the bonding should change when C-Sn-C deviates. The variation in $J_{119Sn-CH_3}$ values[13] (Table A2.1) reflects this change. There must be some compensating effects which keep $\{Me\}^{oct}$ effectively constant. Two such effects are apparent. First, as the S character of the Sn-C bond decreases (making {Me} more negative[14]), the bond length increases (making {Me} more positive). Except for compounds 1, 3 and 4 in Table A2.1, there is a general increase in bond length as the C-Sn-C angle increases, but the errors in the bond length are too large to allow a firm trend. Second, it is likely that this effect applies to $\{L\}^{oct}$ also, making $\{Me\}^{oct}$ - $\{L\}^{oct}$ nearly constant.

The two QS values which lie substantially off the octahedral curve in Fig. A2.1 are those for Me_2SnCl_2 and $Me_2Sn(NO_3)_2$. These two compounds are better described as distorted tetrahedral structures, with Me_2SnCl_2 being slightly associated and the bidentate NO_3(O-Sn-O angle of 55°)

Table A2.1 Relevant Parameters for $Me_2Sn(IV)$ Structures

	Compound	Structural Data (Averages)			Mössbauer Data (mm s^{-1})			$J_{^{119}Sn-CH_3}$	
		∠ C-Sn-C°	r(Sn-C) Å	Ref.	C.S.	Q.S.	Ref.	Hz	Ref.
1.	$Me_2SnCl_2(pyO)_2$	180	2.22	a	1.42	3.96	o	93	y
2.	Me_2SnF_2	180°	2.08	b	1.33	4.38	l		
3.	$Me_2Sn(AcAc)_2$	180°	2.14	c	1.16	4.02	p	99	p
4.	$Me_2SnCl_2(Salen\ H_2)$	175°-177°	2.15	d	--	4.27	q		
5.	$Me_2SnCl_2(DMSO)_2$	172°	2.08	e	1.40	4.16	o	86	y
6.	$Me_2SnCl_2NiSalen$	161.0	2.13	f	1.50	4.06	r	114	r
[illegible]	$Me_2Sn(Salen)$	160.0	2.12	s	1.13	+3.46	12	84	x
8.	$Me_2SnCl\ terpy^+$	159	2.07	g	1.41	3.55	j,s		
9.	$Me_2Sn(NCS)_2$	145.9	2.14	h	1.48	3.87	t		
10.	$Me_2Sn(CN)_2$	148.7	2.11	i	—	--			
11.	$Me_2Sn(dtc)_2$	136	2.15	4	1.57	3.14	6,13	84	4
12.	$Me_2Sn[S_2NC(CH_2)_4]_2$	130.0	—	10	1.59	2.85	6,13		
13.	$Me_2Sn(oxin)_2$	110.7	2.16	3	0.88	2.02	u	71.5	4
14.	Me_2SnCl_2	123.5	2.21	j	1.54	3.55	j		
15.	$Me_2Sn(NO_3)_2$	144	2.12	k	1.56	4.20	v	81.6	13
16.	$Me_2SnCl_3^-$	140	2.12	g	1.44	3.51	u		
17.	$Me_2SnCl(S_2NCR_2)$	128	2.19	l	1.28	2.98	w		
18.	$[Me_2SnOHNO_3]_2$	139.9	2.13	m	1.28	3.67	this work		
19.	$Me_2Sn(NCS)_2O$	140.5	2.11	n	1.25	3.38	this work		

References for Table A2.1

a. E. A. Blom, B. R. Penfold and W. T. Robinson, J. Chem. Soc.A, 913,(1969).

b. E. O. Schlemper and W. C. Hamilton, Inorg. Chem. 5, 995,(1966).

c. G. A. Miller and E.D. Schlemper, Inorg. Chem. 12, 677,(1973).

d. L. Randaccio, J. Organomet. Chem. 55, C58,(1973).

e. N. W. Isaacs and C.H.L. Kennard, J. Chem.Soc.A.,1257,(1970).

f. M. Calligaris, L. Randaccio, R. Barbieri and L. Pellerito, J. Organomet. Chem. 76, C56,(1974).

g. F.W.B. Einstein and B. R. Penfold, J. Chem. Soc.A, 3019,(1968).

h. Y. M. Chow, Inorg. Chem. 9, 794,(1970).

i. J. Konnert, D. Britton, and Y. M. Chow, Acta Cryst.B, 28, 180,(1972).

j. A. G. Davies, H. J. Milledge, D. C. Puxley and P. J. Smith, J. Chem. Soc.(A), 2862,(1970).

k. J. Hilton, E. K. Nunn and S. C. Wallwork, J. Chem. Soc.(Dalton), 173,(1973).

l. K. Furue, T. Kimura, N. Yasueka, N. Kosai, and M. Kakudo, Bull. Chem. Soc. Japan, 43, 1661,(1970).

m. A. M. Domingos and G. M. Sheldrick, J. Chem. Soc.(Dalton).475,(1974).

n. Y. M. Chow, Inorg. Chem. 10, 673,(1971).

o. A. G. Davies, L. Smith and P. J. Smith, J. Organomet. Chem. 23, 135,(1970).

p. G. M. Bancroft and T. K. Sham. Can. J. Chem. 52, 1361,(1974).

q. R. Barbieri, L. Pellerito, M. Bertazzi and G. C. Stocco, Inorg. Chim Acta. 11, 173,(1974), ref. 44.

r. L. Pellerito, R. Cefalu, A. Gianzuzza and R. Barbieri, J. Organomet. Chem. 70, 303,(1974).

s. N. W. G. Debye, E. Rosenberg and J. J. Zuckerman, J. Am. Chem. Soc. 3234,(1968).

t. B. Cassenheimer and R.H. Herber, Inorg. Chem. 8, 1120, (1969).

u. R. Parish and R. H. Platt, Inorg. Chim. Acta 4, 65, (1970).

v. D. Potts, H. D. Sharma, A. J. Carty and A. Walker, Inorg. Chem. 13, 1205,(1974).

w. B. W. Fitzsimmons and A. C. Lawbridge, J. Chem. Soc.(Dalton), 1678,

x. A. Vanden Bergen, R. J. Cozens and K. S. Murray, J. Chem. Soc.(A), (1970).

y. V. G. Kumar Das and W. Kitching, J. Organomet. Chem. 13, 523,(1968)

z. J. Chem. 21, 2401,(1968).

effectively occupying a structural position. The expected tetrahedral curve (broken line) was calculated for $\{Me\}^{tet} = -1.37$ mm s^{-1} [2] by use of eq. A2.2. The two compounds lie closer to this curve than to the octahedral curve.

A careful examination of the molecular structure of the Me_2Sn and Ph_2 structures reveals that the very distorted structures always have chelates L_2 ligands with a small bite for the relatively large Sn atom. Among these non-associated structures, there are four or five membered rings, and the small bite of the chelates forces the coordinating atoms into inequivalent positions. A similar situation has been observed in five coordinate structures (Chapter 4).

If the effective bite of the ligand is known, it should be possible to predict qualitatively the Me-Sn-Me angle. In turn, the QS of known structures can be estimated. Since the bonding property of the ligands should be almost constant for Sn(IV) in all compounds, it still seems entirely reasonable, for predictive purposes, to derive a pqs value in the distorted complex using ideal geometry calculations. It will not be possible, however, to use pqs values (derived using distorted structures) for bonding estimates as has been done for regular six coordinate structures [15].

References:

1. G. M. Bancroft and R. H. Platt, Adv. Inorg. Radiochem. 15, 59, (1972); see also Chapters 1 to 5.

2. M. G. Clark, A. G. Maddock, and R. H. Platt, J. Chem. Soc. (Dalton), 210 (1972).

3. E. O. Schlemper, Inorg. Chem. 6, 2012 (1967).

4. T. Kimura, N. Y. Yasueka, N. Kasai, and M. Kakudo, Bull. Chem. Soc. Japan 45, 1649 (1972).

5. M. Calligaris, G. Nardin, and L. Randaccio, J. Chem. Soc. (Dalton), 2003, (1972).

6. J. L. K. F. De Vries and R. H. Herber, Inorg. Chem. 11, 248 (1972).

7. M. G. Clark, Mol. Phys. 20, 257, (1971).

8. P. G. Harrison, J. J. King and J. A. Richards, J. Chem. Soc. (Dalton), 1723, (1973).

9. L. Coghi, C. Pelizzi and G. Pelizzi, Gazzetta, Chim, Italiana, 104, 873 (1974).

10. P. F. Lindley and P. Carr, J. Cryst. Molec. Struct., 4, 173 (1974).

11. D. Petrides and B. W. Fitzsimmons, Inorg. Chem. 60, 233, (1973).

12. R. C. Poller, Chemistry of Organotin Compounds, Academic Press, N. Y., 1970.

13. G. M. Bancroft and A. T. Rake, Inorg. Chim Acta, in press.

14. G. M. Bancroft, J. G. K. Das, and K. D. Butler, J. Chem. Soc. (Dalton), 2355, (1974).